ISWRRI-52

COMPLETION REPORT

Natural Mixing and Transfer Processes for

Thermal Loads in Streams

Project No. A-040-IA 1/

Duration: July, 1970 - June, 1973

Iowa State Water Resources Research Institute

Ames, Iowa 50010

Date of this report: August, 1973

VERTICAL MIXING OF HEATED EFFLUENTS IN OPEN-CHANNEL FLOW

by

E. J. Schiller and W. W. Sayre

Iowa Institute of Hydraulic Research
The University of Iowa
Iowa City, Iowa

Office of Water Resources Research Agreement Nos.:

14-31-0001-3215
14-31-0001-3515
14-31-0001-3815

1/ Project financed in part by a grant from the U. S. Department of Interior, Office of Water Resources Research under Public Law 88-379 and made available through the Iowa State Water Resources Research Institute.

FOREWORD

The general aim of the Iowa State Water Resources Research Project No. A-040-IA, "Natural Mixing and Transfer Processes for Thermal Loads in Streams", identified on the title page of this report, was to obtain a better understanding of the processes by which a heated water discharge is mixed with flowing streamwater and the excess heat is transferred to the surrounding environment. The way in which these two processes combine to produce the resulting temperature distribution pattern in the stream was also a goal of this study. More specifically, the objectives were: (1) to investigate the vertical, transverse, and longitudinal mixing of heated effluent water in a laboratory flume in situations where turbulence and velocity differentials in the ambient flow are the principal mixing agents; (2) to investigate the influence of the density difference between the heated effluent and the ambient water on the mixing processes; (3) to investigate the influence of the boundary conditions at the water surface and the channel perimeter on the mixing processes for a heated effluent; and (4) to compare the mixing processes for a heated effluent with those for a conservative, neutrally-buoyant tracer, and to relate the differences to the buoyancy and boundary condition effects indicated in objectives 2 and 3.

After the first year of the project, a grant was obtained for a Title II Project, "Mixing and Transfer of Heat in Open Channel Flow" (OWRR Project Number C-3140, Funding Agreement Number 14-31-0001-3692),

for a three-year period. This additional grant permitted the depth and scope of the research activity to be substantially increased.

This report marks the completion of the first phase of the combined projects. It focuses on the vertical mixing problem identified in objective 1, as well as on all of the problems identified in objectives 2, 3, and 4, as they relate to the vertical mixing process. To a greater or lesser extent, most of the major objectives were achieved for the idealized case of uniform ambient flow in a laboratory flume with a rough bottom. Specifically, a fairly general mathematical model was obtained which satisfactorily predicts the damping effect of density differences between the heated effluent and ambient water on the vertical mixing process for a wide range of conditions. As anticipated, the results show that the rate of vertical mixing asymptotically approaches the mixing rate for a conservative, neutrally-buoyant tracer as the density difference approaches zero. The objective pertaining to the investigation of heat transfer across the water surface and through the channel perimeter was only partially achieved. In the region close to the source, where longitudinal temperature gradients are the steepest, experimental measurements indicated that the heat loss across the water surface tends to be significantly larger than that predicted by any of the existing surface heat transfer theories. The cause was not positively identified.

The investigations of the transverse and longitudinal mixing processes have not yet reached a reportable stage. These investigations are being continued under the OWRR Title II project.

ABSTRACT

The extensive use of rivers as a sink for waste heat has caused widespread environmental concern. The vertical mixing of heated surface effluents, due to turbulent and convective transport mechanisms of the ambient flow, was investigated in a series of laboratory flume experiments covering flows ranging from well-mixed to nearly stable stratified conditions. Detailed temperature and velocity distribution data were obtained in the mixing region.

The data and analyses based on the convection-diffusion equation were combined to determine (1) required distances for nearly complete mixing, (2) bulk vertical mixing coefficients, and (3) the variation over the depth of the overall vertical heat transfer coefficient. In the more stratified flows, buoyancy effects sharply reduced the value of the vertical heat transfer coefficient in the upper part of the flow. In flows with minimal buoyancy effects the mixing was rapid and the magnitude and distribution of the heat transfer coefficient approached those for the turbulent vertical momentum transfer coefficient. Finally, using a finite-difference representation of the steady state convection-diffusion equation and an empirical function for the vertical heat transfer coefficient, downstream temperature profiles were predicted for selected representative experimental conditions. The predicted profiles agreed closely with the experimental ones.

KEY WORDS: Diffusion, Dispersion, Heat Flow-water, Heat Transfer,

Mixing in Natural Waters, Stratification-water, Stratified Flow, Temperature-water, Thermal Pollution, Turbulent Flow.

ACKNOWLEDGEMENTS

Except for minor revisions this report is identical to the thesis submitted by the senior writer in partial fulfillment of the requirements for the degree of Doctor of Philosophy in the Department of Mechanics and Hydraulics at the University of Iowa. The junior writer served as research advisor.

In addition to the funding from the Iowa State Water Resources Research Institute and the Offices of Water Resources Research, a Teaching-Research Fellowship from the Graduate College of the University of Iowa provided financial support for the senior writer for three years.

In preparation of the IBM-1801 computer program, and in problems of instrumentation the assistance of Drs. J. R. Glover and F. A. Locher was most helpful. The shop crew under the capable leadership of Mr. Dale Harris is to be commended for their ability to turn out first class craftsmanship, often on very short notice.

TABLE OF CONTENTS

LIST OF TABLES

LIST OF FIGURES

LIST OF SYMBOLS

Symbol	Definition	Dimensions	Units
A	Cross sectional area	L^2	$ft.^2$
$B(\eta:t,r)$	Beta distribution with parameters t and r		
C	Concentration of a neutrally-buoyant substance		
$\overline{C}$	Average concentration of a neutrally buoyant substance in a cross section		
C_a	Area correction factor for the beta distribution		
C_p	Specific heat of water		$\frac{BTU}{lb_m\ ^\circ F}$
D_{75}	Gravel diameter of which 75% is finer	L	ft.
DX	Longitudinal increment for numerical computation		
DY	Vertical increment for numerical computation		
d	Depth of flow	L	ft.
E_c	Width-averaged vertical convective dispersion coefficient	$\frac{L^2}{T}$	$\frac{ft.^2}{sec.}$
E_{My}	Width-averaged vertical mass transfer coefficient	$\frac{L^2}{T}$	$\frac{ft.^2}{sec.}$
E_{MOy}	Width-averaged vertical momentum transfer coefficient	$\frac{L^2}{T}$	$\frac{ft.^2}{sec.}$
E_{Ty}	Width-averaged vertical heat transfer coefficient	$\frac{L^2}{T}$	$\frac{ft.^2}{sec.}$

Symbol	Definition	Dimensions	Units
F_{DO}	Initial densimetric Froude number $= \frac{U}{\sqrt{g r_b (\rho_{eff} - \rho_{amb})/\rho_{amb}}}$		
F_{DX}	Cross-sectional densimetric Froude number $= \frac{U}{\sqrt{g r_b (\rho_{\eta=.08} - \rho_{\eta=.96})/\rho_{\eta=.08}}}$		
$\bar{F}_i$	Body force in the i'th direction	$\frac{ML}{T^2}$	lb_f
g	Acceleration due to gravity	$\frac{L}{T^2}$	$\frac{ft.}{sec.^2}$
K	Surface heat exchange coefficient		$\frac{BTU}{^\circ F\text{-}ft.^2\text{-}sec.}$
K_w	Overall coefficient of heat transfer for walls of flume		$\frac{BTU}{^\circ F\text{-}ft.^2\text{-}sec.}$
K_b	Overall coefficient of heat transfer for bottom of flume		$\frac{BTU}{^\circ F\text{-}ft.^2\text{-}sec.}$
K_x, K_y, K_z	Constant diffusion coefficients in the x,y and z directions.	$\frac{L^2}{T}$	$\frac{ft.^2}{sec.}$
k_s	Equivalent sand grain diameter	L	ft.
p	Pressure	$\frac{M}{LT^2}$	$\frac{lb_f}{ft.^2}$
Q_{tot}	Total measured discharge	$\frac{L^3}{T}$	$\frac{ft.^3}{sec.}$

Symbol	Definition	Dimensions	Units
R	Hydraulic radius	L	ft.
R_i	Richardson number		
R_{ix}	Gross Richardson number for a cross section		
R_N	Open-channel Reynolds number $= \frac{4UR}{\nu}$		
r_b	Effective flow depth	L	ft.
S	Slope of the flume		
T_{air}	Air temperature		°F
T_{amb}	Temperature of the upstream ambient water		°F
T_b	Effective temperature near flume bottom		°F
T_E	Equilibrium temperature		°F
$T_{max}, T_{top}, T_{\eta = .96}$	Average horizontal temperature at $\eta = .96$		°F
$T_{min}, T_{bot}, T_{\eta = .08}$	Average horizontal temperature at $\eta = .08$		°F
T_{eff}	Temperature of the effluent water		°F
T_S	Water surface temperature		°F
T_w	Effective temperature near flume wall		°F
$\overline{T}^w$	Width-averaged temperature of the flowing fluid		°F
$\overline{T}_x$	Average temperature for a cross section weighted by area		°F

Symbol	Definition	Dimensions	Units
T_*	Normalized temperature, T_{amb} as datum $= \frac{\overline{T}^w - T_{amb}}{\Delta T}$		
$\hat{T}$	Normalized temperature, T_E as datum $= \frac{\overline{T}^w - T_E}{\Delta T}$		
U	Average velocity in the longitudinal direction	$\frac{L}{T}$	$\frac{ft.}{sec.}$
u,v,w	Local time-averaged velocities in the longitudinal, vertical and transverse directions	$\frac{L}{T}$	$\frac{ft.}{sec.}$
u_*	Shear velocity	$\frac{L}{T}$	$\frac{ft.}{sec.}$
W	Width of the flume or river	L	ft.
x,y,z	Space co-ordinates in the longitudinal, vertical and transverse directions	L	ft.
X	Distance downstream from the spreader	L	ft.
y_o	Thickness of effluent flow at spreader	L	ft.
ΔT	Temperature difference between heated effluent and ambient fluids		^oF
$\Delta\rho$	Density difference between the ambient and the effluent fluids.	$\frac{M}{L^3}$	$\frac{lb_m}{ft.^3}$

Symbol	Definition	Dimensions	Units
$\Delta\rho_x$	Density difference between the bottom (η = .08) and top (η = .96) for a cross section at X	$\frac{M}{L^3}$	$\frac{lb_m}{ft.^3}$
$\varepsilon_M, \varepsilon_{My}$	Local vertical mass transfor coefficient	$\frac{L^2}{T}$	$\frac{ft.^2}{sec.}$
$\varepsilon_{MO}, \varepsilon_{MOy}$	Local vertical momentum transfer coefficient	$\frac{L^2}{T}$	$\frac{ft.^2}{sec.}$
$\varepsilon_{Tx}, \varepsilon_{Ty}, \varepsilon_{Tz}$	Local coefficients of turbulent heat transfer (due to diffusion)	$\frac{L^2}{T}$	$\frac{ft.^2}{sec.}$
κ	Von Karman turbulence coefficient		
η	Normalized vertical position = y/d		
ϕ_n	Net rate of heat exchange		$\frac{ft.-^oF}{sec.}$
ϕ_s	Heat flux through the water surface		$\frac{ft.-^oF}{sec.}$
ϕ_b	Heat flux through the flume bottom		$\frac{ft.-^oF}{sec.}$
ρ	Density	$\frac{M}{L^3}$	$\frac{lb_m}{ft.^3}$
ρ_a	Density of the ambient fluid	$\frac{M}{L^3}$	$\frac{lb_m}{ft.^3}$
ρ_b	Density of the fluid at the bottom of the flume	$\frac{M}{L^3}$	$\frac{lb_m}{ft.^3}$

Symbol	Definition	Dimensions	Units
σ	Standard deviation of N measurements		
σ_m	Standard deviation of the means		
τ_{xy}	Shear stress in the x-direction acting on a plane normal to the y axis	$\frac{M}{LT^2}$	$\frac{lb_f}{ft.^2}$

Chapter 1

INTRODUCTION

Electrical energy consumption in this country is currently increasing at a rate of about seven per cent per year. Nuclear power plants will produce an increasingly larger share of this electrical power, but because of their lower thermal efficiency, they reject even more waste heat than fossil fuel plants. The dispersion of this waste heat will pose an increasingly troublesome problem. The use of rivers as a source of once-through cooling water is becoming more and more difficult as available sites are used up and environmental protection criteria become more exacting. Because of this, in the future we shall need to predict the behavior of heated effluents more accurately. If it can be shown that for a certain site, the environmental effects of heated effluents are negligible then from a total resources point of view it would be wasteful to resort to a more complicated cooling procedure.

At present, the use of natural waterways to dissipate the heat of discharged cooling water is widely practiced. There are essentially two different ways to introduce the heated discharge into the flowing stream. The hot water can be introduced as a submerged jet. In this case there is rapid turbulent mixing of the discharge with the ambient stream and entrainment of ambient fluid into the jet.

Temperatures are rapidly reduced by dilution and the heat from the discharge water is carried along by the entire ambient flow and gradually transferred to the atmosphere. The other method is to introduce the heated discharge at the surface of the flowing stream, usually at or near the average velocity of the ambient stream. In this case the warmer, lighter fluid tends to stay on top of the flowing stream, thus permitting a more rapid heat loss directly to the atmosphere. Depending on the parameters of the flowing stream, the heated water may remain in the upper part of the flow in a stratified state, or be rather rapidly mixed downward into the flow by the turbulence of the flowing stream. Stratified flow provides a maximum rate of heat loss to the atmosphere, whereas rapid downward mixing reduces the temperature most rapidly. Each of the above cooling methods has its own advantages, but each likewise presents its own ecological hazards. Stratified flow will alter the reaeration process at the surface, upset the natural heat balance in the river and have various effects on the aquatic life in the river as reported by Parker and Krenkel (18). A rapidly mixed heated effluent will also tend to alter the habitat of bottom-growing plant and animal life.

In this study the heated effluent was introduced at the water surface at both the average and water surface velocities. The focus of the investigation was then on the far-field or passive-diffusion mixing region. In this region the mixing is assumed to be due predominantly to the turbulence of the flowing ambient stream,

and entrance effects are considered to be minimal. As the velocity of the flowing stream increases, the mixing process becomes increasingly insensitive to the entrance conditions. However at the lower velocities, the entrance conditions became more critical, so a brief investigation of this phenomenon was made.

The goal of this study was to provide a better insight into the basic mechanism by which a heated effluent at the surface, with no excess momentum, mixes with the underlying ambient stream. A further objective was to evaluate parameters based on the convec-vection-diffusion equation that enable prediction of the mixing rate. It is thus hoped that the results of studies such as this will reduce the future need for expensive and time-consuming model studies.

The basic approach was to simulate the process in a laboratory flume at different flow conditions, monitor temperatures and velocities, and then analyze the resulting experimental data. The IBM-1801 Computer in the Hydraulics Laboratory was used in data acquisition, and the University of Iowa IBM-365 Computer was used in the subsequent analysis.

After a review of previous investigations related to this problem, the basic theoretical background is developed in Chapter III. This is followed by a description of the apparatus and the experiments which were conducted. The heart of the study is in Chapters V and VI which present, utilize and analyze the experimental results. Chapter VII then summarizes the main findings of the study.

Chapter II

REVIEW OF PREVIOUS WORK

The phenomenon of thermal pollution in natural waterways is a relatively new area of scientific investigation. It is only within the last five to ten years that an extensive body of literature has developed around this subject. In 1969 Parker and Krenkel gathered together data on the status of this emerging art (18,19). Harleman has done excellent pioneering work on the nature of stratified flow (9) together with applications to condenser water discharges (19), but his work did not consider in detail the role of passive turbulent diffusion in flows with continuous density gradients. In 1971 and 1972 the Massachusetts Institute of Technology sponsored two Summer Sessions on the Engineering Aspects of Heat Disposal (10). The two chapters from Summer Session Notes most relevant to this work are Chapter 1, "Environmental Heat Transfer," by Ryan and Stolzenbach which reviews the various mechanisms of heat transfer between a water surface and the environment, and Chapter 9, "Temperature Distributions in the Far Field Region - Partial Mixing," by Ditmars, which provides some of the analytical framework for the present study.

Historically the investigation of the mixing of heated effluents has evolved out of the study of the mixing of neutrally buoyant substances, particulate matter such as sediments and the

mixing of saline density-stratified flows. Ellison and Turner (6,7) in a series of experiments on saline stratified flows laid much of the ground work for future investigations. Their first set of experiments, reported in 1959, showed the entrainment coefficient to be a well defined monotonic decreasing function of the overall Richardson number for the layer, defined as

$$R_i = \frac{g(\rho_a - \rho)h}{\rho_a V^2} \tag{2.1}$$

where V, h, and ρ are the mean velocity, thickness and density of the two-dimensional buoyant plume, mixing in an ambient stream of density ρ_a. Subsequent work included further investigation of the rate of spread of the saline effluent which was discharged into a sloping rectangular closed conduit. The rate of spread, was found to depend mainly on the slope α and on the pipe Richardson number, defined by

$$R_{ip} = \frac{D\,g\,(\rho_d - \rho_a)\cos\alpha}{\rho_a V^2} \tag{2.2}$$

where D is the depth of the conduit, ρ_d is the density of the fully mixed discharge and ρ_a is the density of the ambient flow.

In addition, Ellison and Turner presented a simplified model, assuming a parabolic form of the momentum transfer coefficient and a linear variation in vertical density, to investigate the influence of the density difference on the velocity profile. They were able to show that the mass transfer coefficient for the salt, K_s, was influenced much more by the density gradient than was the momentum transfer coefficient K_M. They were then able to represent the ratio

K_s/K_M experimentally as a well defined function of the local Richardson Number

$$R_i = - \frac{g \, \partial\rho/\partial y}{\rho \, (\partial u/\partial y)^2} \qquad (2.3)$$

The work of Jobson (12) and Jobson and Sayre (13) on the vertical mixing of both neutrally buoyant and particulate matter in a two-dimensional turbulent shear flow, provided much of the foundation for this study. In order to determine the vertical mass transfer coefficient for neutrally buoyant dye, Jobson (12,13) introduced certain simplifying assumptions into the convection-diffusion equation. He then integrated this simplified form of the equation and was able to determine experimentally a value for the vertical mass transfer coefficient as a function of depth. In particular the vertical mass transfer coefficient for a neutrally buoyant tracer was found to follow the same parabolic distribution function

$$\frac{E_{My}}{d u_*} = \kappa \eta (1-\eta) \qquad (2.4)$$

as the momentum transfer coefficient. In Eq. 2.4,

E_{My} = the width-averaged vertical mass transfer coefficient

d = depth

u_* = shear velocity

κ = Von Karman's turbulence coefficient

$\eta = y/d$ = normalized vertical position

Finally Jobson's equation (14) for predicting concentration profiles and the accompanying numerical solution was modified for use in the present study.

One important difference in dealing with thermal pollutants as opposed to conservative tracers is that transfer across the boundaries of the system must be considered. In order to determine the boundary conditions for our governing equations, it was necessary to know the rates of heat loss at the boundaries. The literature on heat loss in the environment, especially in relation to heated water bodies, has been growing in both volume and sophistication. Edinger and Geyer (4) linearized the various complex relationships for radiative, conductive and evaporative heat transfer and combined them into a much simpler relationship of the form

$$\phi_n = \frac{K}{\rho C_p}(T_S - T_E) \qquad (2.5)$$

where ϕ_n = net rate of heat exchange (°F-ft./sec.)

K = surface heat exchange coefficient (BTU/ft^2/sec./°F)

T_S = water-surface temperature (°F)

T_E = equilibrium temperature (°F)

Graphs and charts were provided which facilitated the use of this simple concept for predicting heat transfer between bodies of water and the atmosphere. Brady et al. (2) in 1969, made various investigations at actual power plant sites, and further simplified the determination of T_E and K. These simplifications appear to yield results of sufficient accuracy for most practical situations, although they seriously underpredict the case for forced-convection cooling such as occurred in this study. Jobson and Yotsukura (23) recently have investigated the mechanics of heat transfer for both the one and

two-dimensional cases in non-stratified open-channel flows. Their work embodies many of the latest developments of heat transfer in rivers, based on the equation of conservation of thermal energy and the heat transfer relationships at the boundaries. Most recently Ryan (10), has conducted studies of the heat loss from a water surface in a laboratory and presented the results in terms of tabulated values of T_E and K. Unfortunately, however, his experimental conditions apparently differed sufficiently from the ones in the present investigation so that his results are not directly applicable to our situation.

Finally, some studies have been done on the specific problem of introducing a heated effluent at the surface of a flowing ambient stream. However most of these studies concentrated on the near-field mixing zone where jet-type phenomena are dominant. Stolzenbach and Harleman (26) investigated the mixing properties of a surface jet that was introduced at right angles to a flowing ambient stream, but the process was considered only to the point where jet-like behavior ceases. Similarly Motz and Benedict (17) studied surface heated jets in a cross flow, using laboratory data to determine drag and entrainment coefficients, but again their study concentrates on the initial jet mixing zone. Koh and Fan (16) have presented mathematical models for the prediction of temperature distributions in a variety of situations. One of the models is for the case of passive diffusion of a warm surface jet in two-dimensional flow. This can be compared with the prediction model obtained in this study.

Weil (28) investigated the problem of a plume of heated water from a small semi-circular source which was discharged at the local ambient velocity in a turbulent open-channel flow. He was concerned with three gross parameters of the mixing plume: (1) temperatures along the plume axis, (2) plume width, and (3) layer depth, which he presented graphically as functions of flume length. He also presented normalized vertical temperature profiles for some selected runs. He did not make use of the convection-diffusion equation nor did he attempt to formulate a generalized mixing coefficient. In a sense then his work might he considered as a preliminary study to the present project.

Chapter III

ANALYTICAL BACKGROUND

A. Conservation of Heat Equation

The basic equation for this study is the equation of the conservation of energy. The thermal energy equation of fluid mechanics for an incompressible turbulent flow without internal heat sources or sinks, obtained by subtracting the mechanical energy equation from the total energy conservation equation is

$$\underset{(1)}{\frac{\partial T}{\partial t} + u_i \frac{\partial T}{\partial x_i}} = \underset{(2)}{-\frac{\partial}{\partial x_i} \overline{u_i' T'}} + \underset{(3)}{\epsilon_c \frac{\partial^2 T}{\partial x_i \partial x_i}} + \underset{(4)}{\frac{\Phi_T}{\rho C_p}} \qquad (3.1)$$

The various components of Eq. 3.1 are

(1) $\frac{DT}{Dt}$ = rate of change of temperature of fluid particle moving with the flow.

(2) turbulent heat transfer

(3) heat transfer due to conduction

(4) viscous dissipation of mechanical energy into heat.

In Eq. 3.1,

$T(x,y,z,t)$ = temperature averaged over a period just long enough to average out turbulent fluctuations

x_i = distance in the i'th co-ordinate direction

u_i = local flow velocity in the i'th direction, time averaged over a period just long enough to damp out turbulent fluctuations

ρ = mass density of the fluid

ε_c = thermal conductivity coefficient

C_p = specific heat at constant pressure

t = time

ϕ_T = time-averaged viscous dissipation function for turbulent flow.

In the derivation of Eq. 3.1 it is assumed that the variation in ρ, ε_c, C_p and viscosity μ with respect to temperature T is small.

When temperature differences are sufficiently large to create environmental problems, the conduction and dissipation terms in Eq. 3.1 are several orders of magnitude smaller than the other terms, except perhaps in the very last stages of the mixing process. If we then neglect these two terms and introduce the turbulent heat transfer tensor ε_{Tij} by the relationship

$$-\overline{u_i' T'} = \varepsilon_{Tij} \frac{\partial T}{\partial x_j} \tag{3.2}$$

then Eq. 3.1 becomes

$$\frac{\partial T}{\partial t} + u_i \frac{\partial T}{\partial x_i} = \frac{\partial}{\partial x_i}\left(\varepsilon_{Tij} \frac{\partial T}{\partial x_j}\right) \tag{3.3}$$

which has exactly the same form as the convection-diffusion equation for mixing in turbulent flow. Eq. 3.3 can be expressed either in terms of heat or temperature since the two quantities are related by the relationship

$$H = C_p \rho T \tag{3.4}$$

where H = heat per unit volume (BTU/ft.^{3}).

Eq. 3.1 can be written in expanded form as

$$\frac{\partial T}{\partial t} + u\frac{\partial T}{\partial x} + v\frac{\partial T}{\partial y} + \omega\frac{\partial T}{\partial z} = \frac{\partial}{\partial x}\left(\varepsilon_{Tx}\frac{\partial T}{\partial x}\right)$$

$$+\frac{\partial}{\partial y}\left(\varepsilon_{Ty}\frac{\partial T}{\partial y}\right) + \frac{\partial}{\partial z}\left(\varepsilon_{Tz}\frac{\partial T}{\partial z}\right) \qquad (3.5)$$

where x,y,z = space co-ordinates in the longitudinal, vertical and lateral directions

$u,v,w,$ = local time averaged velocities of flow in the $x,y,z,$ directions

ε_{Tx}, ε_{Ty}, ε_{Tz} = local coefficients of turbulent heat transfer in the x,y and z directions.

Fig. 3.1 presents a definition sketch of some of the main flow parameters.

In this experimental study, the flow in the x-direction is approximately two-dimensional , so that a number of simplifications are introduced to reduce the three-dimensional form of Eq. 3.5 to a two-dimensional vertical mixing equation. The turbulent diffusion term in the x-direction reasonably can be assumed to be negligible in comparison to the longitudinal advection term. Near steady-state conditions were achieved in the tests so that even though the ambient temperature rose very slightly with time, the time varying term in Eq. 3.5 was orders of magnitude smaller than the other significant terms. With these simplifications Eq. 3.5 can be written

$$u\frac{\partial T}{\partial x} + v\frac{\partial T}{\partial y} + \omega\frac{\partial T}{\partial z} \approx \frac{\partial}{\partial y}\left(\varepsilon_{Ty}\frac{\partial T}{\partial y}\right) + \frac{\partial}{\partial z}\left(\varepsilon_{Tz}\frac{\partial T}{\partial z}\right) \qquad (3.6)$$

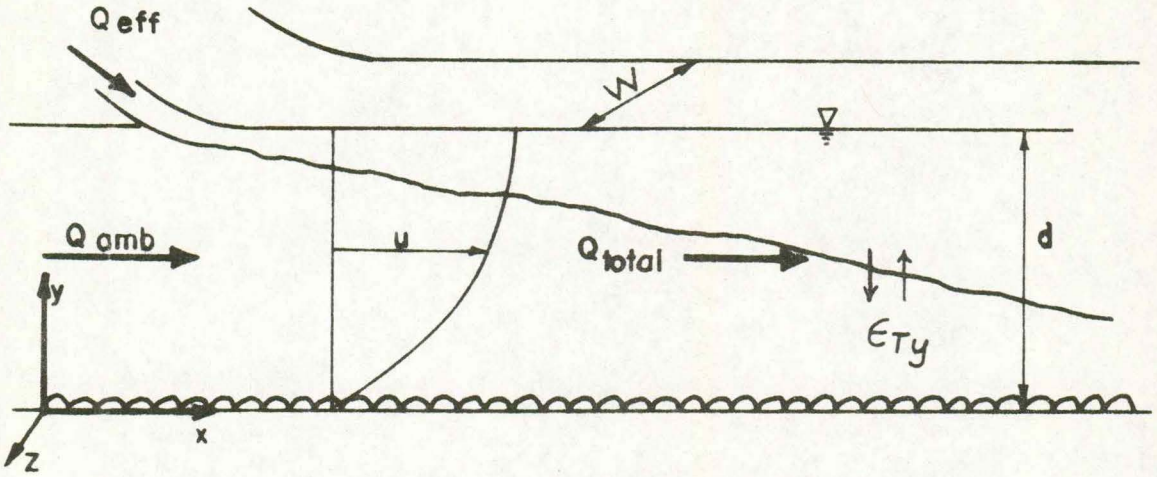

Figure 3.1: Definition Sketch-Flow Parameters.

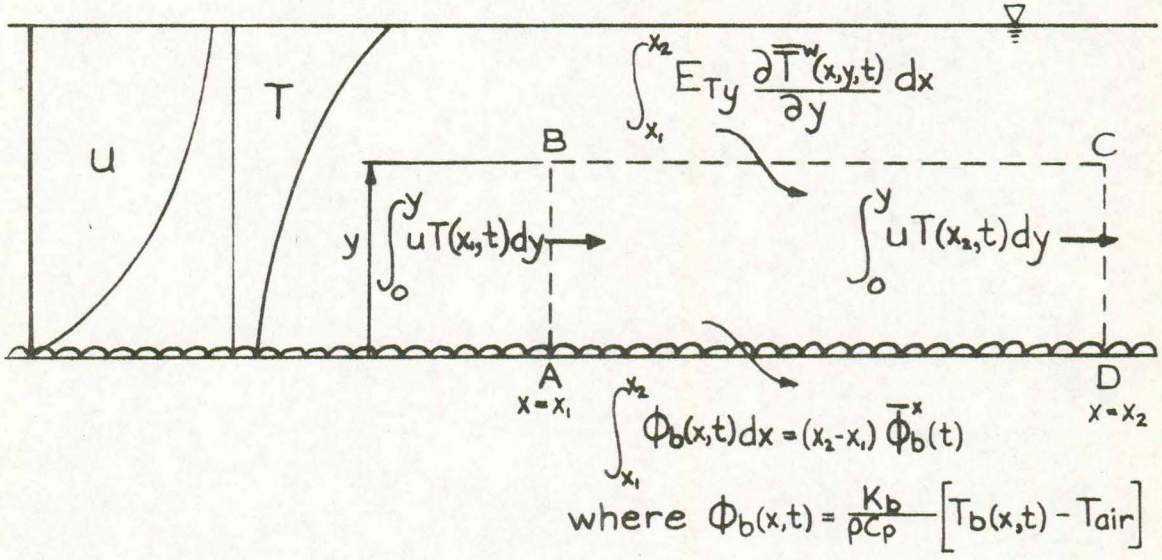

Figure 3.2: Definition Sketch-E_{Ty}.

which when combined with the continuity equation

$$\frac{\partial u}{\partial x} + \frac{\partial v}{\partial y} + \frac{\partial \omega}{\partial z} = 0 \tag{3.7}$$

yields

$$\frac{\partial uT}{\partial x} + \frac{\partial vT}{\partial y} + \frac{\partial \omega T}{\partial z} = \frac{\partial}{\partial y}\left(\varepsilon_{Ty}\frac{\partial T}{\partial y}\right) + \frac{\partial}{\partial z}\left(\varepsilon_{Tz}\frac{\partial T}{\partial z}\right) \tag{3.8}$$

Averaging across the width yields for each term in Eq. 3.8

$$\frac{1}{W}\int_{-W/2}^{W/2}\frac{\partial uT}{\partial x}\,dz = \frac{\partial}{\partial x}\underbrace{\left[\frac{1}{W}\int_{-W/2}^{W/2} uT\,dz\right]}_{\overline{uT}^{W}} = \frac{\partial}{\partial x}\,\overline{uT}^{W} \tag{3.9}$$

$$\frac{1}{W}\int_{-W/2}^{W/2}\frac{\partial vT}{\partial y}\,dz = \frac{\partial}{\partial y}\,\overline{vT}^{W} \tag{3.10}$$

$$\frac{1}{W}\int_{-W/2}^{W/2}\frac{\partial \omega T}{\partial z}\,dz = \frac{1}{W}\,\omega T\Big|_{W/2} - \frac{1}{W}\,\omega T\Big|_{-W/2} = 0 \tag{3.11}$$

since w = 0 at z = ±W/2

$$\frac{1}{W}\int_{-W/2}^{W/2}\frac{\partial}{\partial y}\left(\varepsilon_{Ty}\frac{\partial T}{\partial y}\right)dz = \frac{\partial}{\partial y}\left(\overline{\varepsilon_{Ty}\frac{\partial T}{\partial y}}^{W}\right) \tag{3.12}$$

$$\frac{1}{W}\int_{-W/2}^{W/2}\frac{\partial}{\partial z}\left(\varepsilon_{Tz}\frac{\partial T}{\partial z}\right)dz = \frac{1}{W}\,\varepsilon_{Tz}\frac{\partial T}{\partial z}\Big|_{W/2} - \frac{1}{W}\,\varepsilon_{Tz}\frac{\partial T}{\partial z}\Big|_{-W/2} = \frac{2}{W}\phi_w \tag{3.13}$$

where ϕ_w = local heat flux through a side (°F-ft./sec.). If we then collect the remaining terms, we have

$$\frac{\partial}{\partial x}\,\overline{uT}^{W} = -\frac{\partial}{\partial y}\,\overline{vT}^{W} + \frac{\partial}{\partial y}\left(\overline{\varepsilon_{Ty}\frac{\partial T}{\partial y}}^{W}\right) + \frac{2}{W}\phi_w \tag{3.14}$$

If we write the temperature and vertical velocity in terms of their width-averaged values and the local deviations therefrom, we have

$$V = \overline{V}^w + V' \quad , \text{ but } \quad \overline{V}^w = 0$$
$$T = \overline{T}^w + T'$$

so that using Reynolds' rules of averaging,

$$\overline{VT}^w = \cancel{\overline{V}^w \overline{T}^w}^{\,0} + \cancel{\overline{\overline{V}^w T'}}^{\,0} + \cancel{\overline{V' \overline{T}^w}}^{\,0} + \overline{V'T'}^w$$

By analogy with the analysis of Taylor (25), Elder (5) and Fischer (8) for longitudinal dispersion we assume

$$\overline{V'T'}^w = -E_c \frac{\partial \overline{T}^w}{\partial y} \tag{3.15}$$

where E_c = a width averaged convective vertical dispersion coefficient. If we further assume that

$$\overline{\varepsilon_{Ty} \frac{\partial T}{\partial y}}^w = \overline{\varepsilon_{Ty}}^w \frac{\partial \overline{T}^w}{\partial y} \tag{3.16}$$

which is valid as long as either ε_{Ty} or $\frac{\partial T}{\partial y}$ does not vary appreciably with z, we then have from Eq. 3.14,

$$\frac{\partial}{\partial x} \overline{uT}^w = \frac{\partial}{\partial y}\left[\left(E_c + \overline{\varepsilon_{Ty}}^w\right) \frac{\partial \overline{T}^w}{\partial y}\right] + \frac{2}{w} \phi_w \tag{3.17}$$

from which we can define

$$E_{Ty} = E_c + \overline{\varepsilon_{Ty}}^w \tag{3.18}$$

as an overall vertical mixing coefficient.

The boundary conditions for the flume can be expressed as:

y = d(surface):

$$\left.\begin{aligned} \phi_s = -\varepsilon_{Ty}\frac{\partial T}{\partial y} = \frac{K}{\rho C_p}(T_S - T_E) \\ V = 0 \end{aligned}\right\} \qquad (3.19)$$

y = 0(bottom):

$$\left.\begin{aligned} \phi_b = \varepsilon_{Ty}\frac{\partial T}{\partial y} = \frac{K_b}{\rho C_p}(T_b - T_{air}) \\ u, v, w = 0 \end{aligned}\right\} \qquad (3.20)$$

z = $\pm$W/2(sides):

$$\left.\begin{aligned} \phi_w = -\varepsilon_{Tz}\frac{\partial T}{\partial z} = \pm\frac{K_w}{\rho C_p}(T_w - T_{air}) \\ u, v, w = 0 \end{aligned}\right\} \qquad (3.21)$$

where,

W = flume width (ft.)

d = Flow depth (ft.)

T_{air} = air temperature (°F)

T_S = water surface temperature (°F)

T_w = effective temperature near flume wall (°F)

T_b = effective temperature near flume bottom (°F)

K_w = overall coefficient of heat transfer for flume wall (BTU/(sec.-ft.^{2}-°F))

K_b = overall coefficient of heat transfer for flume bottom (BTU/(sec.-ft.^{2}-°F))

If we insert Eqs. 3.18 and 3.21 into the width-averaged Eq. 3.17 we obtain,

$$\frac{\partial}{\partial x}\overline{uT}^{w} = \frac{\partial}{\partial y}\left(E_{Ty}\frac{\partial \overline{T}^{w}}{\partial y}\right) - \frac{2K_w}{w\rho C_p}\left[T_w(y) - T_{air}\right] \qquad (3.22)$$

Computations indicated that heat losses through the sides were small compared to the other heat loss terms, so that Eq. 3.22 becomes

$$\frac{\partial}{\partial x}\overline{uT}^{w} = \frac{\partial}{\partial y}\left(E_{Ty}\frac{\partial \overline{T}^{w}}{\partial y}\right) \qquad (3.23)$$

Eq. 3.23 can now be integrated from 0 to y, so that using the appropriate boundary condition we have

$$\frac{\partial}{\partial x}\int_o^y \overline{uT}^{w} dy = E_{Ty}\left.\frac{\partial \overline{T}^{w}}{\partial y}\right|_y - \frac{K_b}{\rho C_p}\left(\overline{T}_b^{w} - T_{air}\right) \qquad (3.24a)$$

or,

$$E_{Ty}(y) = \frac{\frac{\partial}{\partial x}\int_o^y \overline{uT}^{w} dy + \frac{K_b}{\rho C_p}\left(\overline{T}_b^{w} - T_{air}\right)}{\left.\frac{\partial \overline{T}^{w}}{\partial y}\right|_y} \qquad (3.24b)$$

Notice that if the bed heat losses can be considered negligible, then the vertical heat transfer coefficient becomes

$$E_{Ty}(y) = \frac{\frac{\partial}{\partial x}\int_o^y \overline{uT}^{w} dy}{\left.\frac{\partial \overline{T}^{w}}{\partial y}\right|_y} \qquad (3.25)$$

Eq. 3.25 was the working equation for the experimental determination of E_{Ty}. It is to be noted that this is the same equation that was used by Jobson (12,13) in his determination of the vertical mixing coefficient for neutrally buoyant dye.

In the above discussion, the temperature can be taken

from any suitable datum. Ditmars (10) has shown that the equations can be expressed in terms of excess heat using the ambient water temperature as the datum. However in our case, since the variation in ambient temperature along the length of the flume was sometimes of nearly the same order of magnitude as the variation of excess temperature, the temperature was referenced to a constant datum of 0°F unless indicated otherwise.

B. Vertical Heat Transfer Coefficient

To understand the significance of the vertical heat transfer coefficient E_{Ty}, consider the control volume depicted in Fig. 3.2.

A two-dimensional control volume ABCD is portrayed with negligible heat loss assumed to occur through the sides. For flows with vertical mixing the longitudinal heat flux increases from section AB to CD by an amount equal to the vertical flux of heat into the upper surface BC minus the vertical heat flux out of the bottom surface AD. The heat transfer from the top is due to the turbulent diffusion and the secondary flow of the flowing stream. This is proportional to the width-averaged temperature gradient, where the coefficient of proportionality, E_{Ty}, has been designated the vertical heat transfer coefficient.

For the limiting case of small Richardson numbers, when buoyancy effects are weak, it is reasonable to suppose that E_{Ty} should approach the vertical mass transfer coefficient, E_{My}, for a neutrally buoyant tracer, which was found by Jobson and Sayre (13) to approximately equal the vertical momentum transfer coefficient E_{MOy}.

Sayre (22) and others have shown that in an open-channel flow with a linearly distributed turbulent shear stress,

$$\varepsilon_{Moy} \approx -\frac{\overline{u'v'}}{\frac{du}{dy}} \approx \frac{u_*^2(1 - y/d)}{\frac{du}{dy}} \tag{3.26}$$

where $\overline{u'v'}$ = the covariance of the longitudinal and vertical turbulent velocity fluctuations.

For a logarithmic velocity distribution

$$\frac{du}{dy} = \frac{u_*}{\kappa y} \tag{3.27}$$

substituting Eq. 3.27 into Eq. 3.26 leads to the parabolic distribution function

$$\varepsilon_{Moy} = \kappa u_* d\, \eta(1-\eta) \tag{3.28}$$

If we can assume Reynolds' analogy for well-mixed flows

$$\varepsilon_{Moy} = \varepsilon_{My} \approx E_{My} \tag{3.29}$$

then Eqs. 3.28 and 3.29 give limiting relations for the case of weak buoyancy effects. In our experimental flume we had nearly two-dimensional flow, so that using width-averaged values we obtain

$$\frac{E_{Ty}}{u_* d} = \kappa \eta (1-\eta) \tag{3.30}$$

and

$$\frac{\overline{E_{Ty}}^{d}}{u_* d} = \frac{\kappa}{6} \tag{3.31}$$

for the limiting case of weak buoyancy effects.

C. Bulk Mixing Coefficient

If the case of a neutrally buoyant dye represents a limiting case for thermal mixing, it should be possible to utilize some of the results from previous mixing studies. If we apply assumptions necessary to reduce Eq. 3.23 to the classical diffusion equation, local velocities are replaced by average velocities and variable mixing coefficients are assumed to be constant so that we have

$$U \frac{\partial \bar{T}^w}{\partial x} = K_y \frac{\partial^2 \bar{T}^w}{\partial y^2} \tag{3.32}$$

This equation has the same form as that for transverse mixing of a neutrally-buoyant substance in a one-dimensional stream

$$U \frac{\partial C}{\partial x} = K_z \frac{\partial^2 C}{\partial z^2} \tag{3.33}$$

where C = concentration.

Using Eq. 3.33 and the reflection principle at the boundaries, Sayre, as shown in Fig. 3.3, (23) has expressed the degree of transverse mixing C_{min}/C_{max} as a function of dimensionless length downstream from a source located at one of the banks.

In our experimental flume, values of $(T_{max} - T_{amb})$, $(T_{min} - T_{amb})$, U, W, the width of the flume, and X, the distance downstream from the spreader, were known for measured cross sections, so that by comparison with the above analysis, the determination of a bulk vertical mixing coefficient Ky is possible. It should be noted that using the analogy of transverse mixing for a neutrally buoyant dye suggests that the parameter Ky will only be directly applicable

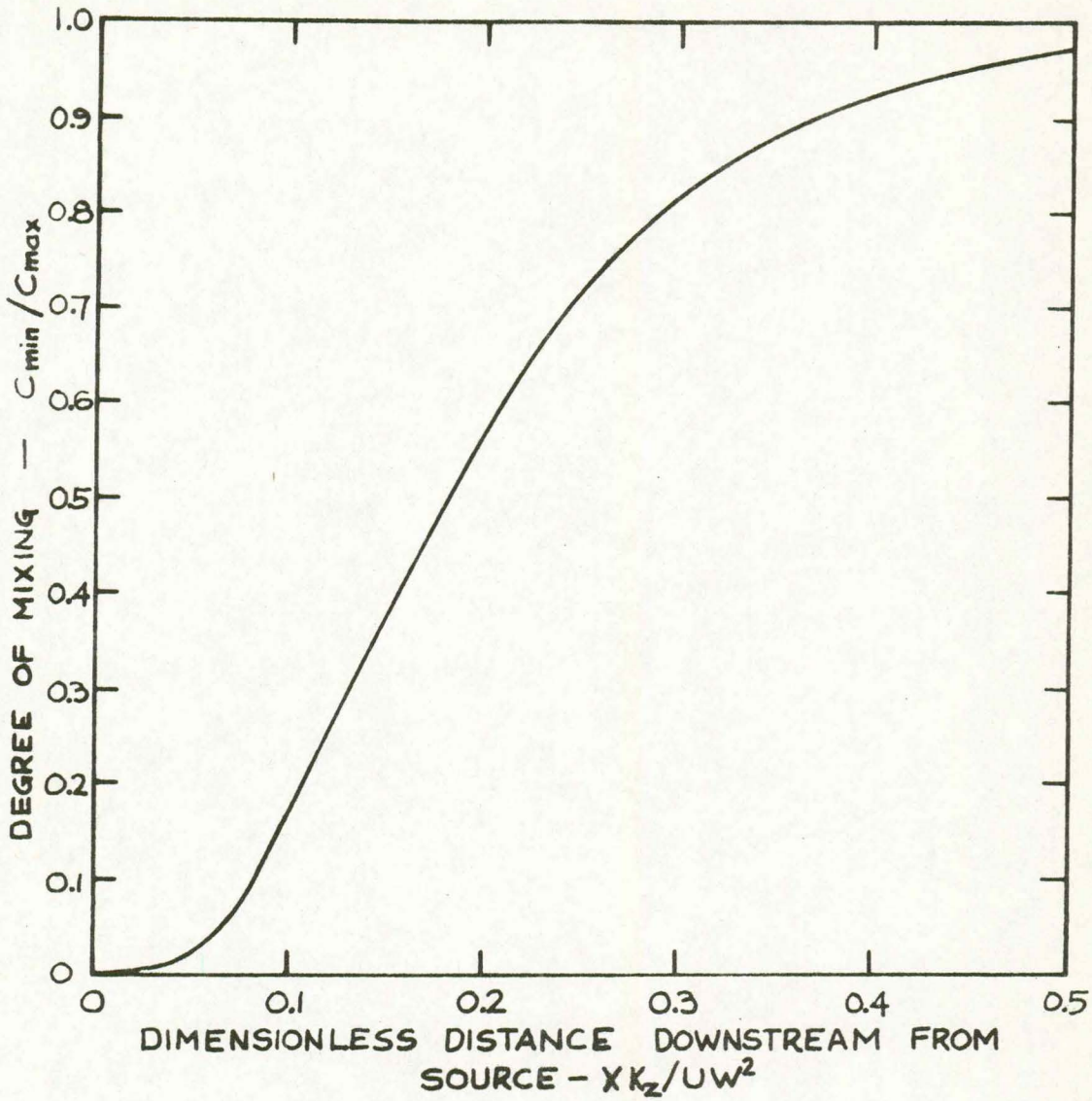

Figure 3.3: Transverse Mixing for a Source at One Bank.

to the well-mixed case. Stratified or partially-stratified flows would not be expected to conform to this analogy. Also, use of the reflection formula implies that $\frac{\partial T}{\partial y} = 0$ at the boundaries, and while this is not strictly true when there is heat loss, it is a reasonable approximation for the cases where rapid mixing occurs.

D. Richardson Number

In order to express the tendency for vertical mixing to occur at a point, a local parameter that is often used is the Richardson number

$$R_i = -\frac{g \frac{\partial \rho}{\partial y}}{\rho \left(\frac{\partial u}{\partial y}\right)^2} \tag{3.34}$$

The significance of the Richardson number is that it is proportional to the density gradient, which represents the tendency to dampen vertical turbulence, and inversely proportional to the square of the velocity gradient which is an indicator of the tendency to generate turbulence. More specifically Harleman (9) has shown that the time rate of increase of potential energy per unit volume is

$$g E_y \frac{\partial \rho}{\partial y} \tag{3.35}$$

where

$$E_y = -\frac{\overline{v'\rho'}}{\partial \rho / \partial y} \tag{3.36}$$

and if it can be assumed that this energy increase is supplied from the mean horizontal motion U, then the rate at which kinetic energy is lost from the mean motion per unit volume is given as

$$\rho \varepsilon_y \left(\frac{\partial u}{\partial y}\right)^2 \tag{3.37}$$

where

$$\varepsilon_y = -\frac{\rho \overline{u'v'}}{\rho \partial u/\partial y} \tag{3.38}$$

The Richardson number is then the ratio of the time rate of increase of potential energy per unit volume (Eq. 3.35) divided by the rate at which kinetic energy is lost from the mean motion per unit volume (Eq. 3.37). Thus at high values of R_i the flow tends to become stratified, whereas at low values of R_i turbulent mixing tends to occur.

E. Densimetric Froude Number

From the definition of the Richardson number, an overall mixing parameter for a cross section located at X can be formulated as follows

$$R_{ix} = \frac{g \Delta \rho_x d^2}{\rho_b U^2} = \frac{1}{F_{DX}^2} \tag{3.39}$$

or

$$F_{DX} = \frac{U}{\sqrt{g d \frac{\Delta \rho_x}{\rho_b}}} \tag{3.40}$$

Therefore a gross Richardson number for the cross section is equal to the inverse of the square of the gross densimetric Froude number, F_{DX}, where $\Delta\rho_x$ = difference between the density ρ_b at the bottom (η = .08) and top (η = .96) for the cross section at X.

While F_{DX} is a useful parameter of the mixing tendency at any cross section, a parameter that describes the initial mixing tendency for a given experiment is the initial densimetric Froude number,

$$F_{DO} = \frac{U}{\sqrt{gd\,\frac{\Delta\rho}{\rho_a}}} \tag{3.41}$$

where $\Delta\rho$ = density difference between the ambient and effluent fluids.

Notice that Eq. 3.41 is a densimetric Froude number related to the total flow rather than merely being a source densimetric Froude number related only to the heated effluent. Thus while F_{DO} characterizes the flow initially in its tendency to mix, F_{DX} is a parameter that can be applied to any subsequent cross section.

F. Equation of Motion

The Reynolds-averaged equation of motion for turbulent flow with variable-density can be written,

$$\rho\,\frac{\partial \bar{u}_i}{\partial t} + \rho\,\bar{u}_j\,\frac{\partial \bar{u}_i}{\partial x_j} = \bar{F}_i - \frac{\partial p}{\partial x_i} - \rho\,\frac{\partial}{\partial x_j}\,\overline{u_i' v_j'} + \mu\,\frac{\partial^2 \bar{u}_i}{\partial x_i \partial x_i} \tag{3.42}$$

where $\bar{F}_i$ = body force in the i'th direction

p = pressure

μ = dynamic viscosity

and the quantities with bars are time-averaged to eliminate turbulent fluctuations.

The equation of motion, which deals directly with forces and their resulting motion, can be used to investigate the influence of

density gradients upon the velocity field. The following analysis closely parallels that of Ellison and Turner (7) for a rectangular conduit. A key assumption of theirs, which is also used here, is that the density gradient does not affect ε_{MO}, so that the parabolic distribution of ε_{MO} applies. If also the Boussinesq approximation is made, in which small changes in fluid density are assumed not to affect the inertia of a fluid element so that $\rho = \rho_a$ = constant in the inertia terms, but do affect the submerged weight of the fluid, then the two-dimensional equation for steady uniform flow in the x-direction reduces to

$$0 = \rho(y) g S - \rho_a \frac{d\overline{u'v'}}{dy} + \mu \frac{d^2\bar{u}}{dy^2} \tag{3.43}$$

For the idealized case where the density decreases linearly from ρ_a at the bottom to $(\rho_a - \Delta\rho)$ at the surface, so that

$$\rho(y) = \rho_a \left[1 - \frac{\Delta\rho}{\rho_a} \frac{y}{d}\right] \tag{3.44}$$

integrating Eq. 3.43 with respect to y yields,

$$C_1 = \rho_a g S \left[y - \frac{1}{2} \frac{\Delta\rho}{\rho_a} \frac{y^2}{d}\right] - \rho_a \overline{u'v'} + \mu \frac{d\bar{u}}{dy} \tag{3.45}$$

where C_1 = a constant of integration. The boundary conditions at $y = 0$, $\overline{u'v'} = 0$ and $\mu \frac{d\bar{u}}{dy} = (\tau_{xy})_o$ yield $C_1 = \tau_o$. Also, by definition $\overline{u'v'} = -\varepsilon_{MO} \frac{d\bar{u}}{dy}$ so that Eq. 3.45 becomes

$$(\nu + \varepsilon_{MO}) \frac{d\bar{u}}{dy} = \frac{(\tau_{xy})_o}{\rho_a} - g S \left[y - \frac{1}{2} \frac{\Delta\rho}{\rho_a} \frac{y^2}{d}\right] \tag{3.46}$$

For turbulent flow, away from the boundaries $\nu << \varepsilon_{MO}$, and also $\frac{(\tau_{xy})_o}{\rho_a} = u_*^2 = gSd$ so that Eq. 3.46 becomes

$$\frac{d\bar{u}}{dy} = \frac{u_*^2}{\varepsilon_{MO}}\left[1 - \frac{y}{d} + \frac{1}{2}\frac{\Delta\rho}{\rho_a}\left(\frac{y}{d}\right)^2\right] \tag{3.47}$$

Eq. 3.47 upon integration yields a velocity distribution of the form

$$\frac{U-\bar{U}}{u_*/K} = \ln\eta + 1 - \frac{\Delta\rho}{2\rho_a}\left[\eta + \ln(1-\eta) + \frac{1}{2}\right] \tag{3.48}$$

Eq. 3.48 indicates that as $\frac{\Delta\rho}{\rho_a}$ increases there will be a tendency for the velocities in the upper depths to increase slightly, with a corresponding decrease in the lower depth velocities. This phenomenon will be most noticeable in flows where $\frac{\Delta\rho}{\rho_a}$ is large and the average velocity is relatively low.

The above analysis is only a preliminary investigation of the modification of the velocity profile by the density gradient. The mathematical model presented is a very simple one and three-dimensional effects have been ignored. It is interesting to compare the above results with those of Monin and Obukov as reported by Turner (27). They considered the atmospheric boundary layer, and using the energy equation for turbulent flow they determined that for the stable case the velocities in the upper heights would also tend to increase.

Chapter IV

DESCRIPTION OF APPARATUS AND EXPERIMENTS

A. Experimental Apparatus

Figs. 4.1 and 4.2 present overall views of the experimental apparatus which was located on the second and third floors of the Iowa Institute of Hydraulic Research. The main components consisted of the experimental flume, the hot water system, the temperature measuring system and the velocity measuring equipment. These are described in some detail below.

1. Experimental Flume: The flume is 85 ft. long, 2.5 ft. wide, and has 10-in.-high side walls. The side walls are made of 1/4-in.-thick glass, as is the bottom. Overlaying the glass bottom was another 1/4 in. plate of glass, which was coated with closely packed gravel fixed to the glass with epoxy paint. The gravel was sifted between sieves having openings of 0.223 in. and 0.265 in. and thus had a geometric mean diameter of 0.243 in. The suspension system supporting the flume is equipped with a motor drive that ennables it to be set at any desired slope between +0.03 and -0.0013.

The flow depth could not be considered as the distance from the water surface to the top of the glass, but was somewhat less because of the presence of the gravel layer. To determine the depth correction Δd, the effective roughness height k_s was calculated using

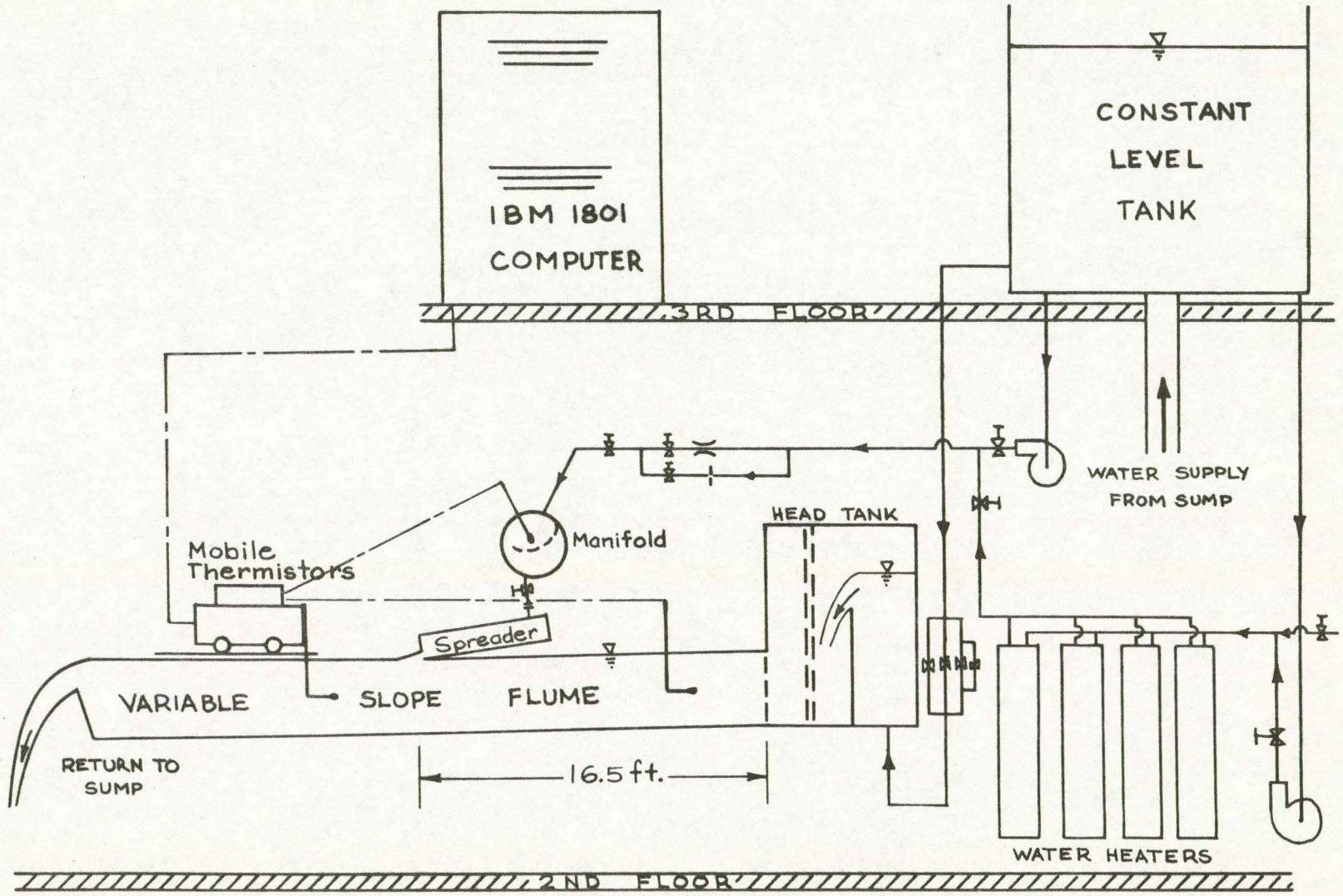

Figure 4.1: General Sketch of Experimental Apparatus.

standard logarithmic resistance and velocity distribution laws and hydraulic parameters measured in uniform flows. The gravel bottom was treated as a rough boundary and the side walls as a hydrodynamically smooth boundary. Computations were made for different values of Δd and the computed values of k_s for each trial were compared with the actual particle size, which was assumed to be $k_s = D_{75}$. In this manner a depth correction of $\Delta d = 0.017$ ft. was established.

Flow into the head tank is regulated by four valves situated in parallel lines, their sizes being 12 in., 6 in., 3 in., and 1 in. A 90° vee-notch weir located in the head tank measured the ambient flow discharge. A tailgate for adjusting the flow depth is located at the downstream end of the flume.

2. Hot Water System: Hot water was provided by four 75,000 BTU/hr. natural-gas heaters connected in parallel. When greater amounts of heat were required, these heaters could be coupled with five additional heaters of the same type located on the first floor. Near the flume head tank the hot-water flow was mixed with the cold water at a tee-joint. The mixed flow was measured by one of two flow metering devices, either a 1-in. venturi meter located in the main 2-in. pipeline or a 0.4-in. orifice meter located in a parallel 1-in. pipeline. The water next passed to a manifold header pipe, located immediately above and at right angles to the flume. The manifold had an internal deflecting baffle plate and five outlets. Each outlet was equipped with its own regulating valve and orifice meter to ensure a uniform distribution of heated effluent flow across

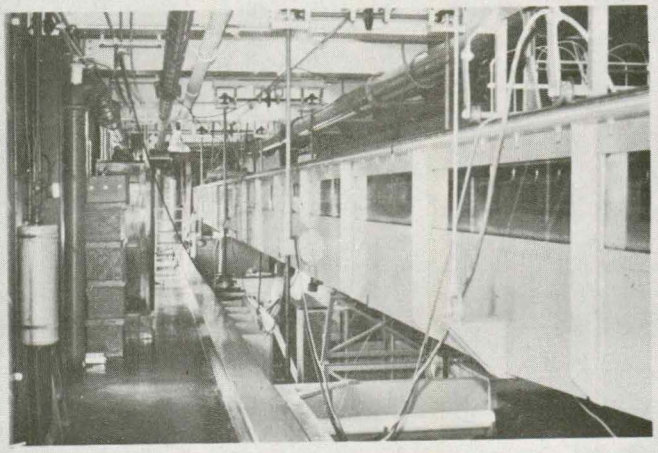

Fig. 4.2. Experimental Flume.

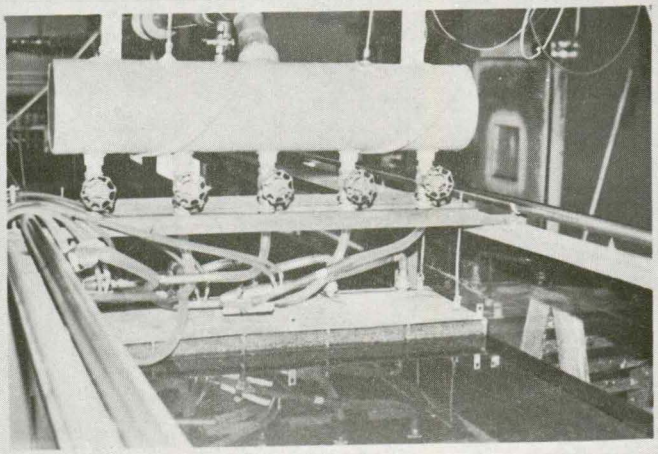

Fig. 4.3. Hot Water Manifold and Spreader.

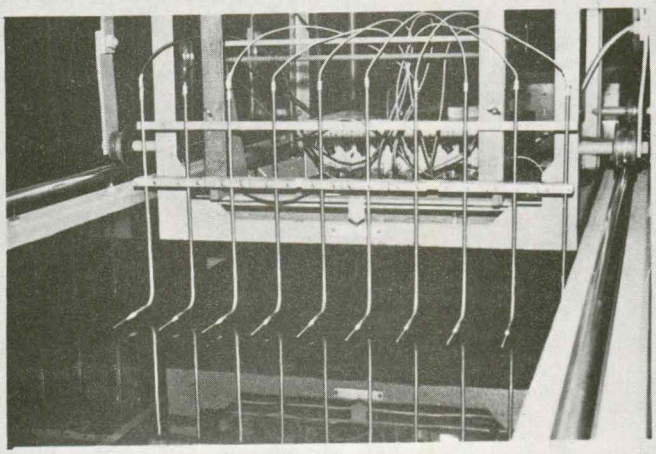

Fig. 4.4. Mobile Thermistors.

the flume. Finally the heated water passed via flexible rubber hoses to a spreader located at the flume water surface. The spreader was filled with a plastic gauze-like material and was subdivided into five sections. The bottom of the spreader sloped gradually into the water surface, and the entire spreader could be raised and lowered so that different entrance conditions could be obtained (Fig. 4.3).

3. Temperature Measuring System: The twelve thermistors used to record temperatures were of type 44004 manufactured by Yellow Springs Instrument Company. One thermistor recorded the upstream ambient temperature, another recorded the heated effluent temperature in the manifold and the remaining ten thermistors were located on a mobile carriage which was capable of traversing the entire length of the flume. The ten thermistors were arranged as a horizontal rake, with the units positioned at the mid points of ten equal increments of flume width (Fig. 4.4).

All twelve thermistors were connected to a 12-channel electronic thermistor resistance indicator interfaced with the Institute's IBM 1801 Data Acquisition System. Each thermistor was incorporated as one resistor of a Wheatstone bridge, the bridge output voltage being -5 mv. to +5 mv. All of the bridges were supplied by a common 5-volt power supply, and the output from each bridge was fed to a relay multiplexer which time-shared a differential amplifier having a voltage gain of 500. The multiplexer and amplifier are integral parts of the IBM 1801 Data Acquisition System. The temperature-measuring system had a resolution of about 0.02°F and a time constant of about

0.7 second. Fig. 4.5 is a schematic drawing illustrating the resistance and thermistor-computer interface circuits. Each of the thermistors was connected to one of twelve multiplexer terminals.

Calibration of the thermistors was achieved by placing the thermistors in an insulated calibration box which was filled with water at the desired temperature. The water was maintained at a uniform temperature by constant stirring while readings were taken. Two precision thermometers with a resolution of .02 °F were located in the insulated calibration box. Thermistor readings were taken over an averaging period of 90 secs. during which time each thermometer was read three times. For each temperature measured, the voltage output from the thermistor circuit could be compared with the temperature obtained from the thermometers. This data was then put in a least-squares fitting program and a second-degree polynomial calibration curve was computed for each thermistor. The coefficients of the calibration curves were then stored on disk for subsequent use during experimental runs. These curves gave excellent agreement when checked with the computer output from known temperature sources. The thermistors were calibrated at the beginning of the experimental program and checked once more during the progress of the tests. Prior to each experimental run a one-point calibration was in effect made by measuring the temperature of the ambient flow close to the bottom.

4. Velocity Measuring Equipment: A Prandtl-type Pitot tube with a 1/16 in. outside diameter was used to measure velocities. The stagnation and static pressures were coupled by a water-air interface

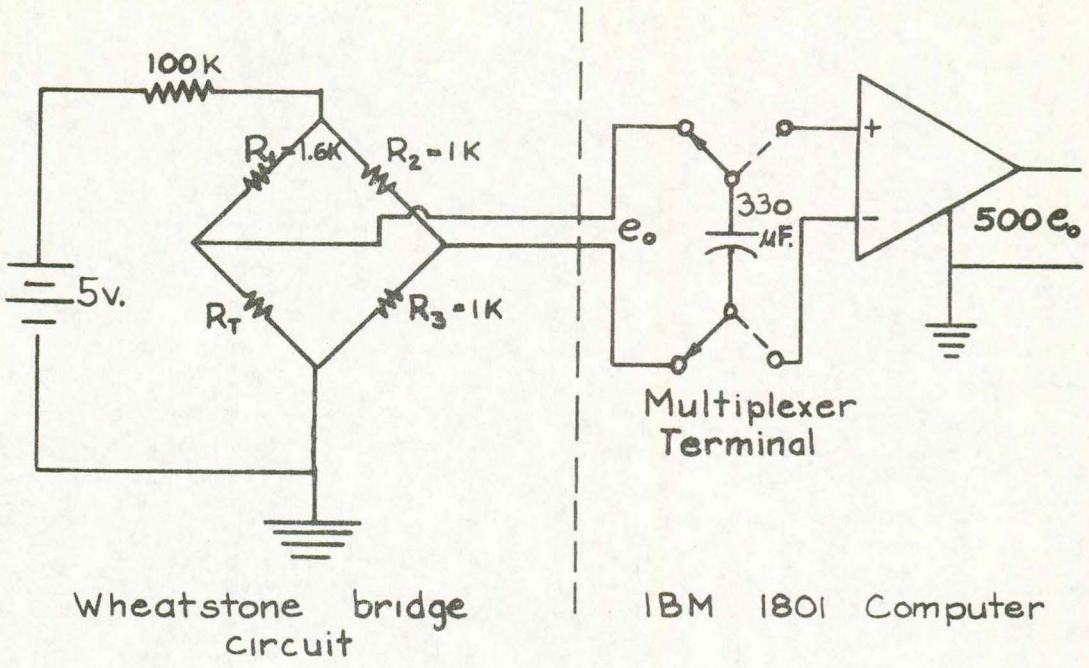

Figure 4.5: Circuitry for Thermistor-Computer Interface.

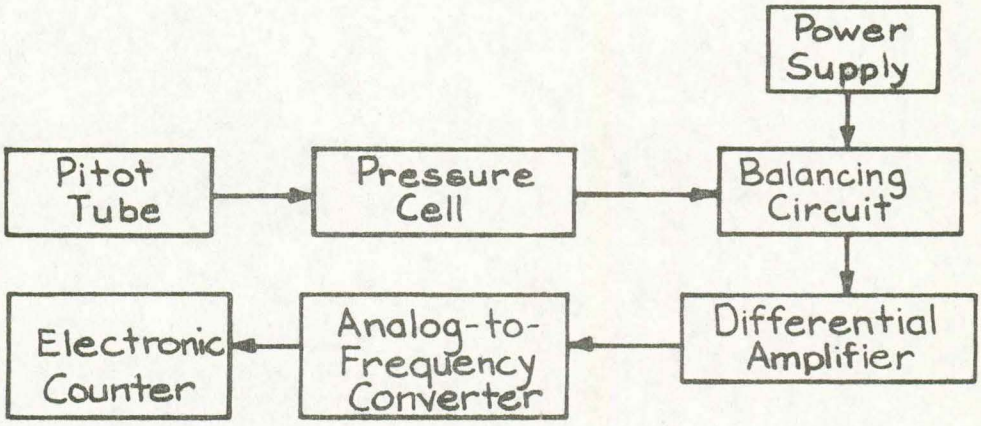

Figure 4.6: Block Diagram of Velocity Measuring System.

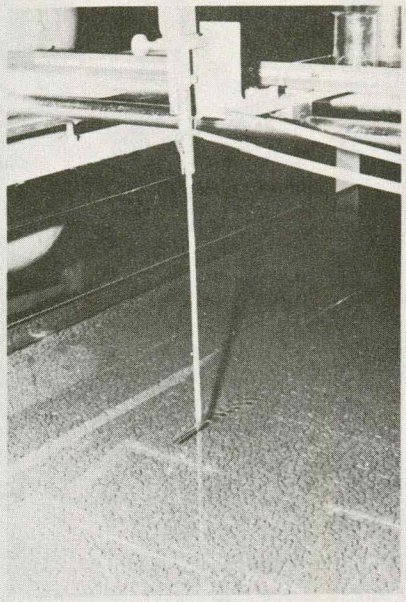

Fig. 4.7. Prandtl-type Pitot Tube.

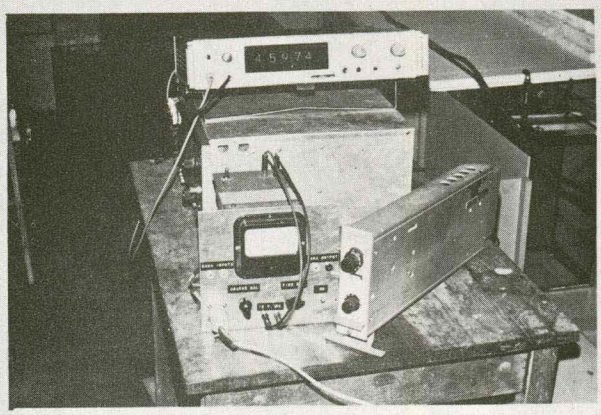

Fig. 4.8. Electronic Velocity Measuring Equipment.

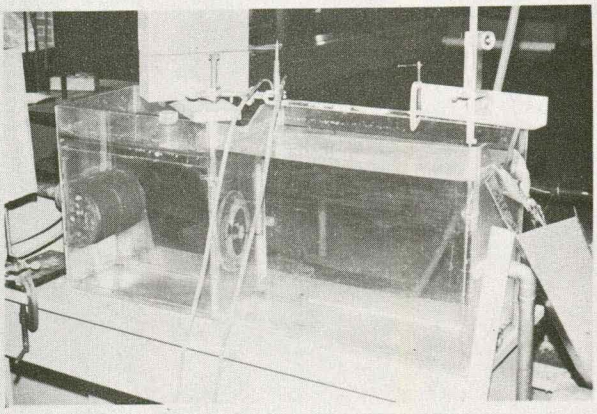

Fig. 4.9. Velocity Calibration Tank.

to a Statham pressure cell, Model PM5-TC, with a maximum range of ± 0.15 psi. The pressure output was amplified by a Dana differential amplifier, Model 2850, and then connected to the analog-to-frequency converter, in a Model Old Gold hot-wire anemometer, manufactured by the Hubbard Instrument Company. The output of the converter was connected to an electronic counter, manufactured by the Computer Measurements Company (Model 603A), which provided a digital display proportional to pressure. A block diagram of the velocity measuring system is shown in Fig. 4.6, and Figs. 4.7 and 4.8 show the equipment in more detail.

The water-air interface joining the pitot tube with the pressure transducer was the source of some difficulties. The pressure difference in the air columns was very sensitive to temperature differences, so that the transducer and air columns had to be well insulated. Also the zero reading tended to vary slowly with time, most likely due to gas transfer across the air-water interface. Because of this, the velocity measuring equipment had to have its zero reading checked at frequent intervals.

Calibration of the velocity measuring system was conducted in a special calibration tank shown in Fig. 4.9. This consisted of an enclosed head tank from which water issued through a standard ISA flow nozzle. Nozzles of 1-in. and 2-in. diameter were used. The velocity was found to be essentially uniform across these nozzles. Inlet flow from the constant storage tank was regulated by a valve and the outlet flow was measured volumetrically using a 2000-ml. graduated cylinder and a stopwatch. The pitot tube was located just downstream from the

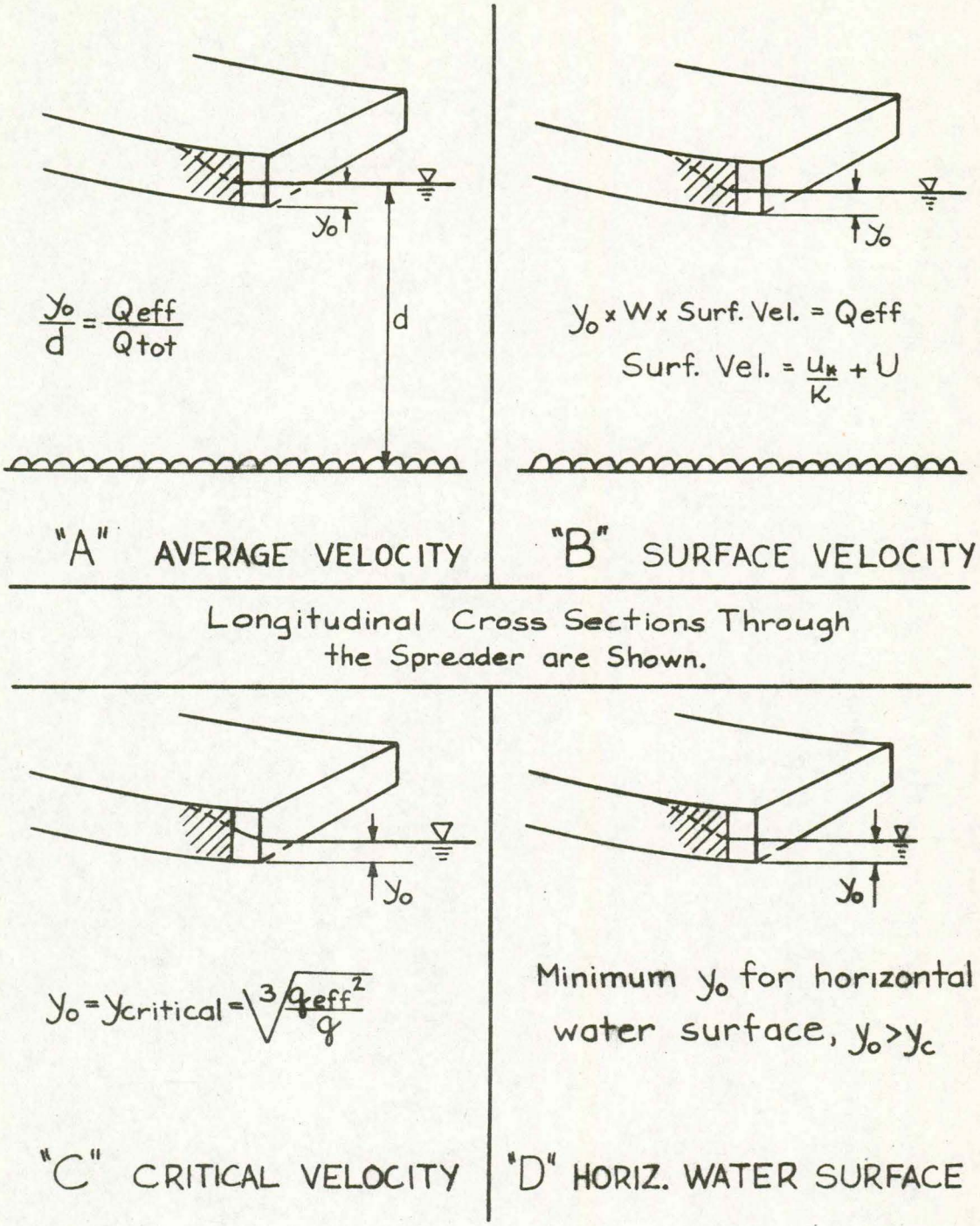

Figure 4.10: Entrance Conditions.

measuring nozzle and was connected to the pressure transducer and accompanying electronic instrumentation in the same way as in the experimental runs. Good reliability could be achieved with velocities of 0.3 f.p.s. and greater, but as the velocity approached 0.1 f.p.s., errors approached ± 10%. For this reason no velocity readings in flows with an average velocity of less than 0.3 f.p.s. were taken.

B. Experimental Procedures

1. Basic Experimental Parameters: A total of 44 experimental test runs was conducted. Average flow velocities ranged from 0.1 f.p.s. to 1.5 f.p.s., while the temperature difference between the hot and cold water varied from 5 to 25 °F. Most runs were conducted at a depth of 0.25 ft., though for some runs the depth was 0.50 ft. The most frequently used discharge ratio (Q effluent/Q total) was 1/10 and for most of the runs the heated effluent was introduced into the flume at the average velocity of the ambient flow. Table A.1 in Appendix A lists the basic parameters for all the experimental runs. The various entrance conditions are depicted schematically in Fig. 4.10.

2. Temperature Measurements: A computer program which governed the operation of the computer during the experimental runs was written and stored on disk. The program could be initiated and terminated from switches located near the flume so that computer operation was completely remote controlled. The thermistor signals were each sampled in rotation about 7 times per second with a running sum kept over a period of 60 seconds. Upon termination of the sampling period, the sum of the signals for each probe was divided to give an

average value and converted to temperatures by the computer, using probe calibration data stored on disk. In addition the temperature differences between heated and ambient flows (ΔT), normalized temperatures ($T_* = \frac{T-T_{amb}}{\Delta T}$), and the average of the ten mobile-thermistor temperatures ($\bar{T}^W$) were calculated. This data was then stored on disk. At the end of an experimental run, this stored data was punched on cards in a format suitable for further computation and processing by the IBM 360/65 System at the University Computer Center.

For each experimental run temperature measurements were taken at from 4 to 8 cross sections downstream from the spreader location. The number and spacing of the cross sections were determined according to the rate of mixing taking place. At each cross section, temperature readings were taken from the top downwards, at vertical locations η = .96, .86, .76, .66, .46, .26 and .08, where $\eta = y/d$ the normalized distance from the bottom. At the uppermost position the thermistors were barely submerged. The last position was the lowest possible, in light of the presence of the gravel bottom. The thermistors were more concentrated in the upper half of the flow due to the greater temperature gradient there.

3. Environmental Measurements: Dry bulb and wet bulb temperature readings in the surrounding air environment were taken before and after each experimental run. The instrument used was a 12 in. sling psychrometer with two thermometers graduated in degrees Fahrenheit. For some of the later runs, psychrometer readings were also taken in the air mass above the water surface between the flume walls.

4. Velocity Measurements: For selected flows, velocity readings were taken across the entire cross section in the reaches where mixing was occurring. Velocity readings were also taken of the ambient flow for the same selected flow conditions. In addition, for some flow conditions, velocity profiles were taken at selected transverse positions at intervals along the flume. In all instances velocity measurements were taken at locations where temperature readings had been taken. A brief tabulation of the velocity measurements which were taken is shown in Table A.2.

Chapter V

PRESENTATION AND REDUCTION OF DATA

This chapter presents the results of the experimental tests. The data is mainly presented in graphical and tabular form, in preparation for the more detailed and integrated analysis and discussion in Chapter VI.

A. Bulk Flow Properties

The previous chapter described the governing parameters for each experimental test run. In addition, there are some derived parameters that are presented in Table A.3 of Appendix A and are briefly described below. In Table A.3 each experimental run is described by the code designation

$$V \;/\; d\text{-}U \;/\; \frac{Q_{tot}}{Q_{eff}} - \Delta T \;/\; ENTRY$$

where V = vertical mixing

d = depth of flow in hundredths of a foot.

U = average velocity in tenths of a foot per second

Q_{tot}/Q_{eff} = ratio of total discharge to effluent discharge

ΔT = temperature difference between heated effluent flow and ambient flow in $^{\circ}F$

ENTRY = letter designation for the entrance condition (see Fig. 4.10).

In Table A.3 all the A and B - entry runs are also designated by symbols which are used in some of the subsequent graphs.

A sidewall correction procedure, as outlined in Ref. 15, was applied to the measured depth and resulted in an effective depth r_b. This depth gave good agreement with Jobson's (12) results on vertical diffusivity for neutrally buoyant dye, which served as a limiting case for well mixed flows, and thus r_b was used in the subsequent analysis.

The shear velocity at the bed was computed using the relation

$$u_* = \sqrt{g r_b S} \tag{5.1}$$

where S = slope of the energy gradient.

The Reynolds number of each flow was computed as follows

$$R_N = \frac{4UR}{\nu} \tag{5.2}$$

where R = hydraulic radius and ν = kinematic viscosity

Although all of the experimental runs were in the fully rough zone as depicted in Fig. 5.1 according to the commonly accepted criterion $u_* k_s/\nu > 100$, the resistance coefficient still appears to be somewhat dependent on the Reynolds number. However, for practical purposes, all flows can be considered to be in the fully rough regime.

B. Velocity Distribution

For some selected typical runs, as noted in Table A.2, Appendix A, velocity readings were taken. Ambient velocities were recorded as well as velocities with the heated effluent present. In this section a velocity correction procedure is described after which the velocity distribution in the ambient flow is considered, and

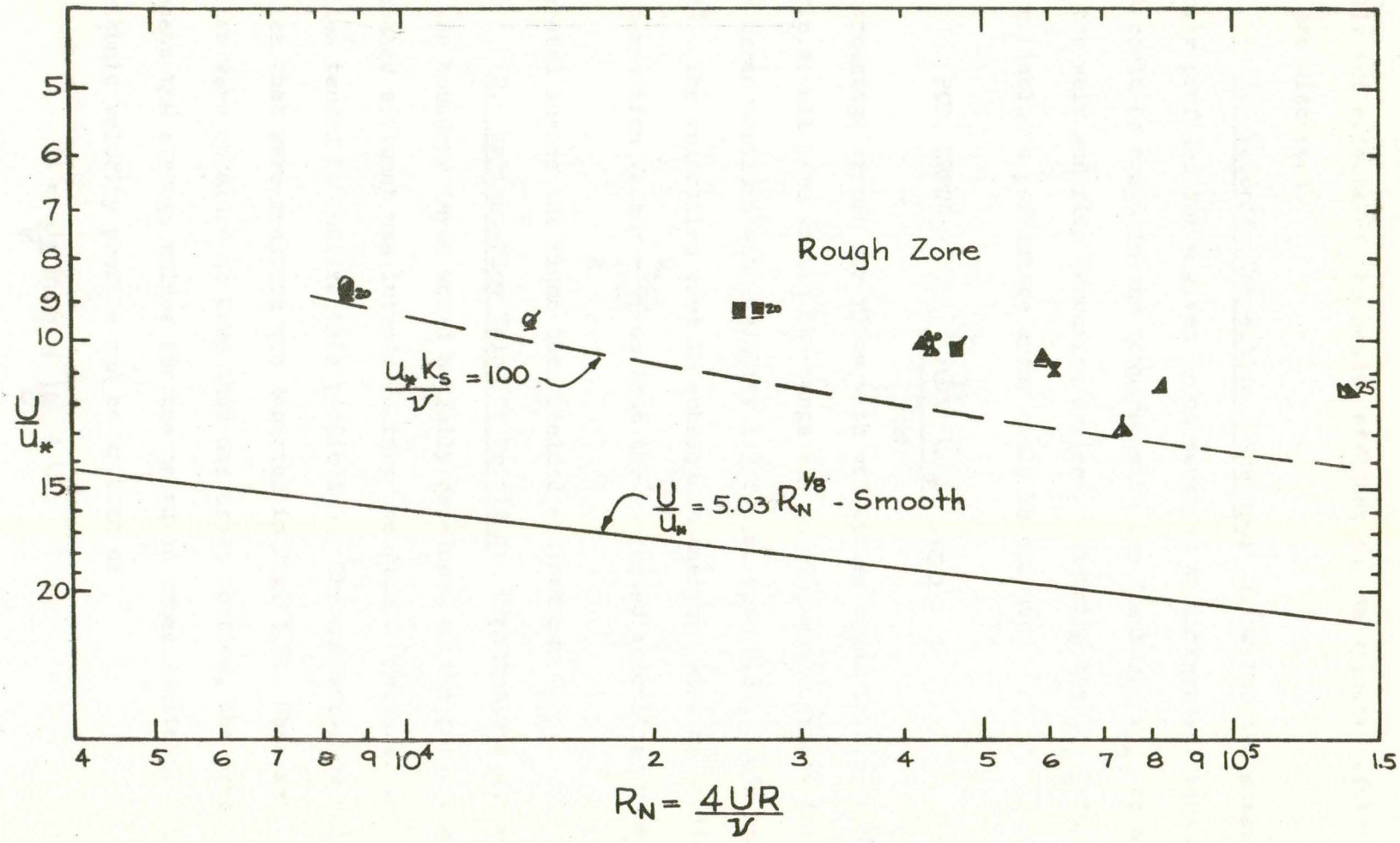

Figure 5.1: Flow Regimes of Experimental Runs.

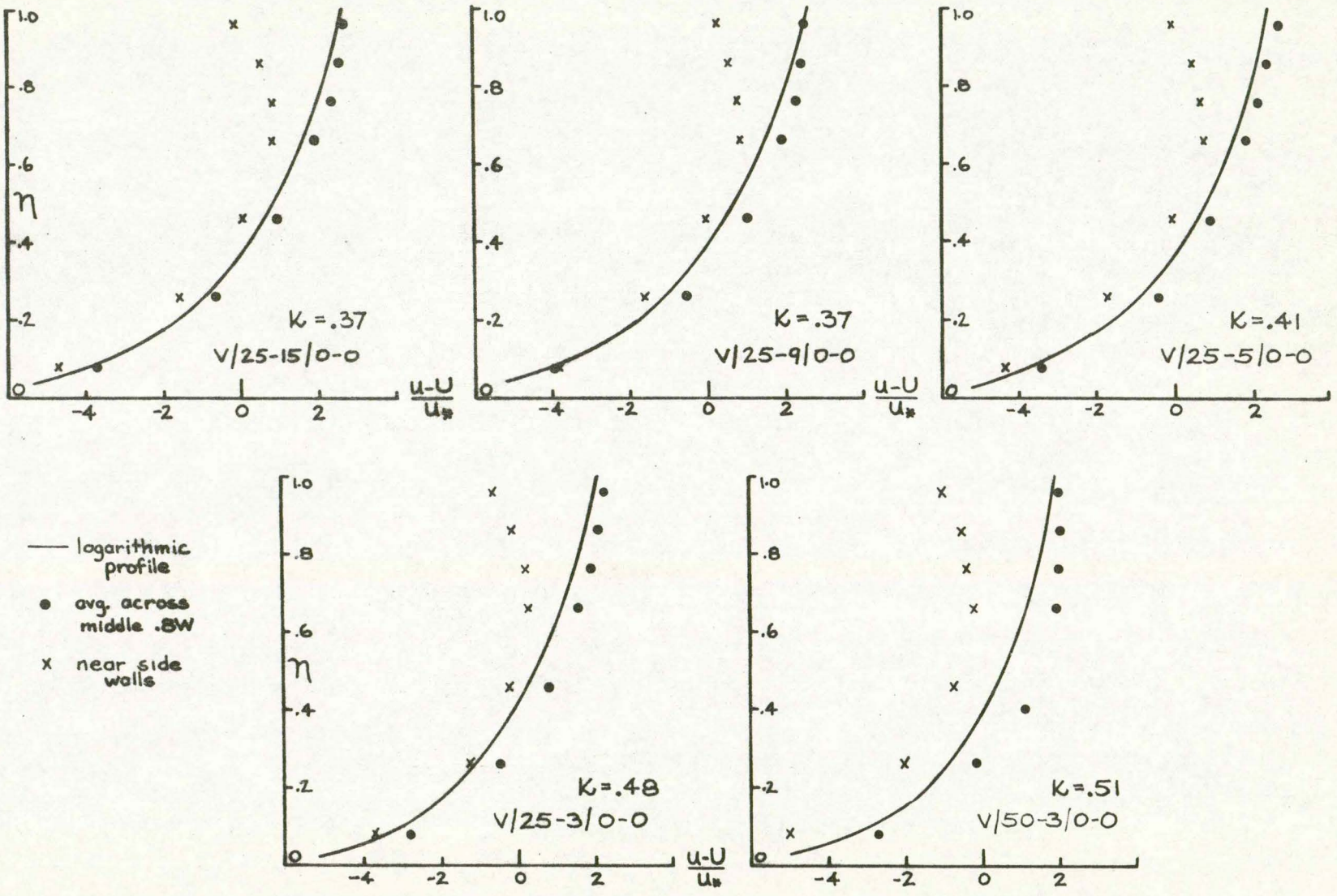

Figure 5.2: Ambient Velocity Profiles.

By plotting u vs. ln. η and obtaining a straight line approximation by linear regression, a value of κ, the Von Karman turbulence coefficient, could be determined from the slope of the line. In this way κ values were obtained from measured velocity profiles. A representative value of κ for the cross section was taken as the average κ value for the middle 8/10 of the flow. It will be noted that the κ value increases as the velocity decreases and/or the depth increases. This phenomenon was accompanied by a progressive increase in the influence of the sidewalls. The increase in the value of κ was likely due to the thicker sidewall boundary layer as the velocity decreased and the depth increased. The logarithmic velocity profile (Eq. 5.4) was plotted for each measured ambient flow in Fig. 5.2. These represented width-averaged values and were thus slightly smaller in magnitude than the middle 8/10 averaged values, because of the retarding effect of the sidewalls. Note that except for the case of depth = 0.5 ft., the shape of the velocity profile in the middle 8/10 of the flow closely approximated the logarithmic profile.

3. Secondary Circulation in the Ambient Flow: A distinct pattern of secondary circulation was indicated by the velocity distribution measurements in the ambient flow. Isovels drawn at cross sections indicated the presence of vertical components of secondary currents, since vertical secondary currents tend to either displace low velocity fluid upward or high velocity fluid downward. The isovel patterns shown in Fig. 5.3 show the helical flow patterns that existed in three of the ambient flows. Notice that for a depth of 0.25 ft. 8

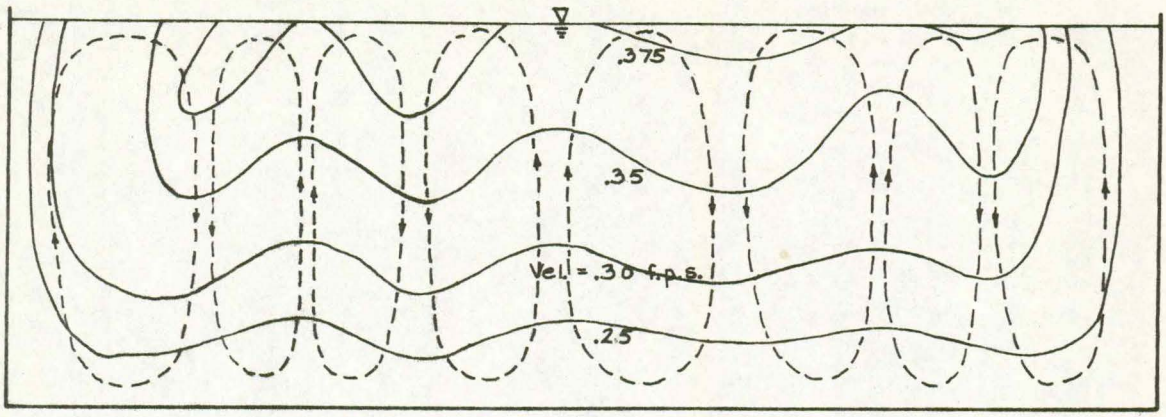

U = 0.3 fps , d = 0.25 ft. , X/d = 50

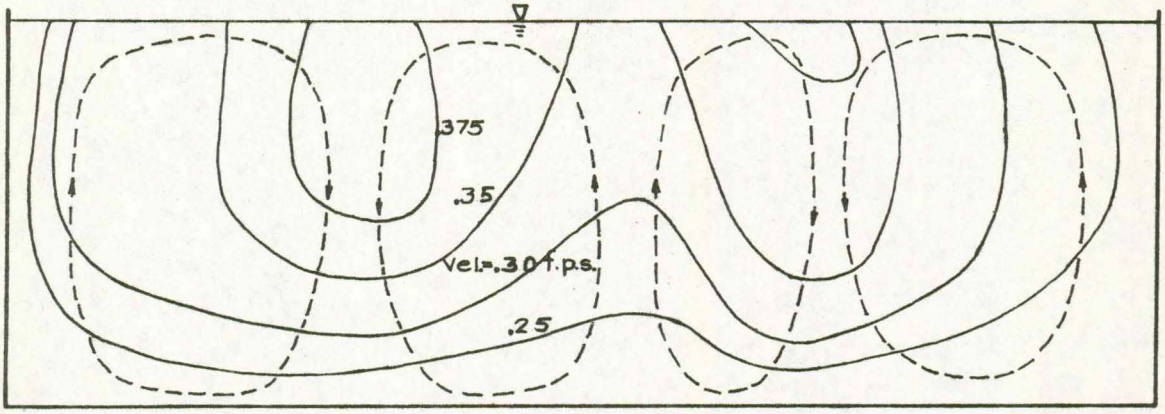

U = 0.3 fps , d = 0.5 ft. , X/d = 45

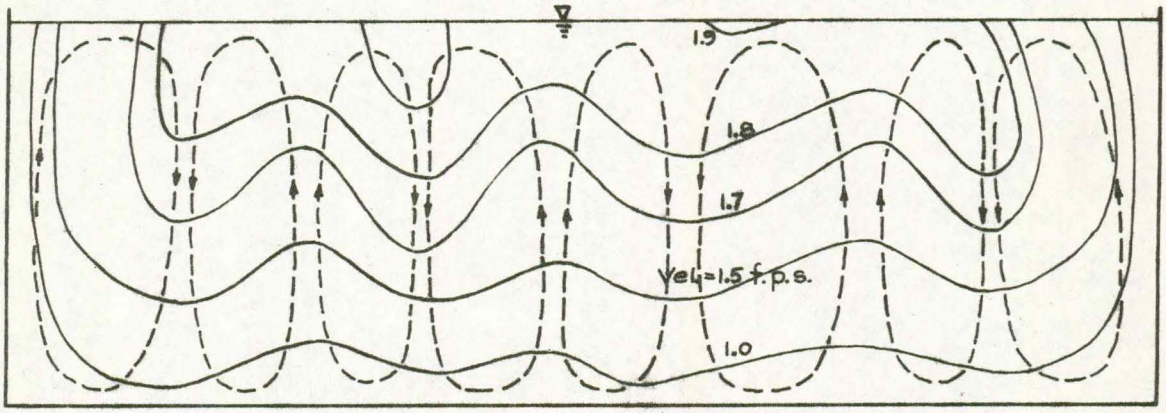

U = 1.5 fps , d = 0.25 ft. , X/d = 20

Figure 5.3: Isovel Patterns Showing Secondary Circulation in Ambient Flows.

cells are present, whereas for a depth of 0.5 ft. 4 cells are present. The cells tend to assume an approximately circular cross section.

4. Influence of the Density Gradient on the Velocity Distribution: The density gradient alters both the longitudinal velocity profiles and the secondary current pattern. These two effects are described below.

(a) Buoyancy Effects: As predicted in the preliminary analysis of Chapter III, the presence of a density gradient should increase the velocities in the upper part of the flow. This phenomenon was indeed observed and was found to be most pronounced for combinations of high temperature differences and low velocity flows. Fig. 5.4 shows the velocity profiles along the flume centerline for three such flows. The dashed lines represent the ambient-flow velocity profiles.

The modification of velocity profiles by buoyancy effects occurred in progressive stages along the flume. Careful inspection of Fig. 5.4 reveals the influence of the entrance condition on the velocity profile near the spreader. Since the effluent flow entered at the average ambient velocity which was somewhat less than the surface velocity, a retarding effect persisted for a short distance downstream from the point of entry. More will be said about the influence of entry conditions in a later section. Also at the higher mixing rates, the upper layer of heated water is increasingly mixed into the ambient flow as one proceeds downstream. This decreases the density gradient and the velocity then reverts back to the logarithmic form as the cause for the difference is removed. Finally, since only

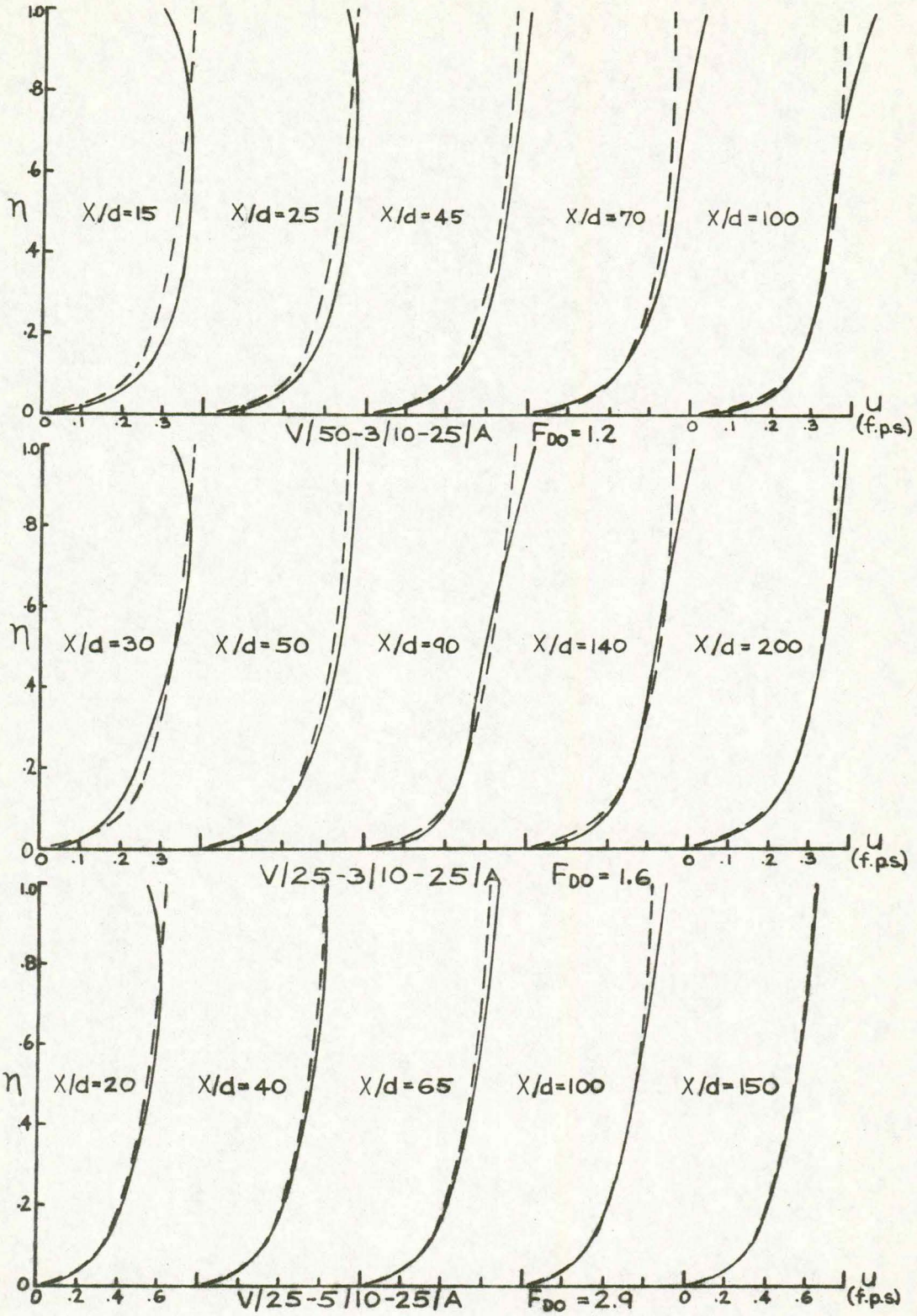

Figure 5.4: Buoyancy Effect on Some Typical Velocity Profiles.

centerline velocity profiles have been presented, the more complex, three-dimensional aspects of this phenomenon are not evident.

(b) Secondary Circulation: The presence of a well defined secondary circulation pattern in the ambient flow was previously described. Fig. 5.5 shows the alteration in secondary currents when 1/10 of the discharge is heated 25 °F higher than the ambient temperature and introduced at the surface. It had been anticipated that a vertical density gradient would reduce the vertical turbulent diffusion. Fig. 5.5 indicates that the secondary flow is also damped, probably because of the barrier to vertical mass transport presented by the density gradient.

5. Influence of the Secondary Circulation on Transverse Temperature Distributions: When the secondary current is strong and the temperature gradient not too large, it is possible for the secondary circulation to alter the temperature field in the flume. The downward movement of the helices tends to move lighter, warmer fluid into the lower depths, while the upward movement carries the denser, colder fluid upwards. This modifies the transverse temperature distribution as shown in Fig. 5.6.

C. Temperature Distribution

In Chapter IV the procedure whereby thermistor readings were averaged, stored on disk and punched out on cards was described. The normalized temperature profiles for each experimental run were then plotted by computer. Fig. 5.7 shows temperature profiles for some typical flow conditions. The tendency for the vertical mixing to be

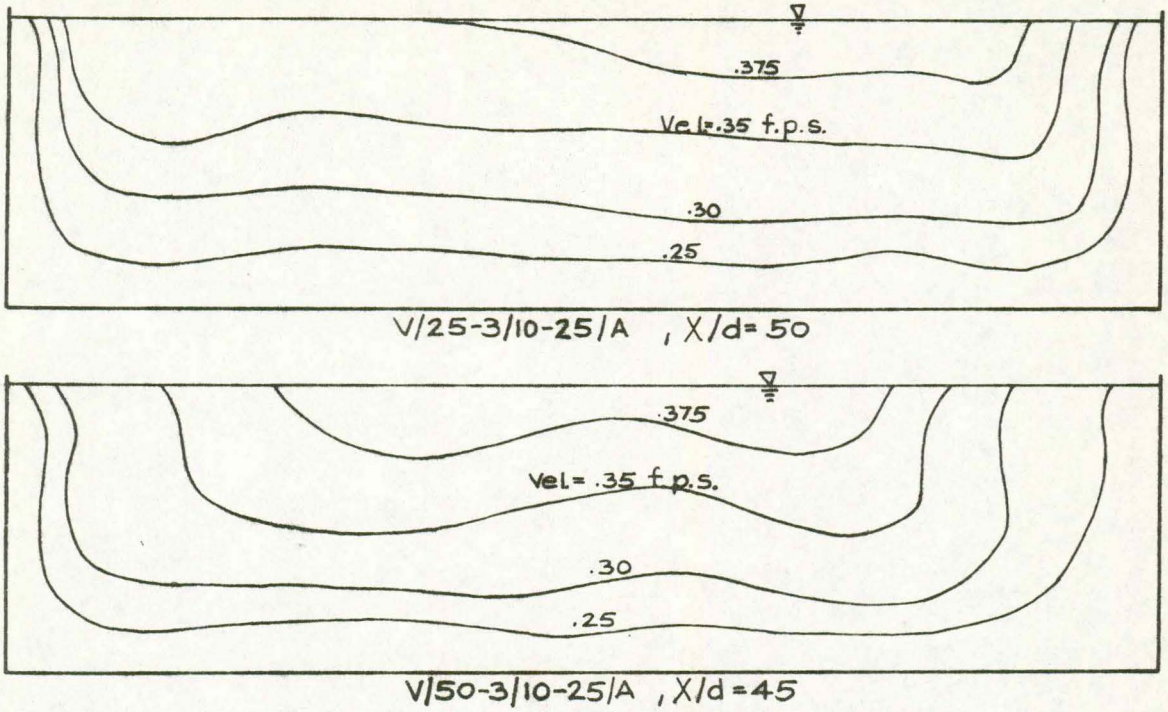

Figure 5.5: Isovel Patterns Showing Modification of Secondary Circulation by Heated Surface Effluents.

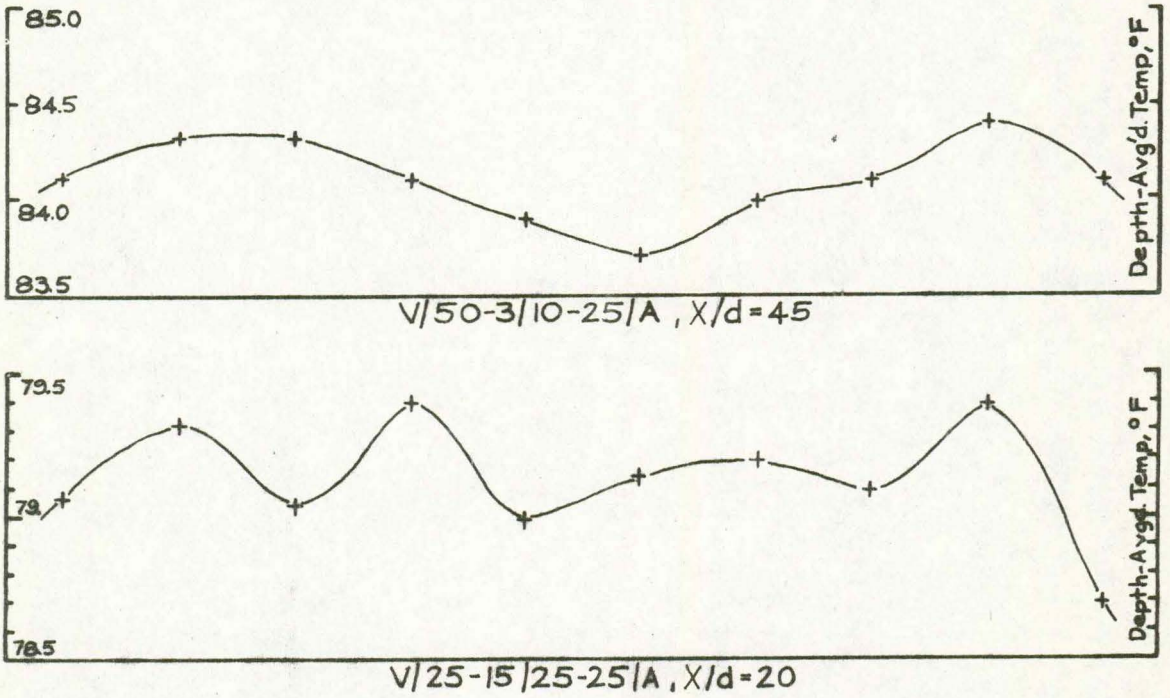

Figure 5.6: The Influence of Secondary Circulation on Transverse Temperature Distributions.

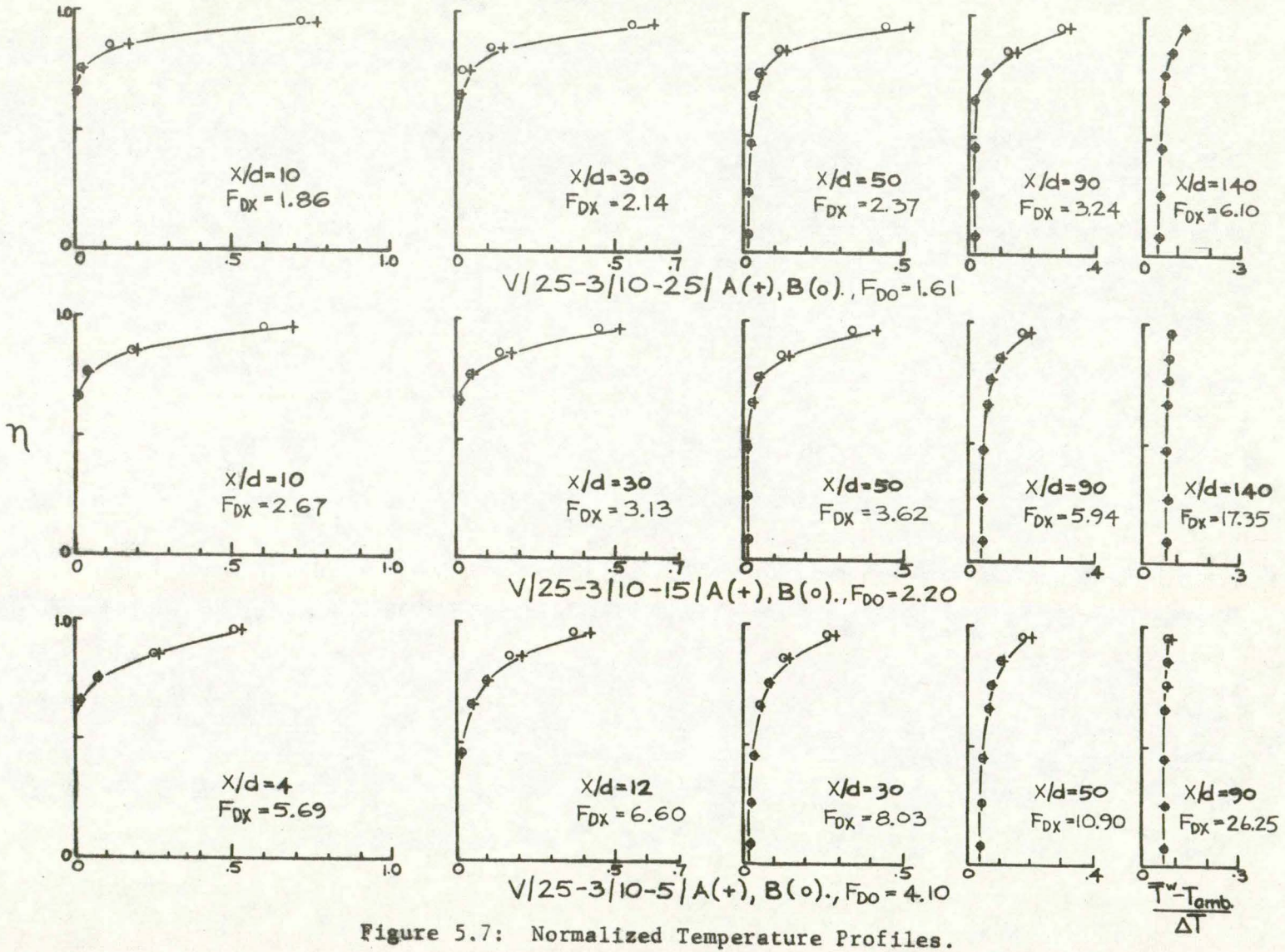

Figure 5.7: Normalized Temperature Profiles.

increasingly inhibited as the density gradient increased can be seen clearly. As the flow conditions approached the stratified state ($F_{DO} \simeq 1.0$), the mixing became minimal and in fact the major contributor to the change in temperature profiles was cooling at the surface. However, as the density gradient was reduced (F_{DO} increases), the mixing became more rapid and a fully mixed condition was easily attained within the length of the flume.

Although there is a continuum of changing characteristics from stratified to rapidly mixing flows, for improved clarity in description, a somewhat arbitrary subdivision is employed in this thesis as follows.

Table 5.1: Flow Designations.

Initial Densimetric Froude Number Range	Flow Designation
$F_{DO} < 1$	Stratified
$1 < F_{DO} < 1.6$	Stratified with Partial Mixing
$1.6 < F_{DO} < 4.0$	Moderate Mixing
$4.0 < F_{DO}$	Rapid Mixing

The photographs in Fig. 5.8 show a representative flow in each of the above designations.

D. Richardson Number Determination

The parameter most influenced by the variation of the velocity distribution from the logarithmic profile was the local Richardson number, R_i. For cross sections where complete velocity measurements were taken, R_i

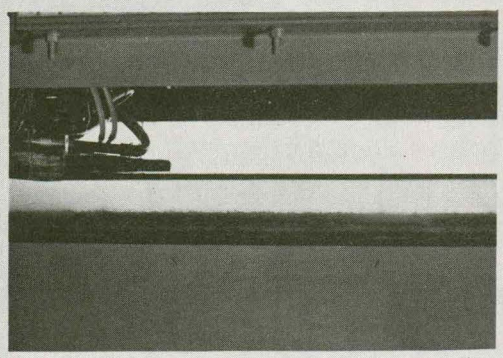

V/25-1/10-25/A, F_{DO} = 0.56
Stratified Flow

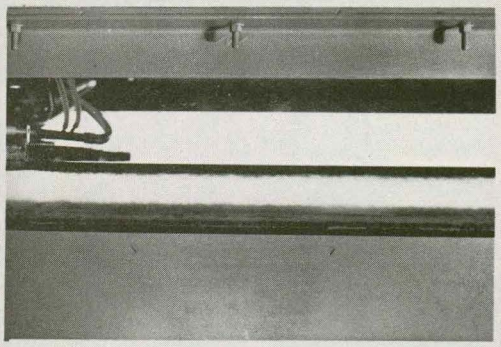

V/25-3/10-25/A, F_{DO} = 1.6
Stratified with Partial Mixing

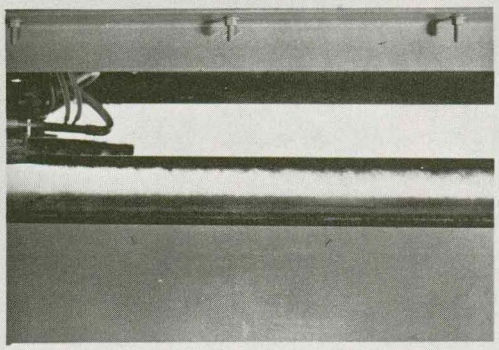

V/25-3/10-15/A, F_{DO} = 2.2
Moderate Mixing

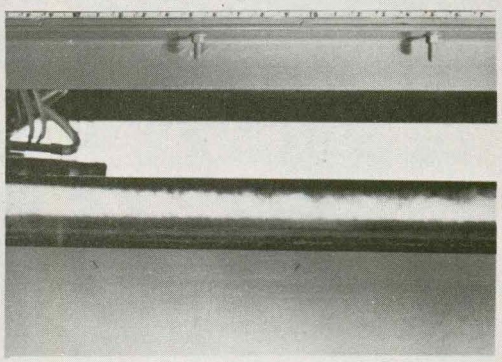

V/25-3/10-5/A, F_{DO} = 4.1
Rapid Mixing

Fig. 5.8. Representative Mixing Conditions.

was computed using both the logarithmic velocity profile and the average of the central 8 velocity readings. By using the width-averaged density and velocity gradients, R_i was computed from

$$-R_i = \frac{g\left(\frac{\Delta\rho}{\Delta y}\right)}{\rho\left(\frac{\Delta u}{\Delta y}\right)^2} \tag{5.5}$$

Typical results from some selected experimental runs are given in Fig. 5.9. This parameter is very sensitive to changes in velocity gradient. This extreme sensitivity, especially in flows with high density gradients, mitigated against its use as a practical parameter in these studies.

E. Effect of Entrance Conditions

Since this study was focused upon the far-field or passive diffusion region, the effect of entrance conditions was not of primary concern. It had been anticipated that the rate of vertical mixing would become independent of slight differences in entrance conditions a short distance downstream from the spreader. Beyond this initial mixing region, it was expected that the mixing would depend only on the properties of the ambient flow, the density difference between the upper and lower layers and perhaps the discharge ratio Q_{tot}/Q_{eff}. This was found to be true for moderately and rapidly mixing flows, but as the velocities became smaller and/or the degree of stratification increased, entrance conditions were found to have profound effects on the mixing processes and the velocity distribution.

1. Initial Mixing: Variations in entrance conditions were

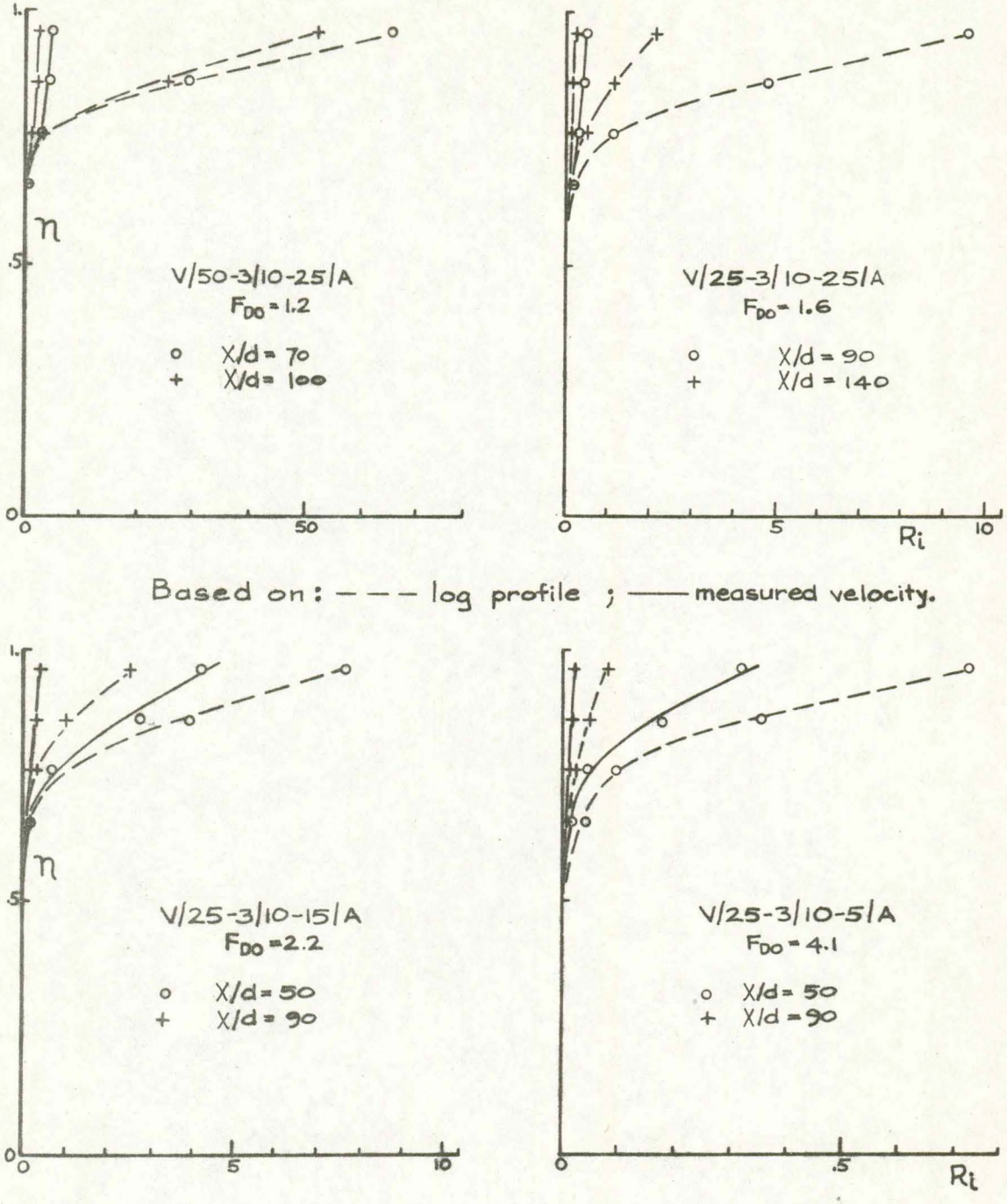

Figure 5.9: The Influence of Velocity Changes on the Richardson Number.

achieved by raising or lowering the spreader. By varying the thickness of the sheet of heated effluent, the average effluent velocity could be controlled. At the low-velocity flows, the depth to which the spreader was set had a critical influence on the mixing processes. Fig. 5.10 illustrates three markedly different mixing conditions that were obtained simply by varying slightly the vertical location of the spreader at the same flow condition. Photographs for the same three runs showing the heated effluent mixed with dye to make the mixing process visible are presented in Fig. 5.11.

The mixing process with entrance condition C was much faster than that predicted by passive diffusion theory. What we had here was essentially a turbulent momentum jet phenomenon. As Silberman (23) has noted, water flowing from a warm water canal with a small density difference can be considered a half-jet with a plane of symmetry at the free surface. Temperature then becomes merely a marker of the water emitted from the canal. Abramovitch (1) discusses the phenomenon of turbulent jets of incompressible fluid in a co-flowing external stream. Data presented graphically by him yields a value of $X \approx 2.3$ ft. from the spreader as the distance at which the warm water marker should reach the bottom. Actually the temperature profiles indicate that the warm water reached the bottom between 1.5 and 2.0 ft. downstream from the spreader. This seems to be reasonable agreement considering that the jet likely had a small downward velocity component at the spreader exit and that Abramovitch's graphical relationship was extrapolated.

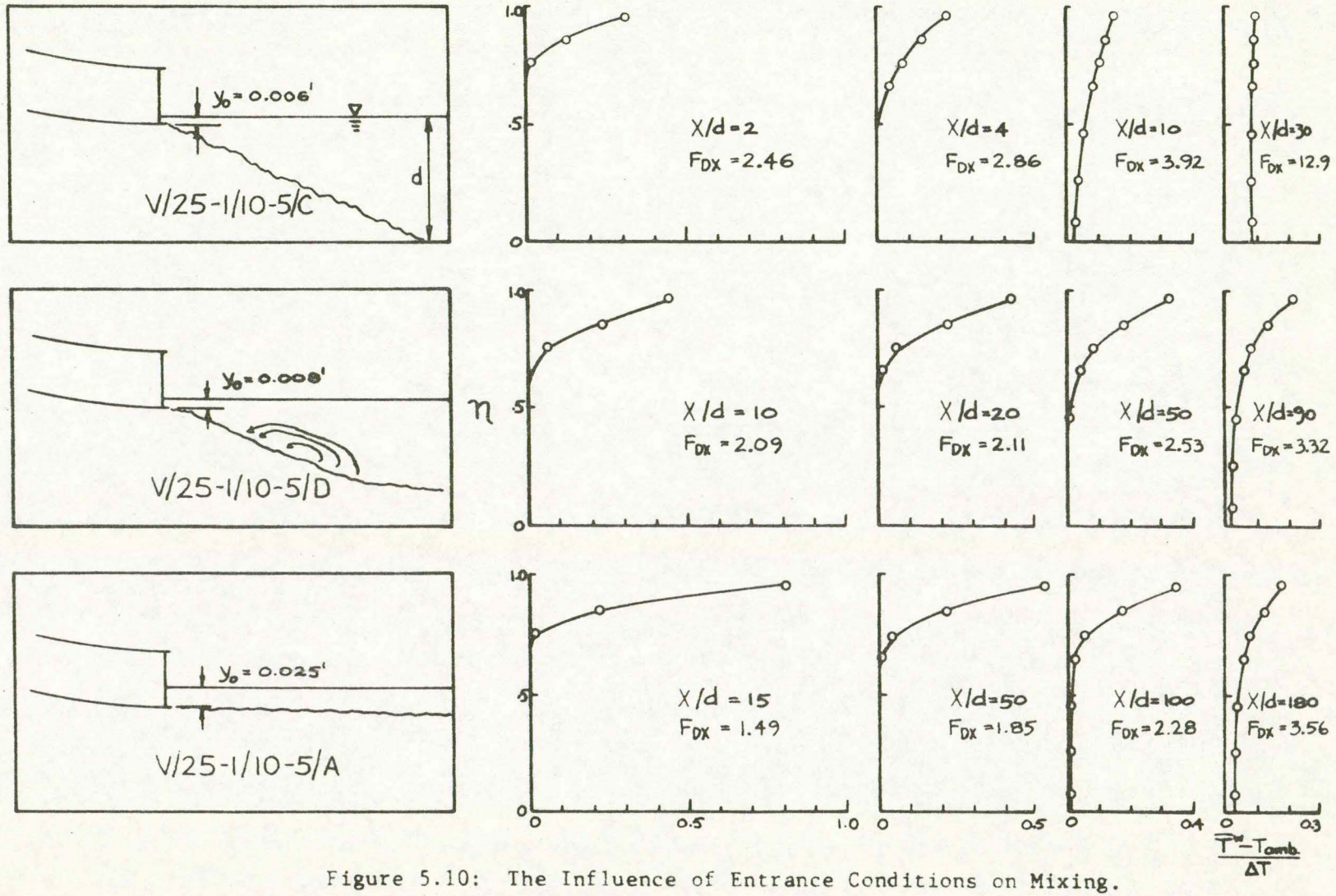

Figure 5.10: The Influence of Entrance Conditions on Mixing.

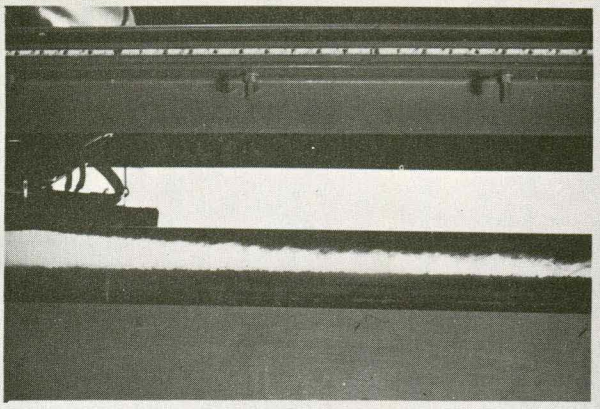

V/25-1/10-5/C

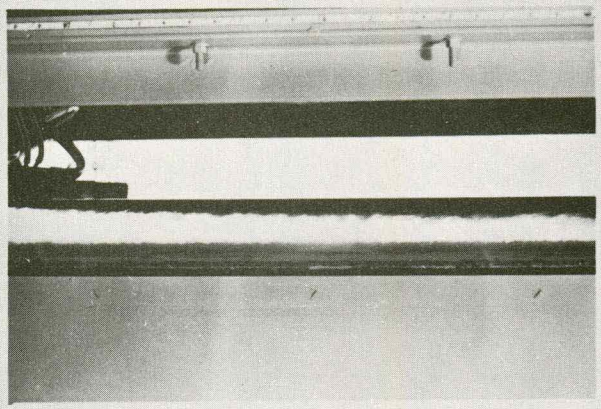

V/25-1/10-5/D

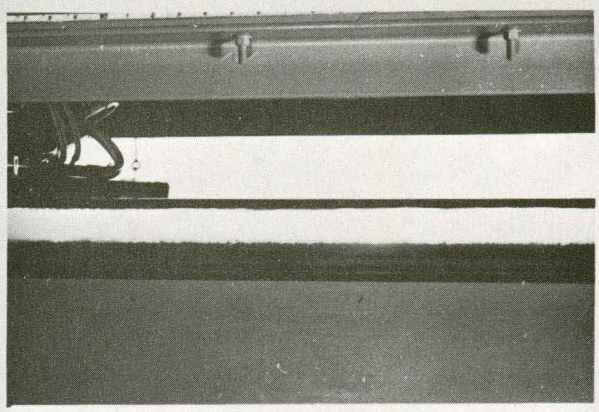

V/25-1/10-5/A

Fig. 5.11. Photographs of Three Entrance Conditions.

The phenomenon of the inverted internal hydraulic jump has been discussed in detail by Yih and Guha (30), Stefan and Hayakawa (24) and Koh and Fan (16). For conditions between that of the momentum jet and stratified flow an inverted hydraulic jump may occur. In this case, the heated plume gradually increases in thickness up to a critical cross section after which the rate of increase of the thickness of the warm layer is greatly reduced. The second flow condition in Figs. 5.10 and 5.11 depicts an inverted hydraulic jump.

The third flow condition of Fig. 5.10 shows that by further lowering the spreader, a nearly stratified flow can be achieved. The influence of the entrance condition on mixing will not be pursued further here except to note that in the design of cooling canals the entrance condition can be critical in determining the kind of mixing that will occur.

2. Velocity Distribution: In most of the experiments the effluent flow was introduced at the average velocity of the ambient flow. This introduced a slight velocity retardation at the surface which persisted for a short distance downstream. However in most cases that were measured, momentum transfer from the ambient flow soon accelerated the effluent flow up to the normal surface velocity. As the degree of stratification increased however, differences in momentum between the effluent and the ambient tended to persist farther downstream, since the mixing process was then limited to a narrower interfacial zone. Fig. 5.12 shows typical velocity profiles at the centerline and near the sidewall for relatively stratified flows with

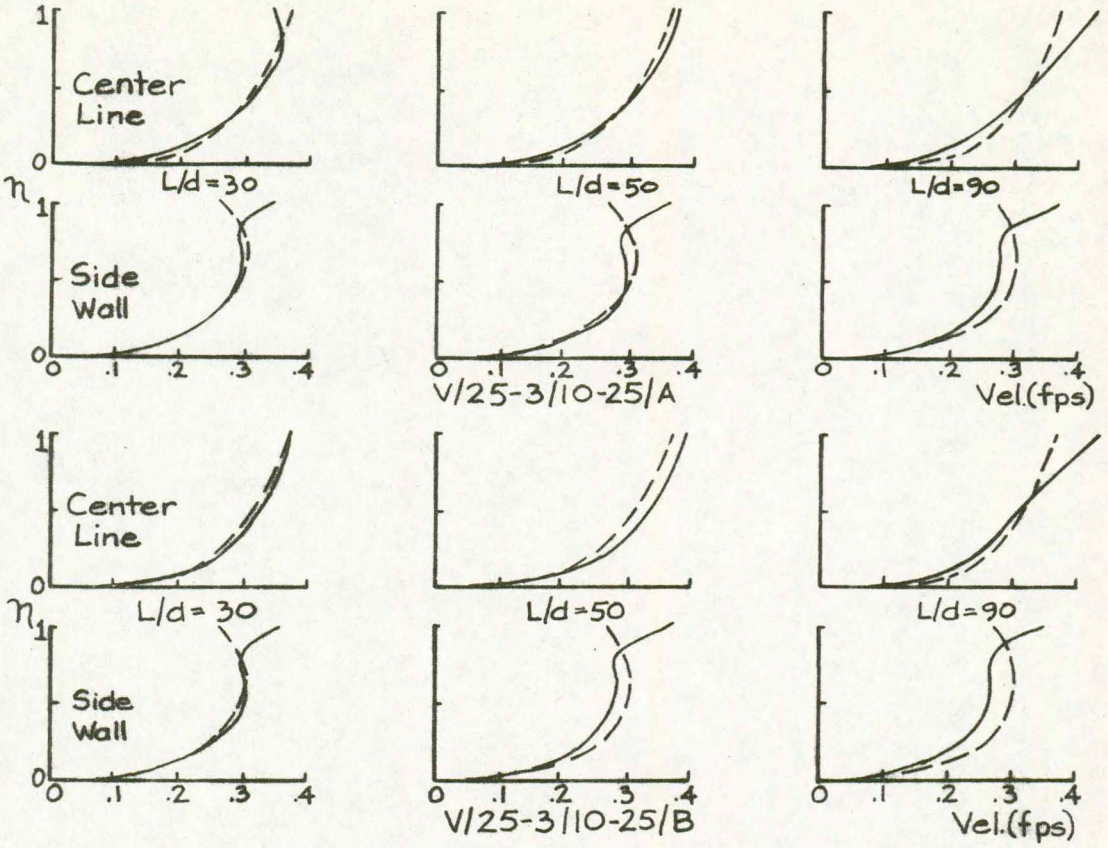

Figure 5.12: The Influence of Entrance Conditions on Velocity Distribution.

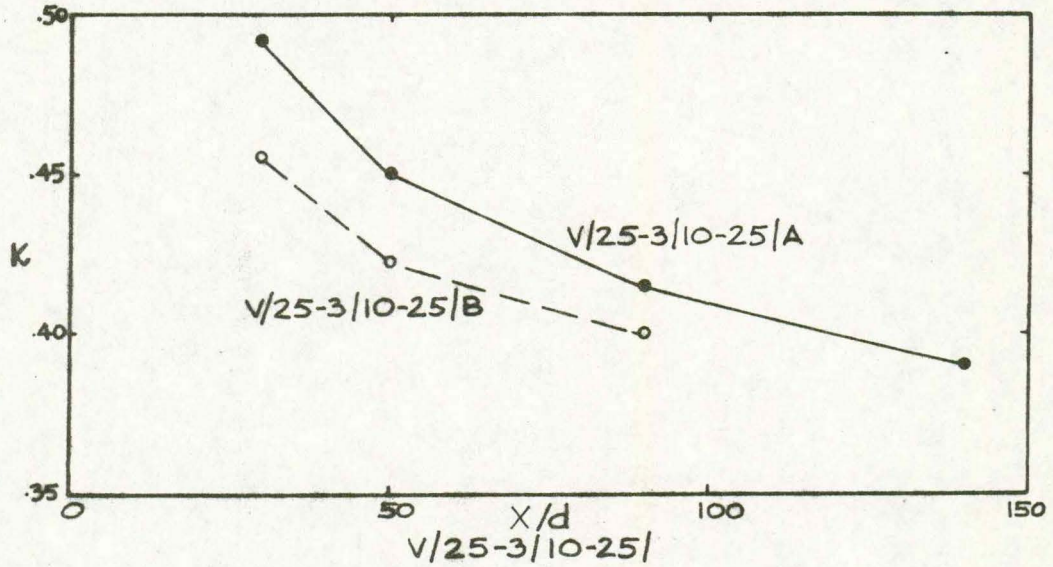

Figure 5.13: The Variation of κ with X/d.

entrance conditions A and B. The dashed lines representing undisturbed velocity profiles are shown for reference.

Some indication is given here of the three-dimensional nature of this phenomenon. The acceleration of the upper-layer flow near the center tends to be compensated by the retardation near the sidewalls. At the sidewalls the injected effluent flow disrupts the sidewall boundary layer near the surface which had developed further upstream. Downstream from the spreader a new sidewall boundary layer slowly develops in the upper portion of the flow.

To depict the general shape of the average velocity profile, the von Karman turbulence coefficient, κ, can be determined and its variation plotted along the flume length. This presents a rather crude indicator of the velocity profiles since κ is usually only defined for logarithmic profiles. Fig. 5.13 shows the values of κ for the two flow conditions depicted in Fig. 5.12. From these two figures we note that the rate of alteration of velocity profiles is the same for both runs, but that the difference in entrance conditions causes an initial distortion in the velocity profiles that persists downstream.

3. Temperature Distribution: Previously in Fig. 5.7 comparative temperature profiles for entrance conditions A and B were shown for 3 selected runs. The faster effluent flow of the B entrance condition results in slightly faster initial mixing. After the initial mixing is completed, the mixing then occurs at an equal rate for both entrance conditions, as evidenced by the constant downstream displacement of the temperature profiles.

The above differences in velocity and temperature profiles

due to entrance conditions are of more academic than practical interest, for it will be shown later that their effect on the vertical mixing coefficient is not significant. The same can be said of the discharge ratio. Within the range of values tested, Q_{eff}/Q_{tot} = 1/5 to 1/25, no significant variations in the rate of vertical mixing were noted.

F. Heat Losses

Heat losses from the flume occurred during the experimental tests. In order to carry out the subsequent analysis, it is necessary to know the heat transfer rates at the boundaries.

1. Environmental Conditions: Table A.4 summarizes the environmental measurements taken during the experimental runs. The range of air temperatures was 69.8 - 77.5 °F, and of relative humidity 57. - 84.5 %. The equilibrium temperature, which represents the temperature toward which the cooling water tends, varied from 65.5 - 72.1 °F. Equilibrium temperature values were determined using the tables derived by Ryan and Stolzenbach (10). The difference between the temperature of the ambient flow and the equilibrium temperature gives an indication of the cooling rate of the ambient water. The range of values for $T_{amb} - T_E$ was 3.79°F - 15.74°F. For some of the later runs psychrometric readings were also taken directly above the flume water surface. These temperature readings are not recorded on Table A.4, but it was found that on the average the dry bulb temperature was 4°F higher and the wet bulb temperature 3°F higher than the corresponding temperatures outside the flume walls. This resulted in approximately equal values of relative humidity

within the flume walls and outside. Interestingly enough there was at most only a 1°F air temperature difference along the entire flume length from spreader to tailgate. A warm moist layer of air was apparently moved along by the flowing water and effectively contained between the flume walls as it slowly rose.

2. Amount of Heat Loss: The heat loss up to a given cross section can be determined by

$$\text{Heat Loss} = \left[Q_{eff}(T_{eff} - T_E) - W\int_o^d (\bar{T}^w - T_E)\, u\, dy \right] \cdot \rho_a \cdot C_p \qquad (5.6)$$

Table A.4 gives the normalized heat loss for each run measured at the cross section farthest downstream. These heat losses are expressed in percent of the heat flux at the spreader using the equilibrium temperature as datum. The effluent heat flux was measured at the same time as the cross sectional heat flux was measured. The heat losses in Table A.4 represent not only losses from the excess heat flux but also losses from the ambient flow. The losses from the ambient flow vary from run to run, being a function of the temperature difference $T_{amb} - T_E$ and K, the surface heat loss coefficient.

The heat losses recorded in Table A.4 were calculated using logarithmic velocity profiles and a constant value of $\kappa = 0.42$. It was found that the change in computed heat losses was very small if the measured velocities were used instead. For example, the difference in percentage heat loss using log velocity profiles and measured velocities was about 0.1% for runs V/25-3/10-5/A, V/25-3/10-15/A and V/25-3/10-25/A. For the stratified case, V/50-3/10-25/A, the

difference in total heat loss was about 0.8%

Fig. 5.14 shows the heat loss curves for five selected runs. Notice that for the rapidly mixing flows most of the cooling occurs near the spreader, after which the rate of cooling decreases as the flow becomes mixed. As the degree of stratification increases, the cooling tends to continue along the entire length of the flume. Also the amount of cooling is greater with the stratified flows, since in this case high surface heat losses can occur over a greater length of the flume and, with the lower velocity, more time is available for cooling.

The heat loss curves depicted in Fig. 5.14 are for the experimental runs that were later selected for checking the downstream temperature profiles predicted by mathematical modeling. For these runs, a smooth heat loss curve was drawn through the experimental points. The heat loss curves had to be modified in the region near the spreader, since the rectangular integration procedure used in Eq. 5.6 tended to give values of the heat flux that were too large in this region. The main reason for this was that the temperature profile from $\eta = .96$ to the surface was unknown and thus an extrapolation of the temperature profile curve was used. This can cause significant error when the temperature gradient is large as, for example, near the spreader. However, the integration procedure became more precise as mixing occurred along the flume.

3. Heat Loss Model: An attempt was made to represent the heat loss completely by a mathematical model for the experimental

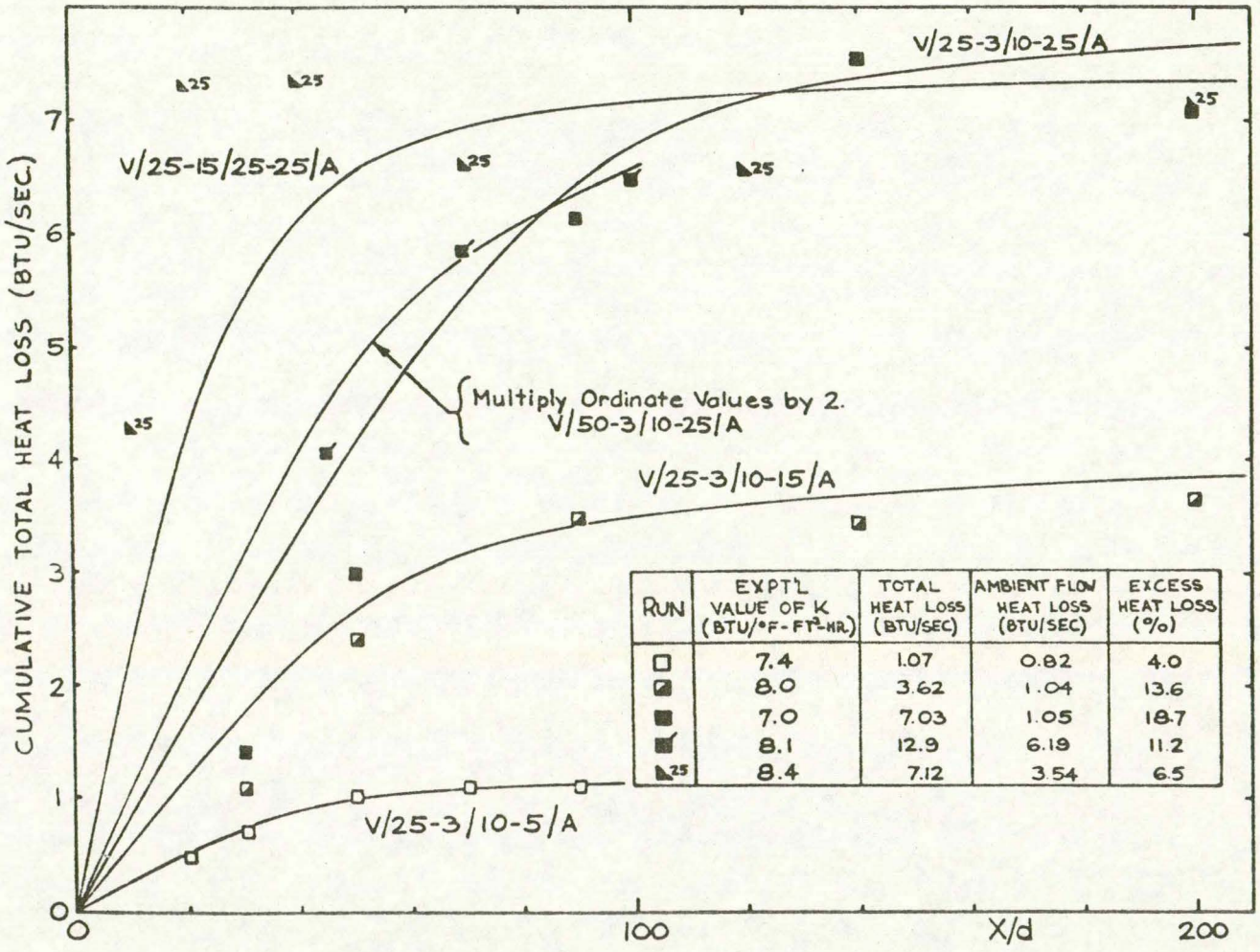

RUN	EXPT'L VALUE OF K (BTU/°F-FT²-HR.)	TOTAL HEAT LOSS (BTU/SEC)	AMBIENT FLOW HEAT LOSS (BTU/SEC)	EXCESS HEAT LOSS (%)
□	7.4	1.07	0.82	4.0
◪	8.0	3.62	1.04	13.6
■	7.0	7.03	1.05	18.7
◪	8.1	12.9	6.19	11.2
▲25	8.4	7.12	3.54	6.5

Figure 5.14: Heat Loss Curves for Selected Runs.

flume. Eventually it was decided to modify this attempt because (1) the heat loss mechanisms throughout the flume length were found to be considerably more complex than first anticipated and (2) there was inadequate monitoring of environmental conditions to enable a detailed heat loss model to be verified. There were indications of high heat losses in the region of the spreader. Also the flume walls inhibited the free movement of convective air and tended to trap a warm layer of moist air above the water surface. Time and space variations in air temperature and humidity were also more important than was originally anticipated.

However, certain insights into the heat loss mechanisms were achieved. The rate of heat loss through the glass sidewalls was determined to be negligible compared to the total heat loss rate. It then remained to allocate the total heat loss between the bottom and the water surface. Measurements of heat losses from the ambient flow in a companion investigation, "Transverse Mixing of Heated Effluents in Open Channel Flow" by T.P. Yeh (29) clearly indicated that most of the heat loss occurred across the water surface. Temperature profiles down the flume were measured for two conditions of ambient flow. Prior to the tests the ambient water was heated so as to be appreciably warmer than the surrounding air. Fig. 5.15 shows a typical width-averaged temperature profile from each of the runs.

The temperature profiles suggest the relative amounts of cooling occurring at the water surface and at the bottom. The heat transfer across a horizontal plane can be expressed as

$$\phi_n = -E_{Ty} \frac{\partial \bar{T}^w}{\partial y} \qquad (5.7)$$

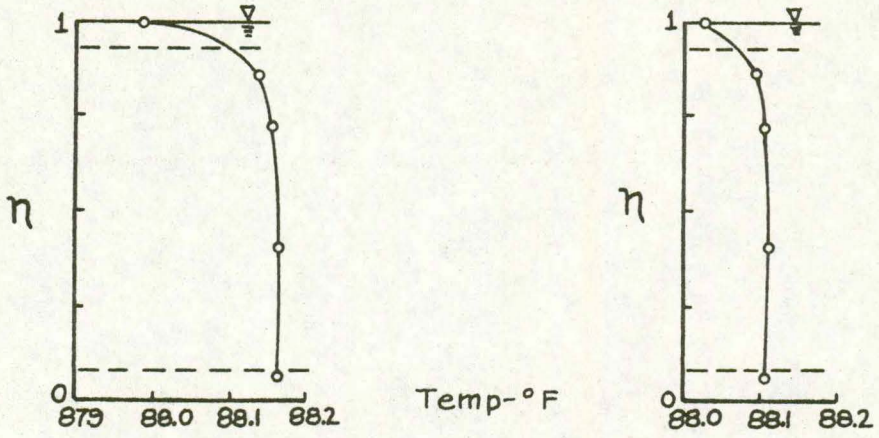

U = 0.3 f.p.s.

d = 0.25 ft.

T_{air} = 79.0 °F

U = 0.5 f.p.s.

d = 0.25 ft.

T_{air} = 78.0 °F

Fig. 5.15. Typical Temperature Profiles of Cooling Ambient Flows.

The flowing ambient stream represents a well mixed case, and it will be shown later that in this case E_{Ty} approaches the theoretical parabolic distribution for mass transfer. The heat flows through the two horizontal planes depicted in Fig. 5.15 will represent the bottom and water surface heat losses. In both cases the flux can be expressed in terms of Eq. 5.7 and the two values of E_{Ty} should be relatively small and approximately equal. The fact that the temperature gradient is much larger near the water surface than near the bed clearly indicates that most of the heat loss occurs through the water surface.

A more detailed analysis of the heat losses was conducted

by T.P. Yeh (29). He considered the heat balance for two control volumes, one for the upper half and the other for the lower half of the flow. He determined the ratio of the heat fluxes through the water surface and through the bottom to be $\phi_s/\phi_b \approx 5$. Average values of the heat exchange coefficient for the water surface and the bottom were found to be

$$K \approx 3.5 \frac{BTU}{ft.^2\text{-}hr.\text{-}^oF}$$

and

$$K_b \approx 0.5 \frac{BTU}{ft.^2\text{-}hr.\text{-}^oF}$$

The value of the surface heat exchange coefficient compares favorably with the values given in the table by Ryan and Stolzenbach (10). They also compare well with the experimental values listed in Fig. 5.14 which were computed using Eq. 2.5 over a reach of the flume sufficiently far downstream from the spreader so that the rate of change of the water-surface temperature was moderate. The above analysis shows that surface heat losses tend to predominate in the flume. This tendency would be accentuated further in the experimental runs where the heated effluent was introduced at the surface.

As stated previously, it was not possible to obtain a complete mathematical heat-loss model for the entire flow. However a model was derived to determine the proportion of the total heat that was lost from the ambient-temperature flow. For this simpler case, the ambient water temperature can be considered to vary only as a function of X. For the steady state case, the rate of change of ambient temperature (T_{amb}) along the flume length can then be expressed as

$$Q\frac{dT_{amb}}{dx} = -\frac{WK}{\rho C_p}\left(T_{amb}-T_E\right)-\frac{WK_b}{\rho C_p}\left(T_{amb}-T_{air}\right) \qquad (5.8)$$

This differential equation yields the solution

$$T_{amb}(X) = T_{amb}(0)\, e^{-C_0X}+\frac{C_1}{C_0}\left(1-e^{-C_0X}\right) \qquad (5.9)$$

where $T_{amb}(o)$ = the average ambient temperature for the experimental run, measured upstream from the spreader.

$$C_0 = \frac{1}{Q\rho C_p}\left[WK + WK_b\right] \qquad (5.10)$$

$$C_1 = \frac{1}{Q\rho C_p}\left[WKT_E + WK_bT_{air}\right] \qquad (5.11)$$

and the other symbols are as defined in Chapter III.

Using Eq. 5.9 the proportion of the total heat that was lost from the ambient flow was computed and tabulated on Fig. 5.14. Notice that for the run with the lowest heat flux (V/25-3/10-5/A), the heat loss from the ambient flow exceeds that from the excess heat flux. The unusually high ambient loss from the 0.5 ft. depth flow (V/50-3/10-25/A) resulted from a high ambient water temperature and the low air temperature and humidity present for that run.

The ambient heat losses were calculated with surface heat exchange coefficients corresponding to ambient water temperatures. Also the air temperature used was that measured outside of the flume. In the experimental run however the water surface temperature was higher than the ambient temperature and a warm body of air lay on top of the water surface. For these reasons the values of ambient flow

heat loss listed in Fig. 5.14 should be considered as estimates rather than exact determinations.

The values of excess heat loss tabulated on Fig. 5.14 were computed using the relationship,

$$\frac{\text{Total Loss-Ambient Loss}}{Q_{eff}\cdot(T_{eff}-T_{amb})\cdot\rho_a\cdot C_p} \times 100 = \frac{\text{Loss of Excess Heat}}{\text{Input Excess Heat}} \times 100$$

where total heat loss is defined by Eq. 5.6 and Ambient Loss = $Q_{tot}\cdot(T_{amb(o)} - T_{amb(x)})\cdot\rho_a\cdot C_p$.

G. Determination of Mixing Parameters

The main point of interest in this investigation is the rate of vertical mixing of the heated effluent and the factors that affect it. In this section three measures of the rate of mixing are presented in order of increasing sophistication.

1. Dimensionless Mixing Length: A simple measure of the rate of mixing is the distance downstream from the spreader at which the normalized temperature difference between the top and bottom reaches a specified value. The specified value was

$$\frac{T_{top} - T_{bot}}{\bar{T}_x - T_{amb}} = 0.2 \qquad (5.12)$$

where $\bar{T}_x$ = average temperature for the cross section weighted by area.

This specification was chosen to represent a reasonably well-mixed condition. Beyond this degree of mixing, the longitudinal rate of change of mixing tends to become asymptotic and large errors in the computation of the mixing length are possible. Fig. 5.16 shows a dimensionless mixing length $(\frac{X_{0.2}u_*}{dU})$, where $X_{0.2}$ is the distance from the

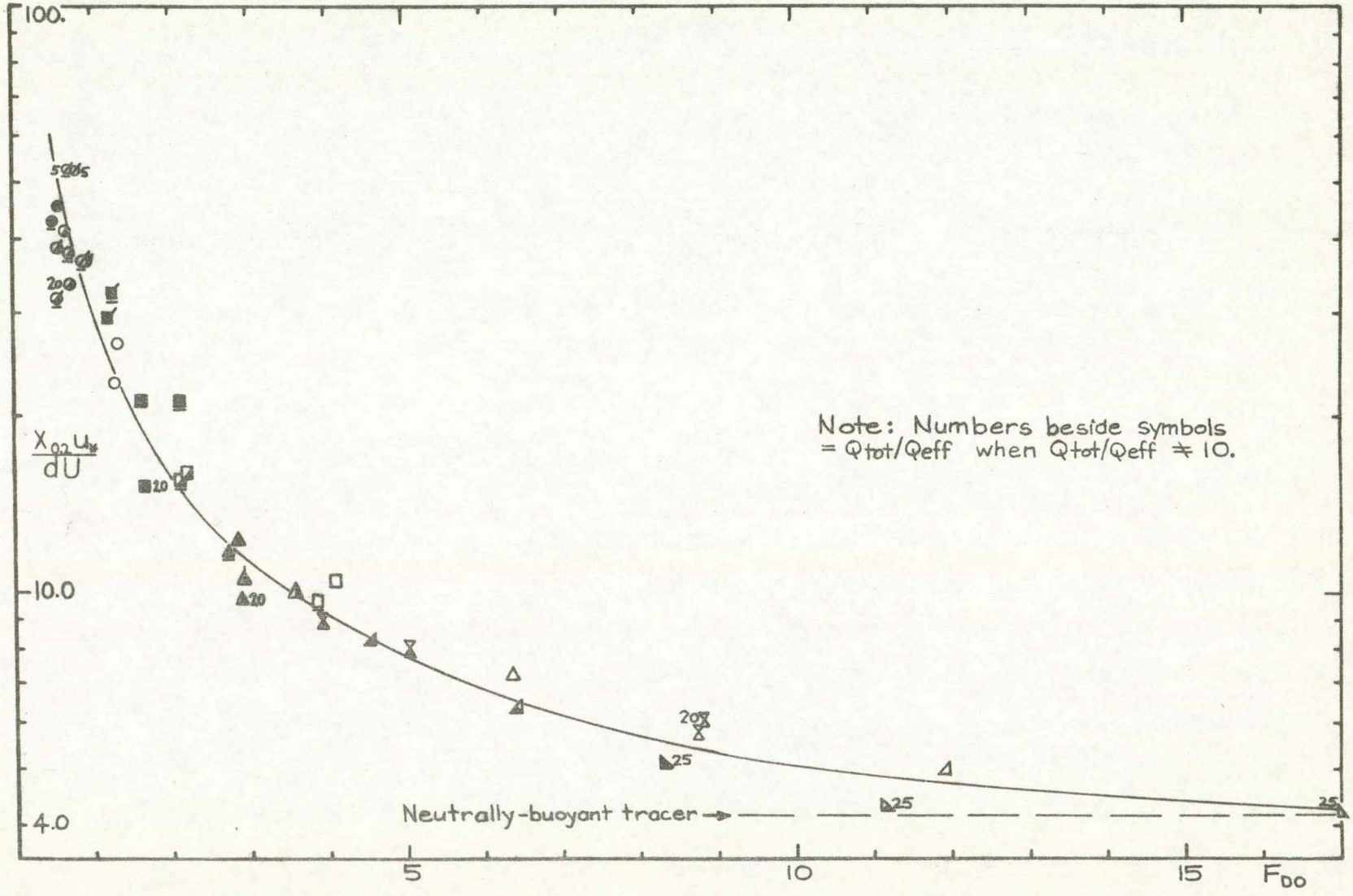

Figure 5.16: Dimensionless Mixing Length vs. Initial Densimetric Froude Number.

spreader to the cross section where $\frac{T_{top} - T_{bottom}}{\overline{T}_x - T_{amb}} = 0.2$, plotted against the initial densimetric Froude number, F_{DO}. The scaling factor for the length downstream, $X_{0.2}$, is made dimensionless by dividing it by $\frac{Ud}{u_*}$ which is a length scale for vertical mixing by passive turbulent diffusion.

All experimental runs are plotted in Fig. 5.16 except those with entrance conditions designated "C" and "D". Otherwise this figure includes the entire range of experimental conditions. The data thus define a 'universal' curve that would be useful in the field for providing a first estimate of the distance required for nearly complete mixing. It should be noted that cooling rates can alter this curve, so that this curve is only applicable for conditions of moderate surface cooling, such as occurred in these experiments. The dashed line represents the dimensionless length for which the ratio $\frac{C_{.96} - C_{.08}}{\overline{C}} = 0.2$ is attained using neutrally-buoyant dye introduced at the surface of a two-dimensional flowing stream. This asymptotic limit was determined from Jobson's (12) data and mathematical model. With increasing F_{DO} the data obtained in the present study clearly approaches the limit for a neutrally buoyant tracer.

A study by Weil (28) computes the length needed for mixing a semi-circular jet introduced at ambient velocity into turbulent channel flow. Though his situation is different from the present study, his results indicate that for nearly complete mixing as defined in this section, a dimensionless length of about 4.3 is required for moderately to rapidly mixing flows. This also agrees well with the results of the present study.

2. Bulk Mixing Coefficient: Using the Fickian diffusion model with total reflection at the boundaries, it is possible to determine a gross mixing coefficient for rapidly-mixing flows as described in Chapter III. Fig. 5.17 shows the bulk mixing coefficients for a selected set of the experimental runs plotted in Fig. 5.16. Not all of the runs in Fig. 5.16 appear in Fig. 5.17. because only cross sections where

$$0.1 < \frac{T_{\eta=.08} - T_{amb}}{T_{\eta=.96} - T_{amb}} < 0.9 \qquad (5.13)$$

were considered in Fig. 5.17. Points outside of this range are subject to large interpolation errors in using Fig. 3.3. Also, limiting points to those within this range effectively eliminated highly stratified flows for which the present analogy is not suitable. Even for the cases of runs that are plotted in Fig. 5.17, only some of the cross sections in the runs met the criterion of Eq. 5.13. The values of $K_y/u_* r_b$ that are plotted represent the average values for the cross sections that met the specified criterion. In some experimental runs only one cross section met the criterion and these are designated with a^1 in Fig. 5.17. The asymptotic value of $K_y/u_* r_b = 0.0633$ is the mean of the most probable value from Jobson's experimental data for neutrally-buoyant dye (12).

3. Vertical Heat Transfer Coefficient: The final mixing parameter is E_{Ty}, the width-averaged heat transfer coefficient, which has been described in Chapter III. Assuming negligible heat loss through the bottom, the equation for determining E_{Ty} is

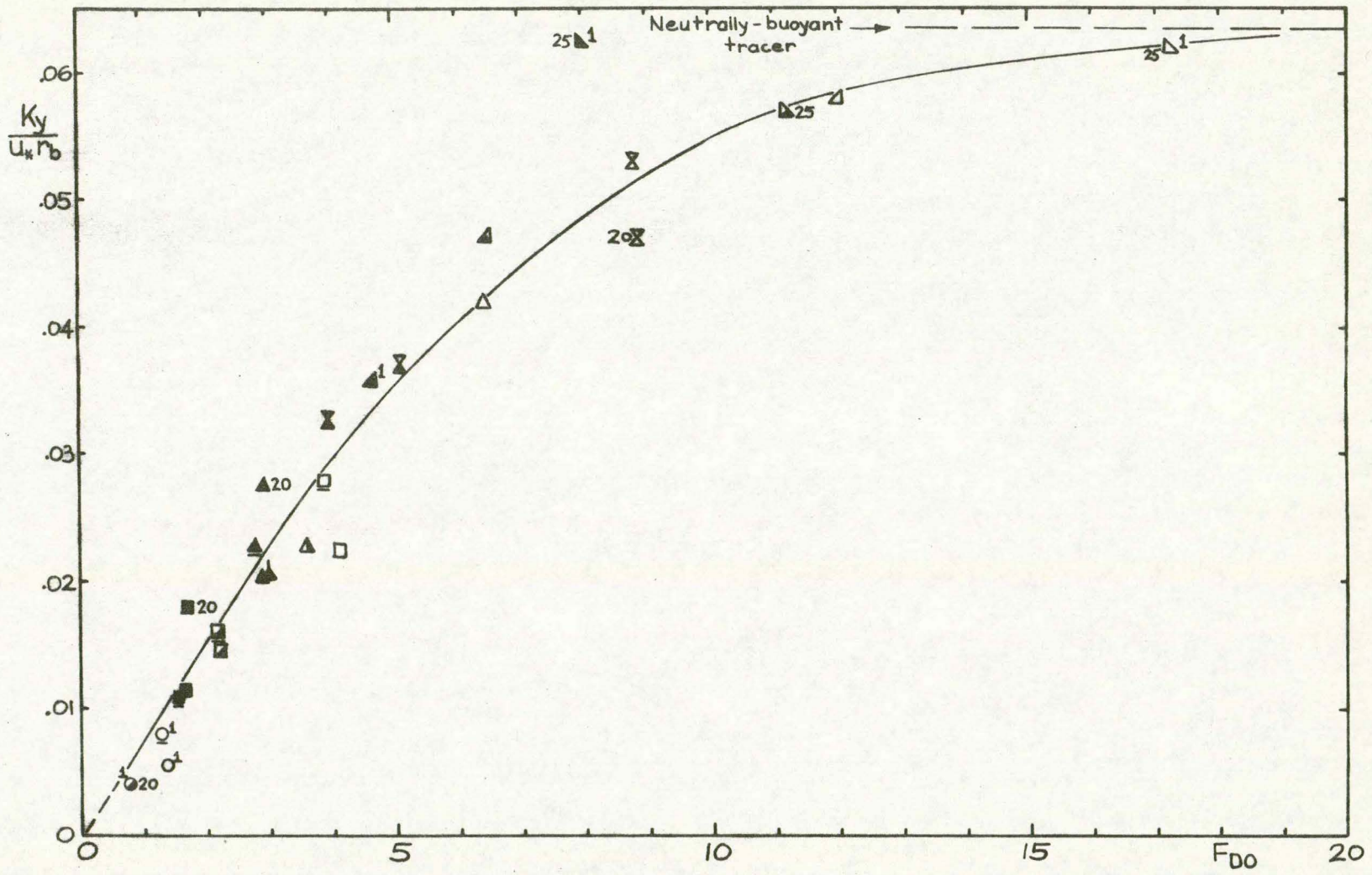

Figure 5.17: Average Values of $Ky/u_* r_b$ vs F_{DO}.

$$E_{Ty} = \frac{\frac{\partial}{\partial x}\int_0^y \overline{uT}^w dy}{\left.\frac{\partial \overline{T}^w}{\partial y}\right|_y} \qquad (3.25)$$

Computation of E_{Ty} involved integration of the heat flux from the flume bottom upwards. Computations were carried out for each cross section only up to $\eta = .96$ thus eliminating the need to utilize the troublesome water surface boundary condition. The logarithmic velocity profile corresponding to the experimental conditions was assumed to exist across the flume width and was used in the computations. For the integration of the numerator the trapezoidal rule was used. The longitudinal gradient of the heat flux was determined as the average of the linearized gradients over the reaches between the cross section in question and the closest upstream and downstream measuring cross sections.

An inquiry was made into the computational error in determining the longitudinal gradient of the flux term in Eq. 3.25. Based on the computational error inherent in the trapezoidal rule (2) it was determined that the error would be less than 1% for moderately and rapidly mixing flows but could be as high as 5% for the more stratified flows.

Notice from Eq. 3.25, that if the slope $\left.\frac{\partial \overline{T}^w}{\partial y}\right|_y$ approaches zero then the value of E_{Ty} is apt to become unreliable. To avoid this potential source of grief, a limiting constraint on the temperature gradient was built into the computer program. Any cross sections wherein the minimum vertical temperature gradient did not meet this

constraint were not used in the computation for E_{Ty}. The limitation on $\frac{\partial \overline{T}^w}{\partial y}$ was obtained by requiring that any two adjacent width-averaged temperature readings must differ by at least by $\pm 2\sigma_m = \pm .008°F$, where σ_m is the standard deviation of the means of the ten thermistors given by

$$\sigma_m = \frac{\sigma}{\sqrt{10}} \tag{5.14}$$

The standard deviation of the ten thermistors readings, σ, was obtained from thermistor readings in a uniform temperature water bath. Using the above procedure, the constraints on the temperature gradient were determined to be

$$\left.\begin{aligned} \frac{\partial \overline{T}^w}{\partial y} &\geq 0.36\,°F/ft. \quad \text{for } d = 0.25\,ft. \\ \text{and} \\ \frac{\partial \overline{T}^w}{\partial y} &\geq 0.72\,°F/ft. \quad \text{for } d = 0.50\,ft. \end{aligned}\right\} \tag{5.15}$$

The values of $E_{Ty}/u_* r_b$ vs. η for some typical runs are given in Fig. 5.18. The theoretical parabolic distribution of the vertical momentum transfer coefficient is shown by the dashed curve. The amount of deviation shown for the nearly mixed flows from the theoretical parabolic limit is typical for the nearly mixed flows.

These curves indicate the following general trends in the variation of E_{Ty}. For highly stratified flows, the values of E_{Ty} are small, and with increasing mixing the values of E_{Ty} increase, approaching the theoretical parabolic distribution for a neutrally-

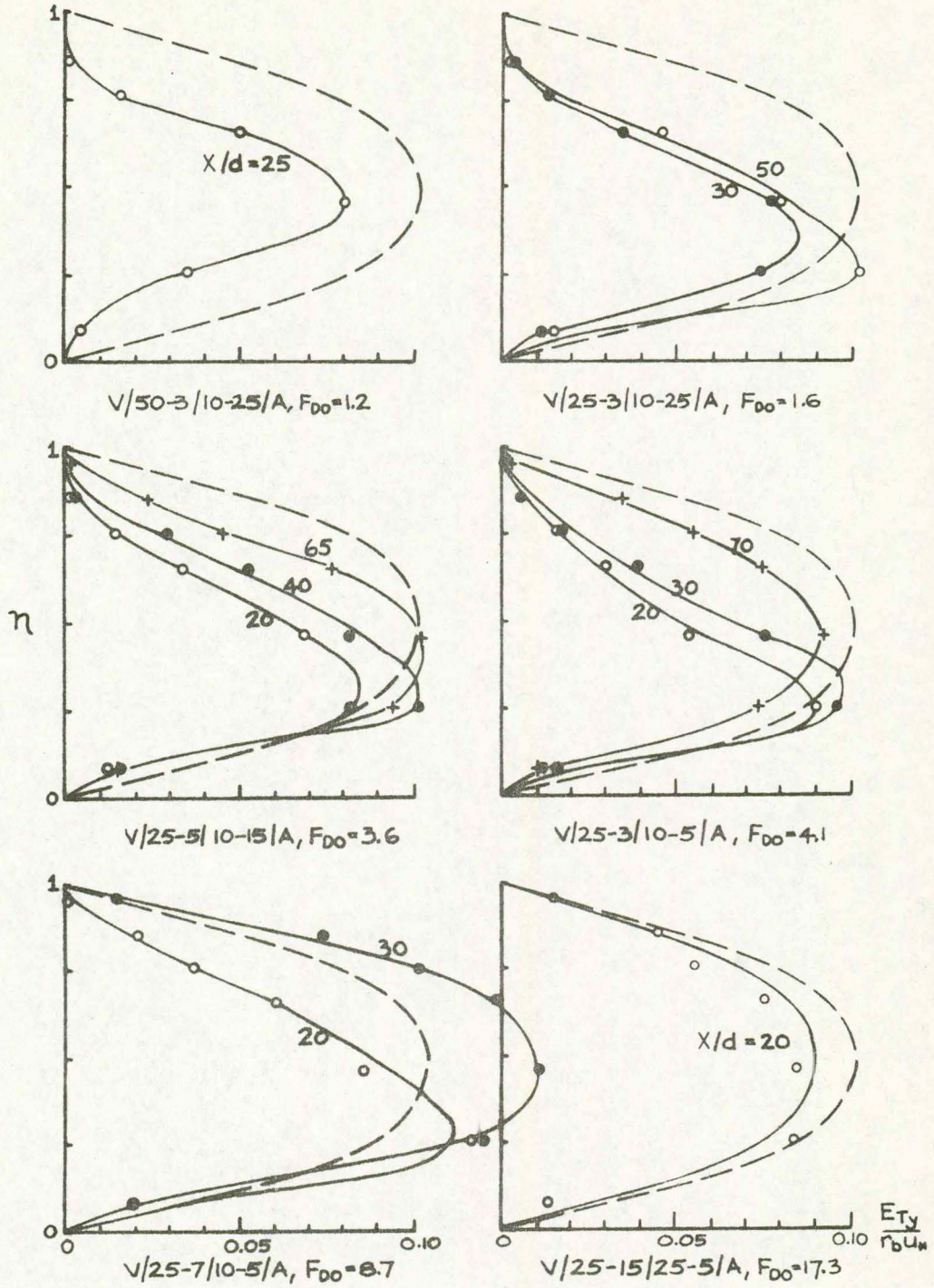

Figure 5.18: $E_{Ty}/u_* r_b$ vs. η for Increasing F_{DO}.

buoyant tracer. The presence of a warm layer of water at the surface suppresses the mixing process, so that when a significant temperature gradient is present, the values of E_{Ty} in the upper reaches of the flow are lower than the values recorded for a neutrally buoyant effluent. In the highly stratified flows and in the rapidly mixing flows the temperature gradient $\frac{\partial \overline{T}^w}{\partial y}$ is very small over long reaches of the flume so that many of the further downstream cross sections do not satisfy the criterion in Eq. 5.15. However, in the zone of moderate mixing, several cross sections satisfy this requirement. In a typical experimental run, as the heated effluent mixes downwards, the value of E_{Ty} increases as η decreases until a maximum value is obtained in the neighborhood of $\eta \simeq 0.25$. Proceeding further downstream the shape of the E_{Ty} distribution tends to evolve towards the limiting case of the parabolic distribution. In the next chapter the distribution of E_{Ty} will be analyzed further and presented in a generalized format.

When complete velocity measurements were taken, the determination of E_{Ty} was repeated using the average value $\overline{uT}^w$ over the middle 8/10 of the flume. Compared with the use of the logarithmic velocity profile, the difference produced in the values of E_{Ty} was well within the variations attributable to experimental errors and computational procedures. The reason for this small deviation is that near the surface where the velocity differences are the greatest, the value of E_{Ty} is small, being suppressed by the presence of heated fluid. Fig. 5.19 shows the influence of changes in velocity distribution on the distribution of E_{Ty}.

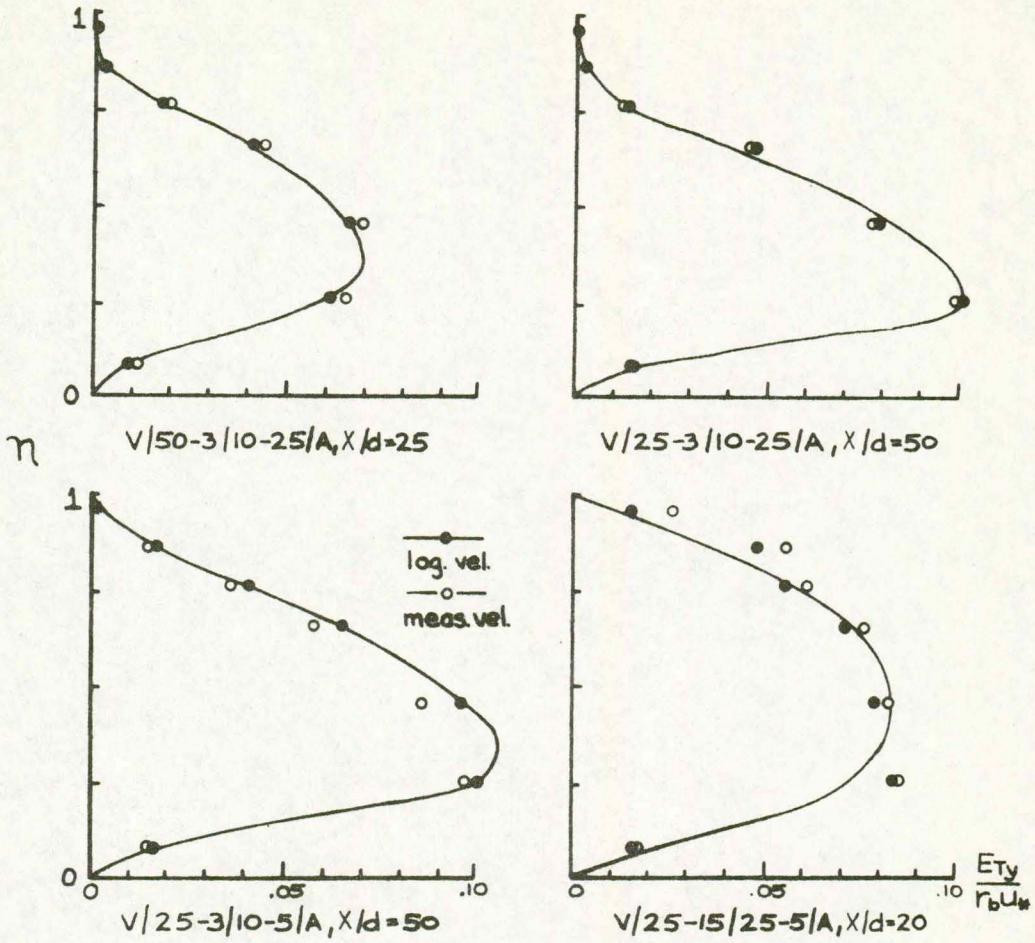

Figure 5.19: Influence of Velocity Changes on E_{Ty}.

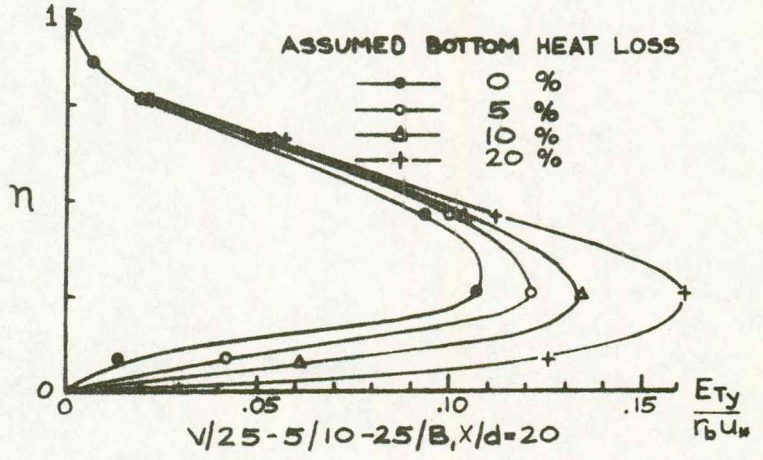

Figure 5.20: Influence of Bottom Heat Losses on E_{Ty}.

The preceding computations of E_{Ty} have been based on the assumption that all of the heat loss occurred at the water surface. Previous tests have demonstrated the reasonableness of this assumption. Chapter V is concluded with an indication of the possible errors introduced into the computation of E_{Ty} by this assumption.

An experimental run with high heat loss , V/25-5/10-25/B, was investigated to study the effect of possible bottom losses on the determination of E_{Ty}. For this run $T_{amb} - T_E$ was 14.94°F and the relative humidity was 67%. The cross section considered was at L/d = 20 where the heat loss rate was 0.857 BTU/sec./ft. With this high heat loss rate, calculations were made for E_{Ty} assuming 0, 5, 10 and 20% of the total heat loss rate occurring through the bottom. Fig. 5.20 shows the results of these calculations. Not surprisingly, the maximum effect occurs at the lower depths. Eq. 3.24b shows that since $\frac{\partial \overline{T}^W}{\partial y}$ is small near the bottom, the effect of a constant bottom heat loss is largest there. As the integration proceeds up from the bottom the heat flux term and the temperature gradient term both increase, resulting in a maximum value of E_{Ty} at about $\eta = 0.25$.

It will be recalled that experiments with a warm ambient flow, conducted by T.P. Yeh, produced a value for the bottom heat loss coefficient of $K_b \approx 0.5$ BTU-in./hr.-ft.^{2}-°F. Using this value in the above selected run gives a value for the heat loss out of the bottom as 9% of the total heat loss. This seems to be a reasonable estimate of the bottom heat loss rate for this particular run. A bottom heat loss of this magnitude produces a maximum error in the computation of E_{Ty} of

about -20% at $\eta \approx 0.25$. While this represents a significant deviation in the value of E_{Ty}, it should be remembered that this run is one of the worst cases. Bottom losses on the other experimental runs will have effects much less than those depicted in Fig. 5.20. The above example then, tends to justify as reasonable the assumption of no heat loss through the bottom in the computation of E_{Ty}.

Chapter VI

ANALYSIS AND DISCUSSION OF RESULTS

In this chapter the experimental results of Chapter V are analyzed further and interpreted, and finally integrated into mathematical models for prediction of downstream temperature profiles. The applicability of the results is stressed throughout.

A. Application of the Bulk Mixing Parameters

1. Dimensionless Mixing Length: The curve of Fig. 5.16 can be used to estimate the length necessary to achieve nearly complete mixing in a straight two-dimensional channel. However, for practical purposes in the field this information can be presented in a more convenient form. The parameters which would most likely be known for a cooling canal would be F_{DO} and ΔT. Thus a graph in terms of $\frac{T_{top} - T_{bottom}}{\Delta T}$ would be most useful. In addition, it is often desired to know the mixing rate along the channel length. Fig. 6.1 is an example of the presentation of the experimental mixing length data in this format.

However, these curves are not universally applicable. The data for these curves were taken from all the A-entry flows with a depth equal to 0.25 ft. and $Q_{tot}/Q_{eff.} = 10$. These curves would only be applicable to other flow situations with similar characteristics.

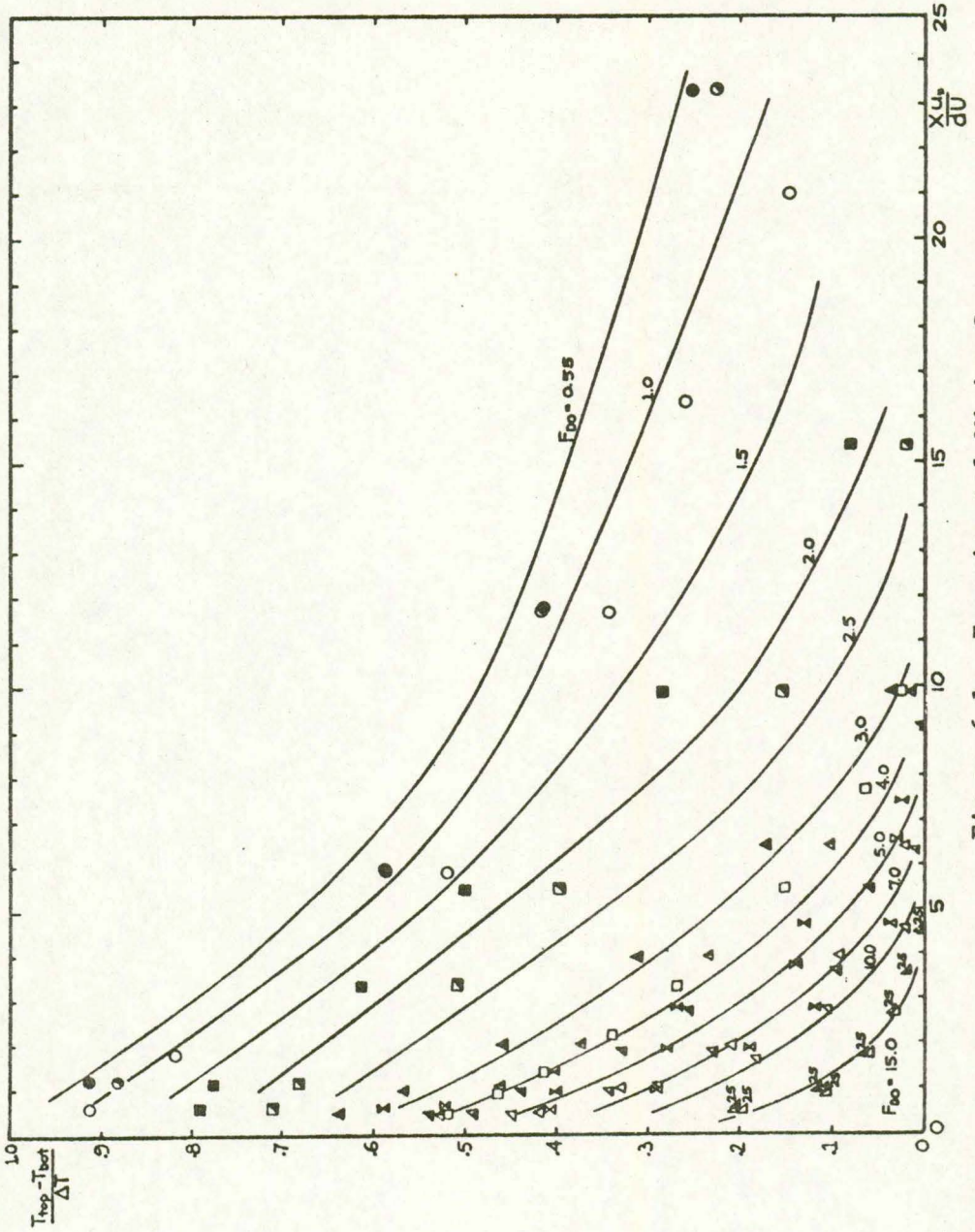

Figure 6.1: Experimental Mixing Curves, $(T_{top}-T_{bot})/\Delta T$ vs. $Xu_*/(dU)$.

The curves also are dependent upon the rate of cooling, this being especially so for the more stratified flows. During these tests, the air temperature varied from 69.5° - 75.5°F and the relative humidity range was 70% - 84%. Finally, the curves in Fig. 6.1 are dependent on the actual temperatures because of the nonlinear relationship between ρ and T. Therefore the curves in Fig. 6.1 would only be applicable within the range of environmental conditions for which it was prepared. It would also be necessary to scale properly the heat loss rate in applying these experimental results to the prototype situation. Granting the above limitations, curves like the ones in Fig. 6.1 could still be useful in the field for predicting the degree of mixing in a given prototype situation for which the experimental flume is a reasonable model.

2. Bulk Mixing Coefficient: Another approach to the degree of mixing can be obtained by the use of the bulk mixing coefficient. For rapidly and moderately mixing flows, values of K_y appropriate for a given initial densimetric Froude number can be selected from Fig. 5.17. This value of K_y can then be used with the Fickian Equation (3.32) to predict the temperature profile at any downstream cross section. In a later section, solutions of Eq. 3.32, obtained by both analytical and numerical methods, are presented for some selected flow conditions.

B. Vertical Heat Transfer Coefficient

The experimental data has indicated a dependence of E_{Ty} upon F_{DX}. It now remains to find a functional link between these two parameters, so that given F_{DX} we may determine E_{Ty}. Since at this

time a theoretical relationship is not available, an empirical relationship has been derived. The relationship used was the beta distribution from probability theory, which was fitted to the experimentally determined distributions of E_{Ty}.

1. Beta Distribution: The beta distribution can be expressed as,

$$B(\eta;t,r) = \frac{\Gamma(t)}{\Gamma(r)\Gamma(t-r)}\,\eta^{r-1}(1-\eta)^{t-r-1} \qquad t\geq 0,\ r\geq 0 \tag{6.1}$$

This distribution was chosen because it has been proven to be a very versatile distribution in describing empirical data. It is able to produce curves of a wide variety of shapes including ones which closely approximate the experimentally determined E_{Ty} distributions. In particular, when the values of the parameters are r = 2 and t = 4, a parabolic curve is generated, so that Eq. 3.30, the limiting case for a well mixed flow, can be exactly represented.

If the area under the experimental curves of $E_{Ty}/r_b u_*$ vs. η are subdivided into seven rectangular increments (based on the seven sampling points) having area a_i, the mean and the second moment can be estimated by numerical integration.

Mean:
$$E(\eta) = \frac{r}{t} = \frac{\sum_{i=1}^{7} \eta_i a_i}{\sum_{i=1}^{7} a_i} \tag{6.2}$$

Second Moment:
$$E(\eta^2) = \frac{(r+1)r}{(t+1)t} = \frac{\sum_{i=1}^{7} \eta_i^2 a_i}{\sum_{i=1}^{7} a_i} \tag{6.3}$$

Eqs. 6.2 and 6.3 are sufficient to determine r and t. It remains to define an area correction factor, C_a. Integrating Eq. 6.1 yields,

$$\frac{\Gamma(t)}{\Gamma(r)\,\Gamma(t-r)} \int_{\eta=0}^{1} \eta^{r-1}(1-\eta)^{t-r-1}\,d\eta = 1$$

or,

$$\int_{\eta=0}^{1} \eta^{r-1}(1-\eta)^{t-r-1}\,d\eta = \frac{\Gamma(r)\,\Gamma(t-r)}{\Gamma(t)}$$

We now define C_a as follows,

$$C_a \int_{\eta=0}^{1} \eta^{r-1}(1-\eta)^{t-r-1}\,d\eta = \sum_{i=1}^{7} a_i$$ = the area under the experimental curve

Thus

$$C_a = \sum_{i=1}^{7} \frac{a_i\,\Gamma(t)}{\Gamma(r)\Gamma(t-r)} \qquad (6.4)$$

Finally, after combining terms,

$$\frac{E_{Ty}}{r_b u_*} = C_a\,\eta^{r-1}(1-\eta)^{t-r-1} \qquad (6.5)$$

For a given $E_{Ty}/r_b u_*$ vs. η distribution Eqs. 6.2, 6.3, and 6.4 will yield the parameters t, r and C_a. For every cross section considered, the values of t, r and C_a were then plotted against the value of the gross densimetric Froude number of the section, F_{DX}. Curves were then fitted graphically to each of the three resulting relationships as shown in Figs. 6.2, 6.3 and 6.4. The dashed lines represent the beta distribution parameters computed by numerical integration for the limiting parabolic distribution of E_{My}. The exact parameters to fit the limiting parabolic distribution would be t = 4, r = 2 and $C_a = \frac{dK}{r_b} \simeq 0.45$. However because of relatively large, unequal increments used, the numerical integration procedure yielded actual values that were somewhat lower than the exact theoretical values.

The following criteria were used in selecting cross sections

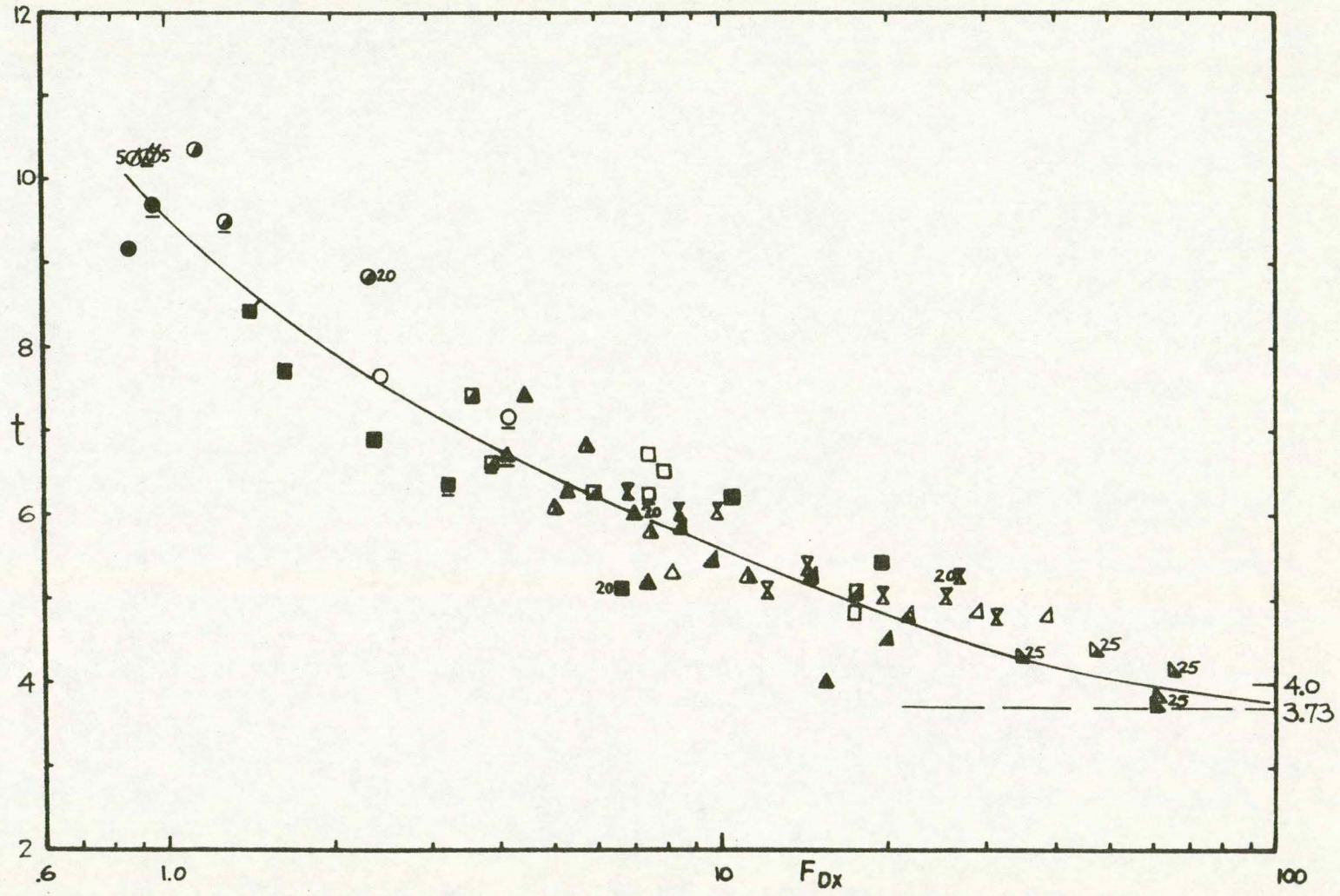

Figure 6.2: Beta Distribution Parameter t vs. F_{DX}.

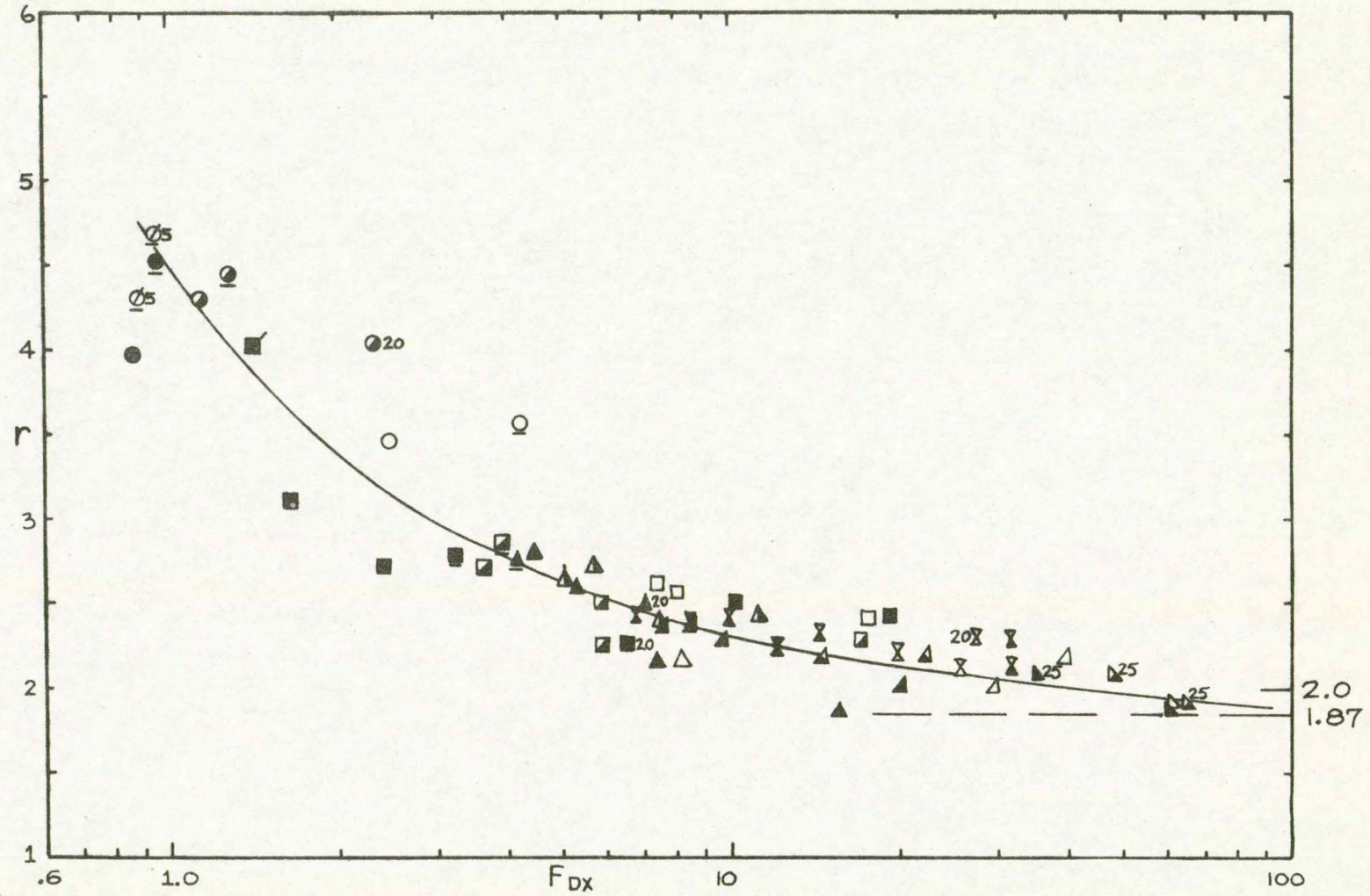

Figure 6.3: Beta Distribution Parameter r vs. F_{DX}.

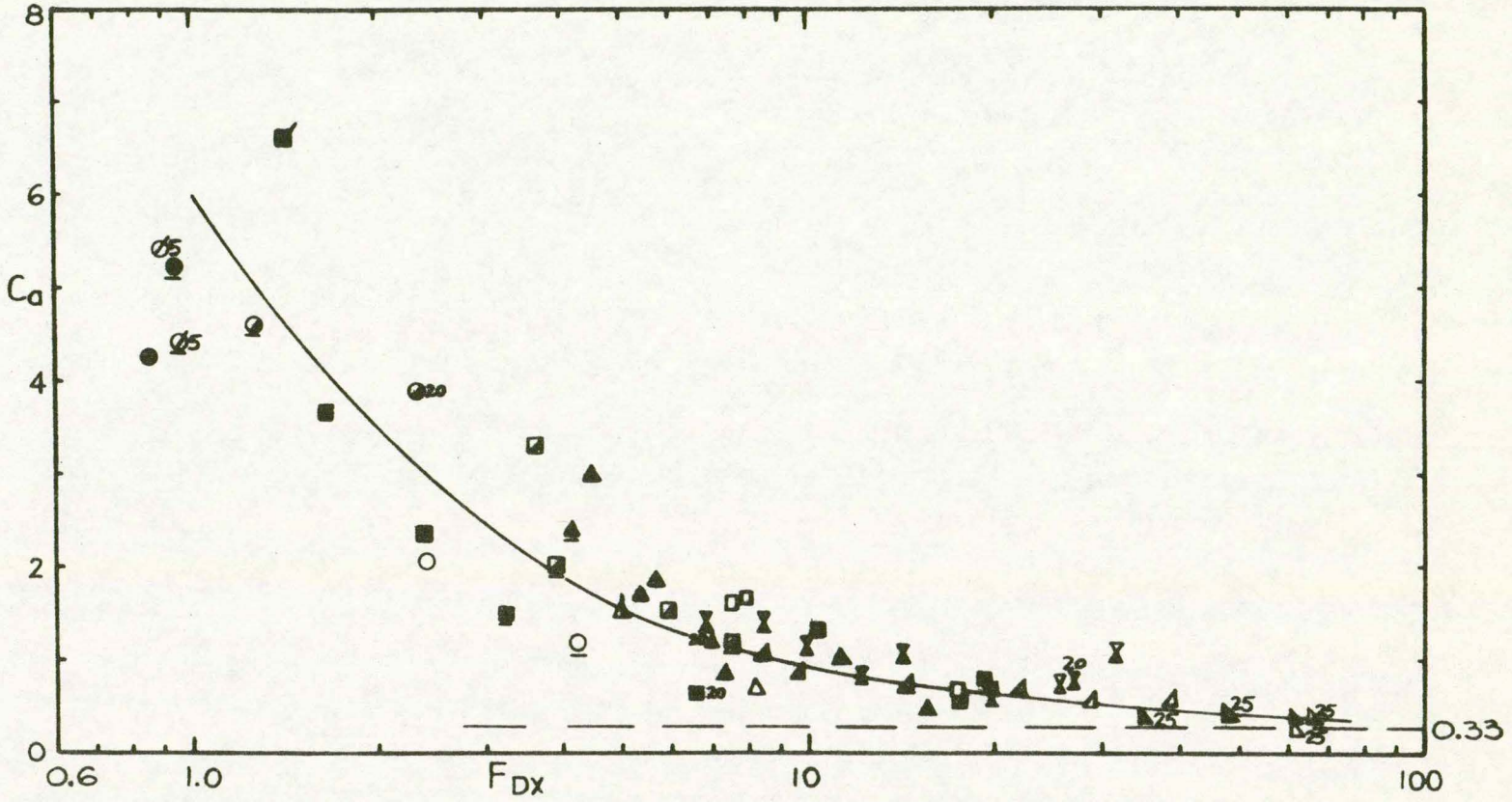

Figure 6.4: Beta Distribution Area Correction Factor Ca vs. F_{DX}.

for the data plotted in Figs. 6.2, 6.3 and 6.4. All cross sections had to meet the previously stated criterion for the minimum temperature gradient (Eq. 5.15). Cross sections meeting this criterion were then chosen from all A-entry, 0.25 ft. depth runs. From this set of cross sections, five additional borderline cross sections were eliminated, having temperature gradients in the range $0.36 \leq \frac{\partial \overline{T}^{w}}{\partial y} \leq 0.52$. Two other cross sections which were only 10 depths downstream from the spreader were also eliminated. In addition to this set of cross sections, one cross section was included from each of the remaining experimental runs where the temperature gradient criterion was met. In this manner a total of 56 cross sections were selected. The cross sections used in Figs. 6.2, 6.3 and 6.4 are marked with an asterisk in Table A.4.

2. Generalized Curves for E_{Ty} vs. η: Using Figs. 6.2, 6.3 and 6.4, it is possible to estimate the distribution of E_{Ty} for a given F_{DX}. A set of curves showing distributions of E_{Ty} for different values of F_{DX} can thus be obtained as shown in Fig. 6.5.

As indicated by the experimental scatter in the beta distribution parameters, the generalized curves in Fig. 6.5 are the result of a smoothing process. All parameters became more scattered as stratified conditions ($F_{DX} \simeq 1.0$) were approached. However Fig. 6.5 does clearly depict the main trends in the E_{Ty} distribution as the degree of mixing increases. Stratified flows tend to have low values of the vertical heat transfer coefficient. As F_{DX} increases, the values of E_{Ty} increase, and the suppression of E_{Ty} near the free surface is more pronounced for

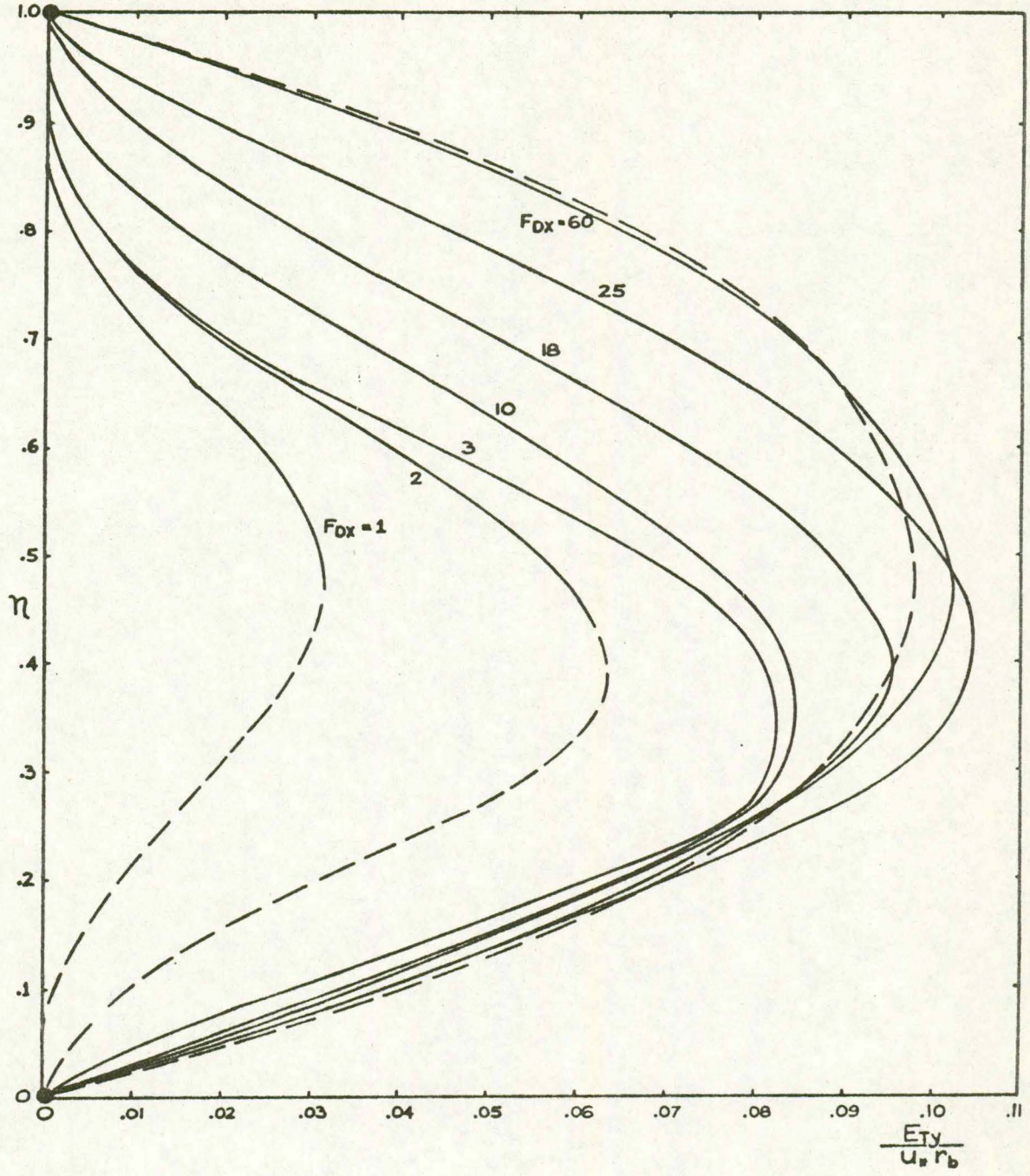

Figure 6.5: Generalized Curves of $E_{Ty}/u_* r_b$ vs. η.

smaller values of F_{DX}. Finally as nearly complete mixing is approached, the warm water tends to become merely a marker for the mixing fluid and the values of E_{Ty} tend to approach those of the mass transfer coefficient E_{My} which is shown with a dashed line in Fig. 6.5.

The distribution of E_{Ty} for $F_{DX} < 3.0$ is marked with dashed lines in the lower half depth of the flow. This is because, although the procedure previously described produced the distribution of E_{Ty} which is depicted, there is some doubt about the physical interpretation of the apparent suppression of mixing at the lower depths. At low densimetric Froude number runs, the flow being relatively stratified, has a small temperature gradient in the lower portion and hence one would expect very little suppression of mixing there. However, the upper layer of heated fluid does tend to alter the secondary flow pattern so vertical convective transfer in the lower depths may be reduced. In any event, even with stratified flows there is a small amount of heat that descends to the lower depths and the model using the given distributions of E_{Ty} seems to predict this quite well. In summary then, with stratified flows, both diffusive and convective transfer are greatly reduced in the upper layer, and convective transfer appears to be reduced in the lower portion also.

For the limiting case of rapidly mixing flows there is reasonably good agreement between $K_y/u_* r_b$ and the normalized depth-averaged value of the vertical heat transfer coefficient $\overline{E_{Ty}}^d/u_* r_b$. There respective values are $K_y/u_* r_b \simeq .0633$ and $\overline{E_{Ty}}^d/u_* r_b \simeq 0.07$. Considering that K_y is based upon Fickian assumptions of constant velocity and

heat transfer coefficient, the above values give reasonably good correlation. At runs with lower densimetric Froude numbers the agreement becomes less precise as the Fickian model represents flows with large density gradients less accurately.

3. Vertical Heat Transfer Coefficient and the Richardson Number: The Richardson number is a local mixing parameter which has been shown to be very sensitive to small disturbances in the velocity distribution. Nevertheless this parameter has been widely used and a number of empirical relationships relating E_{My} and R_i have been derived (16). For cross sections where velocities were measured, values of the vertical heat transfer coefficient normalized by the value of the limiting mass transfer coefficient at the same depth were computed. The ratios $\frac{E_{Ty}}{E_{My}}\Big|_{\eta}$ were then plotted as functions of R_i as shown in Fig. 6.6. The empirical relationship

$$\frac{E_{Ty}}{E_{My}}\Big|_{\eta} = \frac{1}{(1+3.33R_i)^{5/4}} \qquad (6.6)$$

fits the points fairly well and is similar to a relationship derived by Munk and Anderson (16).

Fig. 6.6 substantiates what has been previously said about E_{Ty}. When the degree of mixing is large (i.e. R_i is small) the value of E_{Ty} approaches that of E_{My}. Also as stratification increases (R_i increases), the value of E_{Ty} compared to E_{My} becomes progressively smaller.

The relationship between E_{Ty} and R_i is another way of presenting the mixing parameter and is in good agreement with the

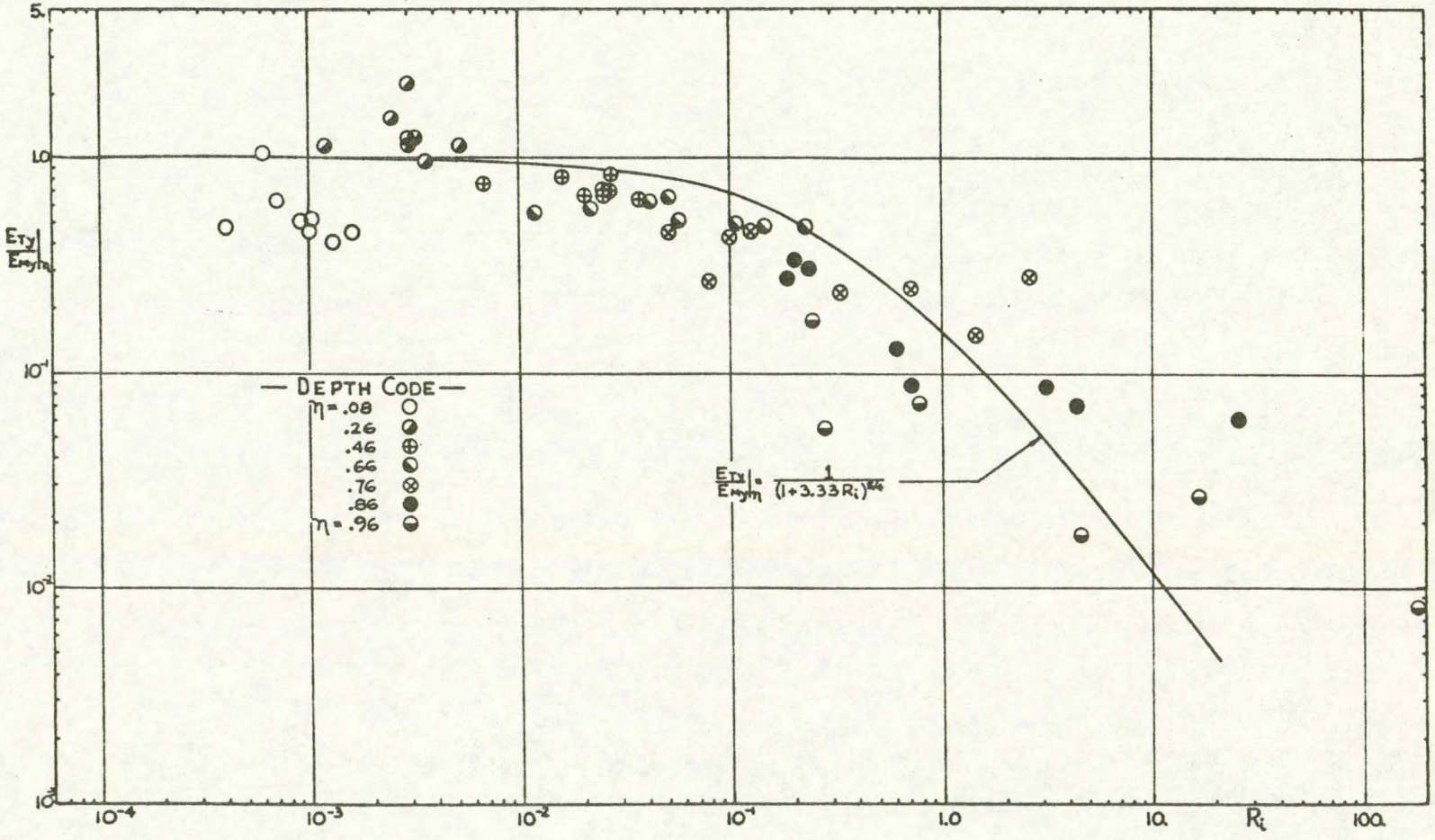

Figure 6.6: Normalized Vertical Heat Transfer Coefficient vs. Richardson Number.

results of other experimenters. However it is not an especially practical form for field applications since the Richardson number as defined here is only a local mixing parameter which is very sensitive to small changes in the velocity distribution. Also, in order for R_i to be a useful parameter, the velocity profile must be known accurately and this is rarely the case in field studies.

C. Convective and Diffusive Components of Vertical Transfer

As previously noted, secondary currents which contribute convective dispersion to the vertical transfer process are present in the flow. An attempt was made to ascertain the relative contributions of convective dispersion and turbulent diffusion. Although no definitive results were obtained, the initial analysis is presented here in the hopes that future investigations will yield an answer to this question.

The presence of a density gradient tends to suppress the well-defined secondary current pattern of the ambient flow. However for the higher velocity flows, as well as for the 0.5-ft.-depth flows, the strong original secondary current pattern tends to persist and influence the vertical mixing process. For some of the runs it was observed that the isotherms as well as the isovels in a cross section were displaced upwards in the updraft and downward in the downdraft regions where the secondary flow had only a vertical velocity component (see Figs. 5.3 and 5.5). At these locations (i.e. $x = x_i$, $z = z_i$) where both $\frac{\partial T}{\partial z} = 0$ and $w = 0$, Eq. 3.8 simplifies to

$$\frac{\partial(uT)}{\partial x} + \frac{\partial(vT)}{\partial y} = \frac{\partial}{\partial y}\left(\varepsilon_{Ty}\frac{\partial T}{\partial y}\right) \qquad (6.7)$$

Integrating Eq. 6.7 from the bottom along a vertical at, x_i, z_i, yields

$$\int_o^y \frac{\partial(uT)}{\partial x}dy + \int_o^y \frac{\partial(vT)}{\partial y}dy = \int_o^y \frac{\partial}{\partial y}\left(\varepsilon_{Ty}\frac{\partial T}{\partial y}\right)dy \qquad (6.8)$$

or,

$$\frac{\partial}{\partial x}\int_o^y (uT)dy + vT\Big|_y - vT\Big|_o = \varepsilon_{Ty}\frac{\partial T}{\partial y}\Big|_y - \varepsilon_{Ty}\frac{\partial T}{\partial y}\Big|_o \qquad (6.8a)$$

Eq. 6.8a, which is referenced to a point x_i, y, z_i, contains two unknowns, v and ε_{Ty}. The values of $\frac{\partial}{\partial x}\int_o^y uTdy$, $\frac{\partial T}{\partial y}$ and T were obtained for adjacent longitudinal x-y planes where only vertical components of secondary flow were assumed to exist. By analogy with Jobson's similar analysis wherein the concentration of sediment was used (12, 13), the value of the temperature T used here was the excess temperature, $T - T_{amb}$. If we assume that the value of ε_{Ty} is constant for a given depth in any cross section and also that in two adjacent planes of updraft and downdraft motion the vertical velocities are equal in magnitude but opposite in direction, then it is possible to apply Eq. 6.8a to these planes and solve for v and ε_{Ty}. This procedure was applied to two runs which had well defined secondary flow patterns (V/25-15/25-25/A and V/50-3/10-25/A), but the results obtained were inconclusive. The direction obtained for the vertical velocity components was often inconsistent with that expected from the isovel pattern for the

flow. Moreover, the magnitudes of the vertical velocity components were very small, being two orders of magnitude less than the average longitudinal velocities for the rapidly mixing flow, and three orders of magnitude less for the stratified flow. Two other methods of solution for Eq. 6.8a described by Jobson (12, 14) were also employed but they also yielded inconsistent results.

The most likely cause of the difficulties here is that the transverse variations in the experimental data were not of sufficient magnitude to reliably evaluate the vertical convective transport. All the methods of solution attempted involved differences in the gradients of the flux terms, $\frac{\partial}{\partial x}\int_0^y uTdy$ and/or the tubulent diffusion transport term, $\varepsilon_T \frac{\partial T}{\partial y}$. Invariably the differences were of an order of magnitude comparable with the probable error in the experimental data upon which they were based. In addition the concept of a longitudinal x-y plane in which there is no net transport in the transverse direction is an idealization which would not be exactly true in the actual flow. Changes in the ambient temperature along the flume were determined to have a negligible effect for both of the runs considered. The influence of heat loss from the bottom would be minimal in the stratified case as the excess heat did not reach the bottom over the reach considered. In the rapidly mixing case the excess heat had just reached the bottom at the cross section under consideration so that bottom heat losses may have been a small contributing factor in this case.

A cautious conclusion that might be advanced, in light of the apparent small magnitudes of the quantities involved, is that in

these experiments convective dispersion is a smaller contributor to the mixing process than turbulent diffusion, and it may even have a negligible influence on the mixing. Also, it appears that in stratified flows convective mixing has less influence than in the more rapidly mixing flows.

D. Prediction of Temperature Distribution

In this section methods for predicting the downstream temperature profiles are described together with the results obtained. Two mathematical models are presented. The first one uses Fickian assumptions in the convective-diffusion equation and the second uses the experimentally determined values of E_{Ty}.

1. Fickian Equation: As previously stated, the Fickian equation

$$U \frac{\partial \bar{T}^w}{\partial x} = K_y \frac{\partial^2 \bar{T}^w}{\partial y^2} \tag{3.32}$$

assumes both a constant velocity, U, and a constant mixing coefficient Ky. In addition, along with the Fickian assumptions, and the assumed reflection conditions at the boundaries, zero heat loss is assumed at the bottom of the flume and at the water surface.

At y = 0:
$$K_y \frac{\partial \bar{T}^w}{\partial y} = 0 \tag{6.9}$$

and at y = d:
$$K_y \frac{\partial \bar{T}^w}{\partial y} = 0 \tag{6.10}$$

For subsequent analysis it is more convenient to work with the dimensionless form of the above three equations. If $\bar{T}^w$ is replaced by the dimensionless term $T_* = (\bar{T}^w - Tamb)/\Delta T$ and if we make the substitutions

$$\mu = \frac{U}{u_*} \qquad \therefore \; U = u_* \mu \tag{6.11}$$

$$\bar{X} = \frac{x}{d} \qquad \therefore \; x = d\bar{X} \tag{6.12}$$

$$\eta = \frac{y}{d} \qquad \therefore \; y = d\eta \tag{6.13}$$

$$\bar{K_y} = \frac{K_y}{d u_*} \qquad \therefore \; K_y = d\, u_* \bar{K_y} \tag{6.14}$$

Then Eq. 3.32 becomes

$$\mu \frac{\partial T}{\partial \bar{X}} = \bar{K_y} \frac{\partial^2 T_*}{\partial \eta^2} \tag{6.15}$$

and the boundary conditions become

at $\eta = 0$: $$\bar{K_y} \frac{\partial T_*}{\partial \eta} = 0 \tag{6.16}$$

at $\eta = 1$: $$\bar{K_y} \frac{\partial T_*}{\partial \eta} = 0 \tag{6.17}$$

In the following discussion dimensionless quantities will be assumed and the distinguishing subscripts and superscripts will be dropped.

(a) Analytical Solution: An analytical solution to the above equations was obtained, a brief outline of which is given below.

For the experimental run which was investigated, the discharge ratio Q_{eff}/Q_{tot} was equal to 1/10 and the effluent water was released into the ambient flow at the average ambient velocity. The initial condition was taken at the spreader and is thus given as

$$X=0,\ 0\leq\eta<0.9\ :\ T=0.0 \tag{6.18}$$

$$X=0,\ 0.9\leq\eta\leq1\ :\ T=1.0 \tag{6.19}$$

A separation of variables technique was used, wherein the solution $T(X,\eta)$ is assumed to be of the form

$$T(x,\eta)=X(x)Y(\eta) \tag{6.20}$$

The general solution of Eq. 6.15 is of the form

$$T(X,\eta)=e^{-\lambda^2 x}\left[C_1\sin\sqrt{\frac{\lambda^2\mu}{K_y}}\,\eta+C_2\cos\sqrt{\frac{\lambda^2\mu}{K_y}}\,\eta\right] \tag{6.21}$$

where C_1 and C_2 are constants and λ is the eigenvalue.

Employing the boundary conditions (Eqs. 6.16 and 6.17) and the initial condition (Eqs. 6.18 and 6.19) eventually yields the particular solution

$$T(X,\eta)=0.1+\sum_{n=1}^{\infty}\frac{-2.\sin(0.9n\pi)}{n\pi}\,e^{-\lambda_n^2 X}\cos\sqrt{\frac{\lambda_n^2\mu}{K_y}}\,\eta \tag{6.22}$$

(b) Finite Difference Form of the Equation: The Fickian form of the convection-diffusion equation (Eq. 6.15) is easily solved by numerical methods. An explicit forward difference scheme yields results with a high degree of accuracy. If we subdivide the flow field into

N rows measured from the flume bottom to the water surface and if we subdivide a unit length of flume into M columns we then have a grid size with dimensions DY = $\frac{1}{N}$ and DX = $\frac{1}{M}$. The temperature T(i,j) is then considered to be the temperature at the center of each grid rectangle located at iDX, jDY. Eq. 6.15 in its forward difference form can then be represented as

$$\frac{T(i,j+1) - T(i,j)}{DX} = \frac{K_y}{\mu} \frac{1}{DY^2}\left[T(i+1,j) - 2T(i,j) + T(i-1,j)\right] \qquad (6.23)$$

so that T(i, j+1) can be solved explicitly as

$$T(i,j+1) = T(i,j) + \frac{DX}{DY^2}\frac{K_y}{\mu}\left[T(i+1,j) - 2T(i,j) + T(i-1,j)\right] \qquad (6.24)$$

The boundary conditions can correspondingly be written, for the bottom row

$$T(1,j+1) = T(1,j) + \frac{DX}{DY^2}\frac{K_y}{\mu}\left[T(2,j) - T(1,j)\right] \qquad (6.25)$$

and for the top row

$$T(N,j+1) = T(N,j) + \frac{DX}{DY^2}\frac{K_y}{\mu}\left[T(N,1) - T(N-1,1)\right] \qquad (6.26)$$

Solutions were obtained numerically for two different initial conditions. In one case the condition at the spreader, X = 0, was used and in the other cases the temperature profile at the first experimentally measured cross section was taken as the initial condition. In each case the initial temperature profile was simply read into the computer at the designated vertical increments of DY = $\frac{1}{N}$. The numerical solution then proceeded stepwise down the flume, printouts being obtained at the cross sections where experimental measurements were taken. As noted by Richtmyer (21), the criterion for stability with this type

of equation is $\frac{DX}{DY^2}\frac{Ky}{\mu} \leq \frac{1}{2}$. In all the calculated runs this condition was easily met. The condition for minimum truncation error, $\frac{Ky}{\mu}\frac{DX}{DY^2} \simeq \frac{1}{6}$, was approximately met for one calculation, V/25-3/10-5/A with DY = .02, where $\frac{Ky}{\mu}\frac{DX}{DY^2} = \frac{1}{8}$, and the results from this calculation were in close agreement with the output for an increased mesh size.

(c) Predicted Temperature Distributions and Experimental Results: In Fig. 6.7 temperature prediction results using the Fickian model are compared with experimentally observed values. The profiles are presented in order of decreasing initial densimetric Froude number, F_{DO}, so that the flow is progressing from rapidly-mixing to stratified. For each case the initial condition is taken as the first measured cross section and the grid sizes are DY = .04 and DX = .01. For run V/25-3/10-5/A the grid size DY = .02, DX = .01 is also used. In addition, for this run the temperature profile is predicted using the initial condition at the spreader. When plotted as in Fig. 6.7, the output for this numerical solution is indistinguishable from the analytical solution.

A number of points should be noted about Fig. 6.7. First, as was expected, considering the assumptions inherent in the Fickian model, the agreement is best for the rapidly mixing case, and then it gradually deteriorates for the more stratified flows. The boundary condition of $Ky\frac{\partial \bar{T}^w}{\partial \eta} = 0$ implies a zero gradient at the boundary. This is greatly at variance with the physical situation, so that the lack of agreement near the surface is quite large. Also the assumption of constant mixing coefficient Ky implies much more mixing in the upper layers of the flow

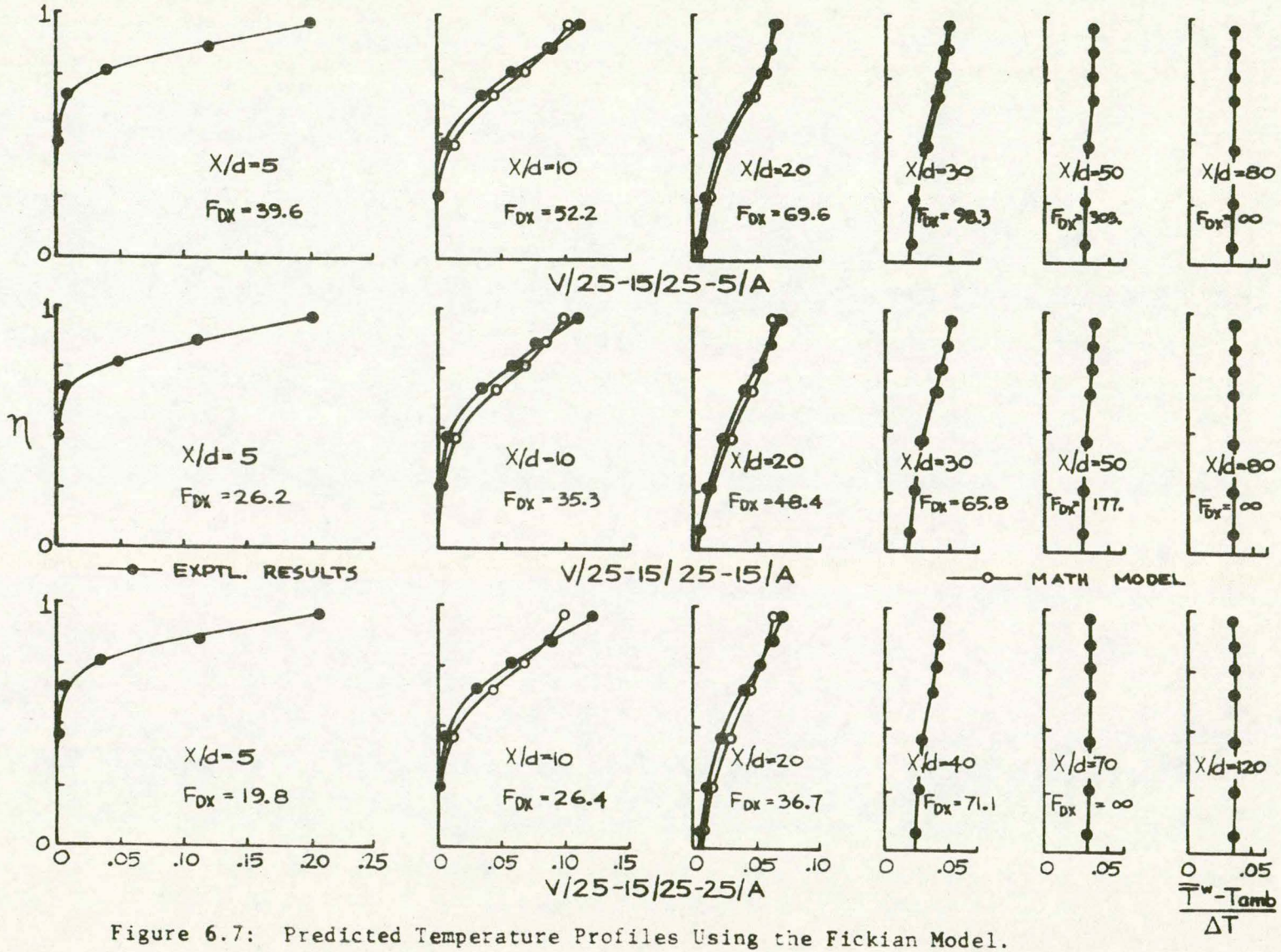

Figure 6.7: Predicted Temperature Profiles Using the Fickian Model.

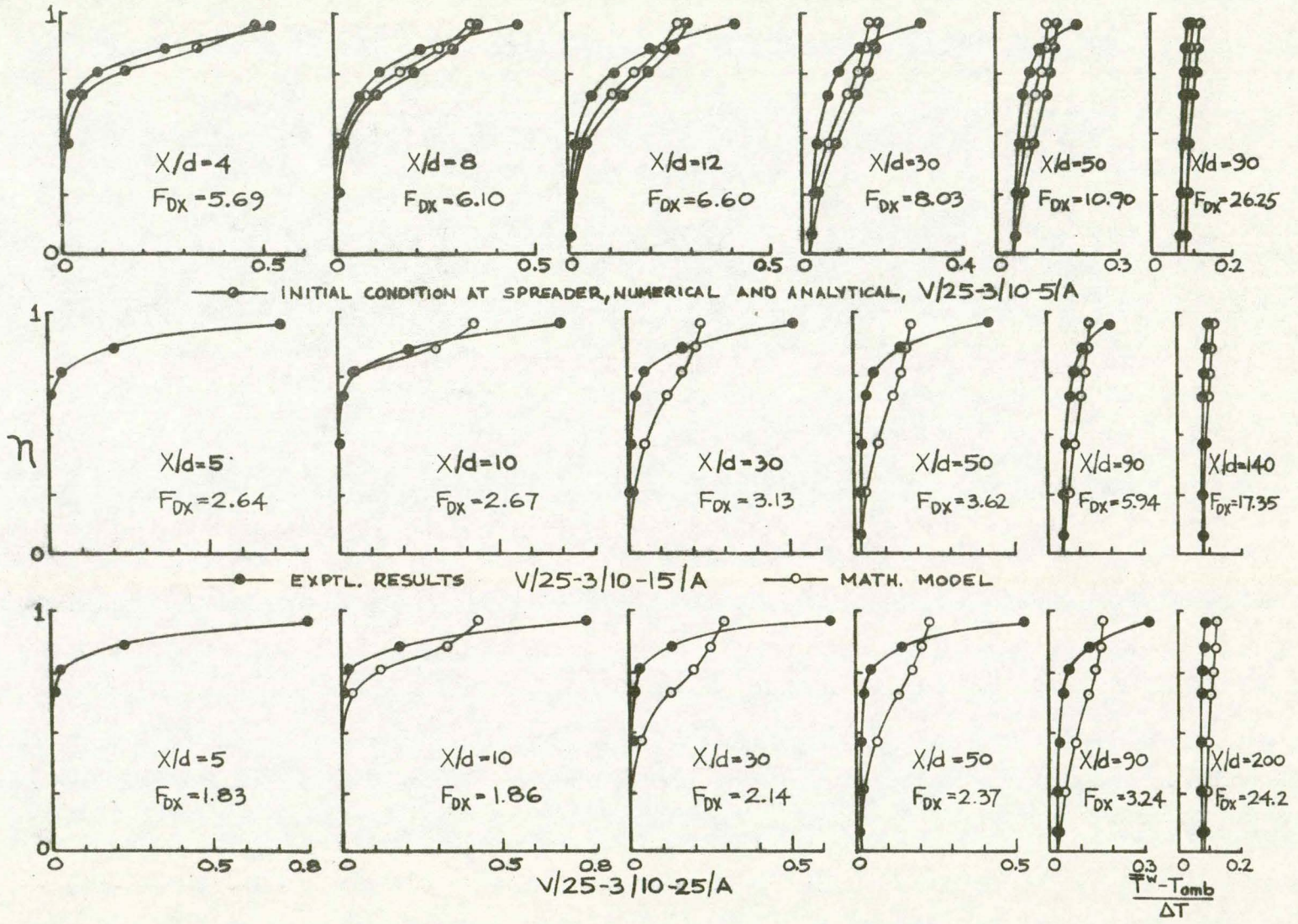

Figure 6.7 (cont.)

than is actually occurring in a flow with a density gradient, so that the Fickian model consistently predicts temperatures that are too low near the surface. Since the Fickian model incorporates the assumption of zero heat loss it is to be expected that the final fully mixed temperature profile depicts a temperature greater than the experimentally observed temperature. The difference between the two temperature profiles represents the heat loss, and this difference increases as the flow becomes more stratified and the cooling losses increase in magnitude.

Comparison of the results using the vertical grid sizes of DY = .04 and DY = .02 in run V/25-3/10-5/A show a high level of agreement, so close in fact, that they are both represented by the same curve. The deviation between the two sets of results was well under 1%, thus indicating that we have a convergent solution. For the same run, using the spreader temperature profile as the initial condition, the agreement between the analytical solution and the numerical solution was also very precise. For all cross sections the two methods of solution yielded results well within 1% of each other and are again represented by the same curve.

The results based on the initial condition at the spreader show a larger discrepancy over most of the flow depth compared with those based on the first measured cross section. This same phenomenon was noted by Jobson (12,14) in his experiments with neutrally-buoyant dye. The discrepancy is even greater when a variable distribution of E_{Ty} is used. In the next section possible reasons for this discrepancy will be considered.

2. Convection-Diffusion Equation with E_{Ty}: In Chapter III we noted that the convection-diffusion equation could be expressed as

$$\bar{u}^w \frac{\partial \bar{T}^w}{\partial x} = \frac{\partial}{\partial y}\left(E_{Ty} \frac{\partial \bar{T}^w}{\partial y}\right) \tag{3.23}$$

Also the boundary conditions are closely approximated by

$$E_{Ty} \frac{\partial \bar{T}^w}{\partial y} = -\phi_n \quad \text{at} \quad y = d \tag{6.27}$$

and

$$E_{Ty} \frac{\partial \bar{T}^w}{\partial y} = 0 \quad \text{at} \quad y = 0 \tag{6.28}$$

where ϕ_n = the rate of total heat loss at the cross section under consideration.

Again, prior to solving these equations it is expedient to express them in a dimensionless form. The surface boundary condition is expressed in terms of total heat loss which includes heat loss from the ambient flow as well as from the heated effluent. For this reason it was decided not to express the numerator of the dimensionless temperature with T_{amb} as a datum, as in the Fickian equation, but instead with T_E, the equilibrium temperature, as a datum. It will be remembered that T_E is the temperature towards which the water tends, given the existing meteorological conditions. Therefore water above a temperature of T_E can lose some of its heat to the atmosphere, whereas water below that temperature takes up heat from the atmosphere. Thus the dimensionless temperature was expressed as

$$\hat{T} = \frac{\overline{T}^{w} - T_E}{\Delta T} \tag{6.29}$$

where ΔT = Teff-Tamb as previously defined. Other dimensionless scaling factors, obtained in a manner similar to Jobson and Sayre (14), are

$$\frac{y}{d} = \eta \qquad \therefore \qquad y = \eta d \tag{6.30}$$

$$\frac{u}{U} = \mu \qquad \therefore \qquad u = \mu U \tag{6.31}$$

$$\frac{E_{Ty}}{E_{My}^{d}} = \frac{6E_{Ty}}{\kappa d u_*} = \psi \quad \therefore E_{Ty} = \frac{\psi \kappa d u_*}{6} \tag{6.32}$$

$$\frac{x}{U}\frac{\overline{E_{My}}^{d}}{d^2} = \frac{x \kappa d u_*}{6 U d^2} = \overline{X} \therefore x = \frac{6 U d \overline{X}}{\kappa u_*} \tag{6.33}$$

Substituting these into Eq. 3.23 yields

$$\mu \frac{\partial \hat{T}}{\partial \overline{X}} = \frac{\partial}{\partial \eta}\left(\psi \frac{\partial \hat{T}}{\partial \eta}\right) \tag{6.34}$$

Similarly, the boundary conditions become

$$-\psi \frac{\partial \hat{T}}{\partial \eta} = \frac{\phi_n 6 \not{d}}{\kappa \not{d} u_* \Delta T} = \phi \quad \text{at } \eta = 1 \tag{6.35}$$

and

$$\psi \frac{\partial \hat{T}}{\partial \eta} = 0 \quad \text{at } \eta = 0 \tag{6.36}$$

Again, in the following discussion, dimensionless quantities will be assumed and the distinguishing subscripts and superscripts will be dropped.

(a) Finite Difference Form of the Equation: The finite difference form that we are about to formulate is based upon distributions of μ and ψ that vary in the η-direction but are considered constant with respect to x-direction. There are in fact slight variations in velocity in the x-direction especially with the more stratified flows, but these are neglected and a logarithmic velocity profile is used. The distribution of E_{Ty} undergoes noticeable change along the flume length as the flow becomes more fully mixed. Accordingly the flume length was divided into segments separated by the cross sections where experimental readings were recorded. The greater the rate of change in the temperature profiles the shorter these segments tended to be. For each segment the value of E_{Ty} was considered constant with respect to X, and was equal to the value computed at the upstream cross-section. Since a relationship between the gross densimetric Froude number at a cross section, F_{DX}, and the distribution of E_{Ty} had been previously specified, it was possible to calculate a new distribution of E_{Ty} for the next segment. Thus the computation progressed downstream, stopping at each experimental cross section to compute a new distribution of E_{Ty}.

The difference equation was formulated and interpreted as follows. The temperature T(i,j) and the velocity $\mu(i)$ are considered to be acting at the centre of the grid rectangle located at iDX, jDY. The normalized heat transfer coefficient $\psi(i,j)$ is the value at the

bottom edge of the grid rectangle at iDX, jDY. Eq.6.34 can then be expressed in explicit forward difference form as

$$\frac{\mu(i)}{DX}\left[T(i,j+1)-T(i,j)\right]=\frac{1}{DY^2}\left\{\psi(i+1)\left[T(i+1,j)-T(i,j)\right]\right.$$

$$\left.-\psi(i)\left[T(i,j)-T(i-1,j)\right]\right\} \quad (6.37)$$

so that T(i, j+1) can be solved for explicitly as

$$T(i,j+1)=T(i,j)+\frac{DX}{DY^2}\frac{1}{\mu(i)}\left\{\psi(i+1)\left[T(i+1,j)-T(i,j)\right]\right.$$

$$\left.-\psi(i)\left[T(i,j)-T(i-1,j)\right]\right\} \quad (6.38)$$

Similarly the difference equations for the boundary conditions become at the flume bottom

$$T(1,j+1)=T(1,j)+\frac{\psi(2)\,DX}{DY\,\mu(1)}\left[T(2,j)-T(1,j)\right] \quad (6.39)$$

and at the water surface

$$T(N,j+1)=T(N,j)-\frac{DX\;\psi(N)}{DY^2\,\mu(N)}\left[T(N,j)-T(N-1,j)\right]-\frac{\phi\,DX}{\mu(N)DY} \quad (6.40)$$

The entire computer program for predicting temperature profiles is given in Appendix B, along with the program for the Fickian model. Again the criterion for stability is that the coefficient of the temperature difference $\frac{DX}{DY^2}\frac{\psi}{\mu}$ be less than 1/2. This coefficient now is variable, but for all runs the criterion for stability was met.

(b) Predicted Temperature Distributions and Experimental Results: The convection-diffusion equation (Eq. 6.34) with the empirical distribution functions for E_{Ty} was used to predict temperature profiles for 5 representative runs, ranging from rapidly-mixing (F_{DO}=8.28) to stratified flow (F_{DO}=1.2). The profiles in Fig. 6.8 show that, unlike the Fickian model, the use of a variable E_{Ty} permits a reasonably accurate prediction of temperature profiles over this wide range of flow conditions.

For all runs a computation was made using DX = .0001 and DY = .04. The choice of DY = .04 was determined by the fact that the highest level at which a thermistor reading could be made for the 0.25 ft. depth flows was at η = .96. Use of an incremental depth smaller than .04 would involve extrapolation beyond the experimental data into a region where high temperature gradients are known to exist. However, for two runs (V/25-3/10-5/A and V/25-3/10-25/A) computations were made with smaller values of DY and the results revealed interesting qualitative information about the nature of the temperature profile very near the surface.

Good agreement between experimental data and the results using the predictive equation is obtained for all runs when $\eta \leq 0.86$. For almost all selected cross sections the difference in this range was within $\pm$2.5%. Larger discrepencies, however, occurred in the uppermost region. The differences in the depth range η=0.86 to 0.96 for these selected runs fell within the range of $\pm$20% based on the normalized temperature as defined here. Above η=.96 large temperature gradients

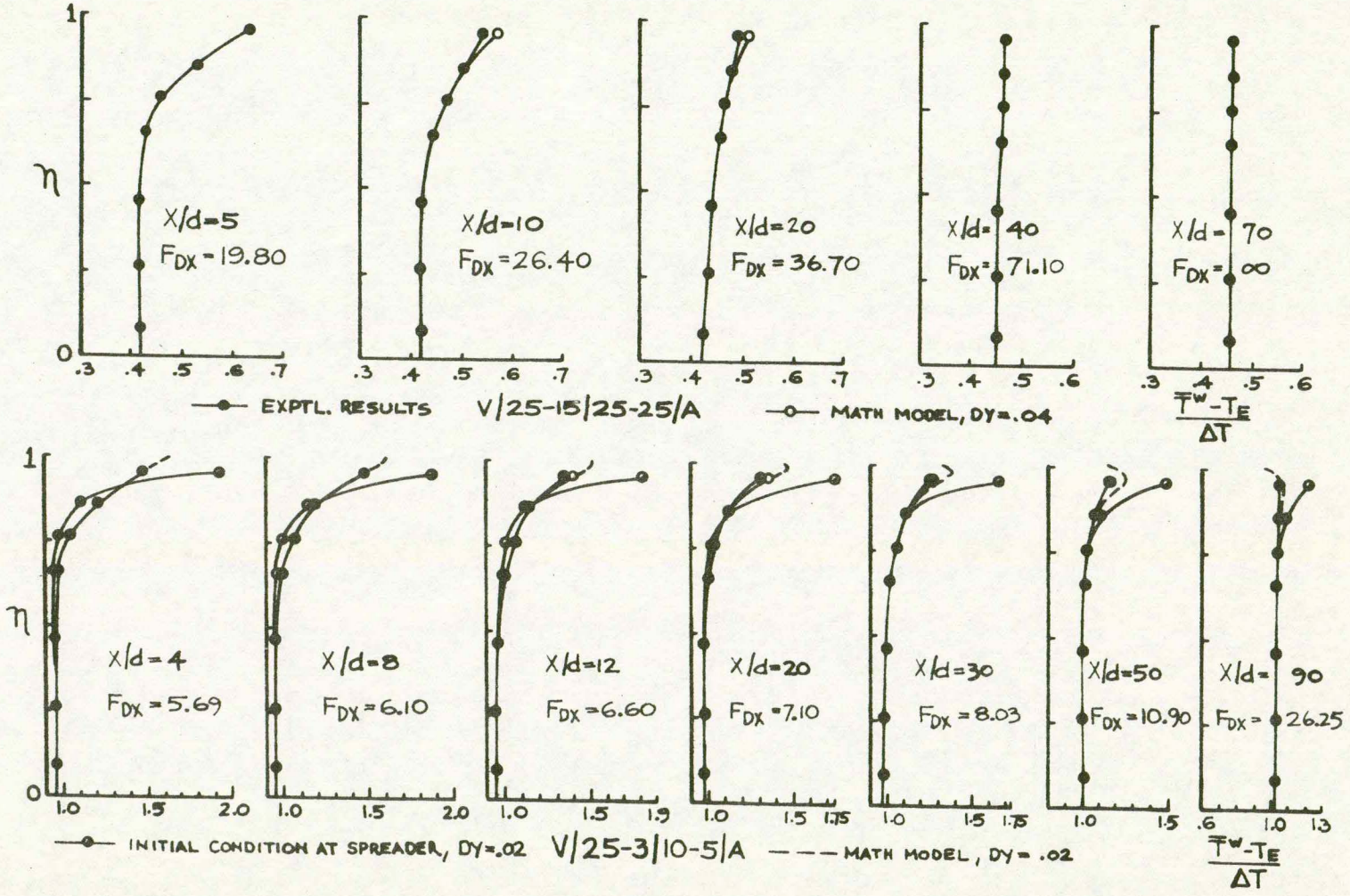

Figure 6.8: Predicted Temperature Profiles Using Empirical Distribution Functions for E_{Ty}.

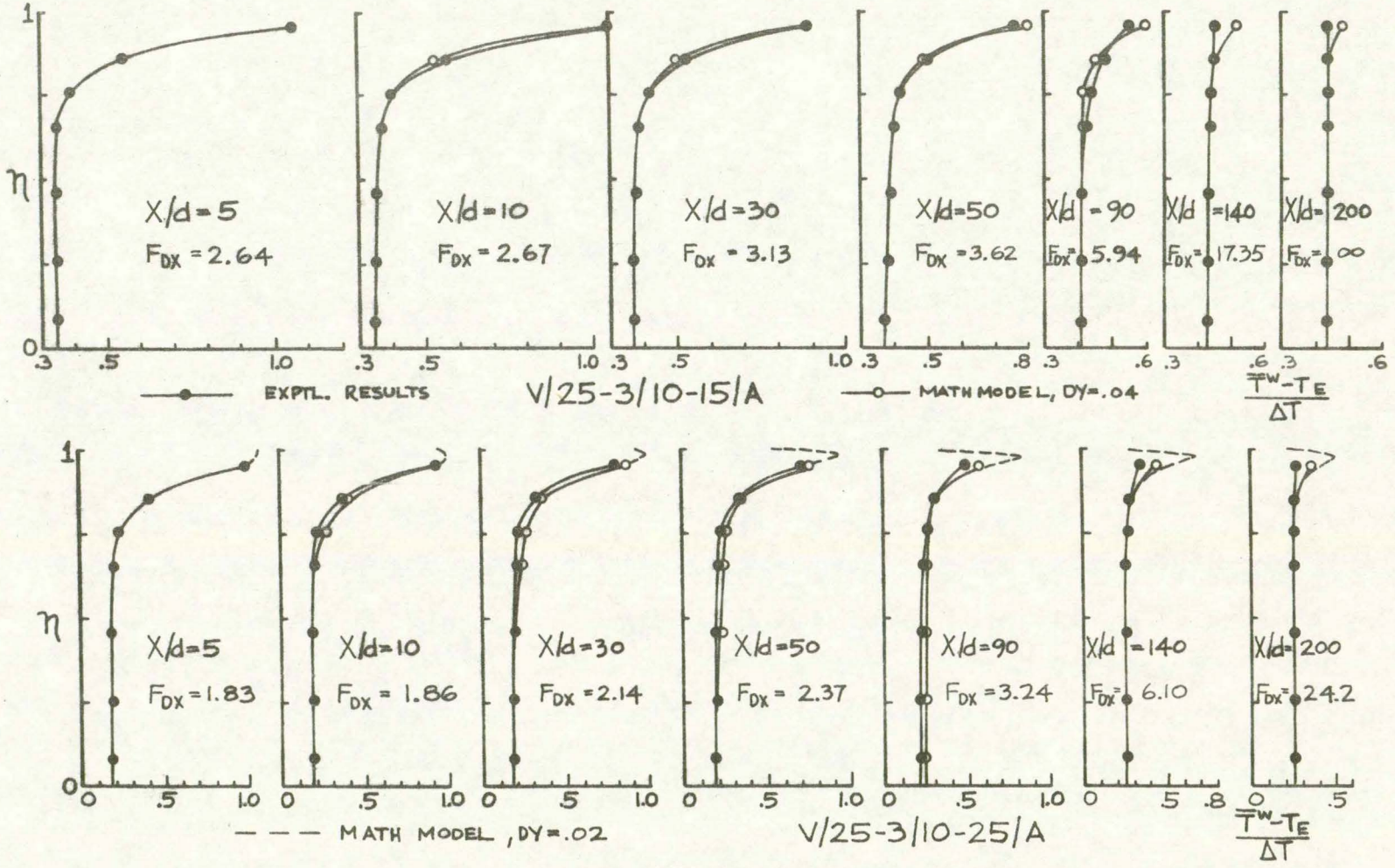

Figure 6.8 (cont.)

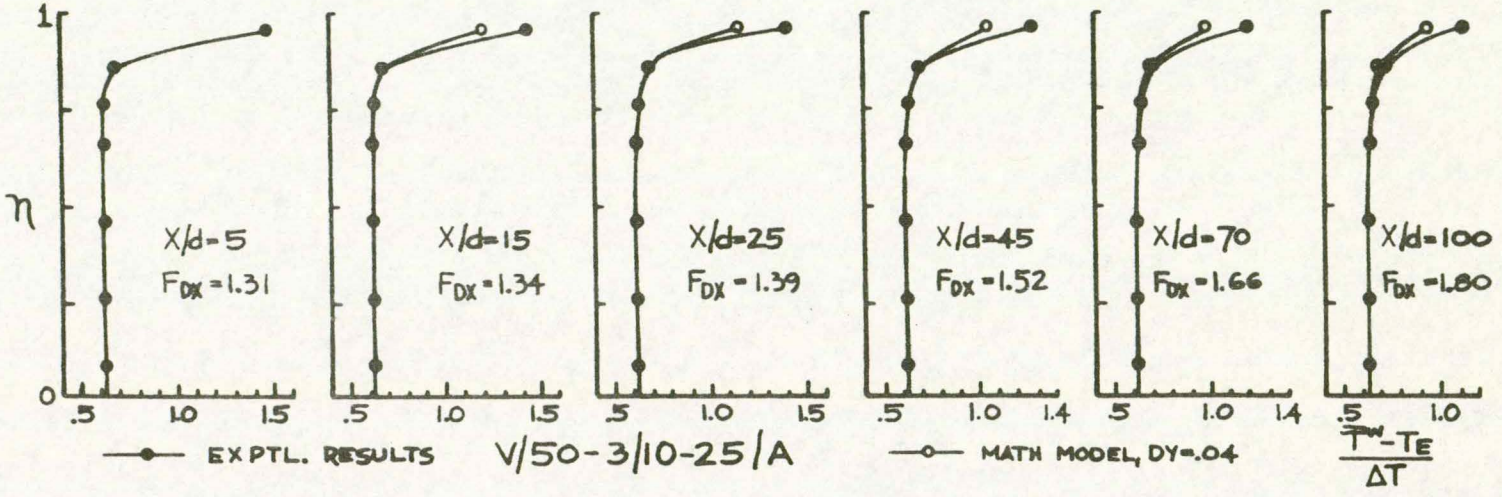

Figure 6.8 (cont.)

were predicted that could not be verified experimentally.

The main causes for the discrepancies in the temperature prediction near the surface are likely two-fold (1) inadequate knowledge of the exact surface heat loss rate and (2) the difficulties in extrapolating from the experimental data to the water surface.

The analysis here is based on the assumption of total heat loss through the upper water surface. It has been previously shown that this is a reasonably accurate assumption although there are surely small heat losses through the sides and the bottom. The presence of these losses would alter the actual heat loss through the water surface and thus account for some deviations in the observed and predicted temperatures near the surface.

Not only the magnitude of the heat losses, but the rate of change of the heat loss along the flume was not known with complete certainty. The heat losses used were those measured experimentally. For each cross section the heat loss was calculated as the difference in the total heat flux between the cross section at the spreader and the cross section under consideration. The heat flux at a cross section was computed using a simple rectangular integration rule with the width-averaged temperature values at the seven measured depths. This method of computation becomes more accurate as the flow becomes mixed but consistently overestimates the heat flux when the temperature gradient reverses sharply, as occurs near the spreader. For this reason curves of heat loss vs. flume length had to extrapolated back from the downstream locations of the flume (where the readings

were more reliable) to the upstream positions near the spreader (where the heat loss readings were less reliable). In addition to the above uncertainty there was an apparent high rate of heat loss very near the spreader. This was probably due to high radiative and convective heat losses as the heated effluent exited from the spreader. Unfortunately it was in this same region where it was least possible to accurately monitor the heat loss rate. Because of all of these uncertainties in computing the true heat loss rate, errors occurred in the predicted temperatures near the surface.

The second reason for discrepancies in predicting temperatures very near the surface, especially when an incremental step size smaller than DY=0.04 was used, is the use of the mathematical model to extrapolate beyond the range of experimental data into a region of large temperature gradients. It is known that for a heat loss to be occurring at the surface a reverse temperature gradient must occur near the surface. This phenomenon, however, was never recorded with our thermistors. The thermistors were situated as close to the water surface as possible for the 0.25 ft. depth flows (η=0.96) without being exposed to the air. One can therefore conclude that the layer over which the reverse temperature gradient occurs is very thin indeed. It is interesting to note that by decreasing the vertical step size DY it is possible to extrapolate beyond the experimental data with the predictive equation and actually predict a reverse temperature gradient. The difficulty is that since the temperature differences are very large and the vertical distances involved are very small, the temperature gradients are thus extremely large

(especially in the more stratified flows) and cannot reliably be represented except at a step size so small that the computing cost would tend to be prohibitive. There is an additional source of error in the uncertainties of the value of ψ near the surface, though the predicted temperature profiles were shown to be relatively insensitive to small changes in the value of ψ near the surface. In spite of these difficulties, a good qualitative picture emerges as to the nature of the temperature profiles near the surface.

In run V/25-3/10-5/A computations were made using DY=.02 (DX=.0001 and DX=.00001) and DY=.01 (DX=.00001). These computer results indicate that the depth over which the reverse temperature gradients exist is very thin at first and it gradually grows in depth as one proceeds downstream. The magnitudes of the temperature predictions near the surface are not to be trusted, since at these high temperatures gradients high precision is not possible. The output with DY=.04 represents an averaged value of the temperature profile near the surface. At all step sizes the values were stable and convergent at the lower depths ($\eta<.86$), so that the deviations near the surface reasonably can be supposed to be due mainly to the cooling effect near the water surface. For the run V/25-3/10-25/A with DY=.02, the same general phenomenon is present. Here the temperature gradients are even higher so that the computed temperature profiles near the surface vary even more. Again, the values of the predicted temperatures near the surface should be considered as only qualitatively valid.

All of the predictive computations, except one, used the

first measured temperature profile as the initial condition. For the run V/25-3/10-5/A a computation was made based on the temperature profile at the spreader as the initial condition. It can be seen that the correlation with the measured temperature profiles is poor. This is due to the fact that the convection-diffusion equation does not accurately predict the mixing phenomena near the spreader. Jobson (12, 14) found the same difficulty in predicting the concentrations of neutrally-buoyant dye. The reasons that he gave are likely also operative in the case of heated effluents. They are that in this region (1) the longitudinal temperature gradient $\frac{\partial \bar{T}^w}{\partial x}$ is not small as assumed in the derivation of the working form of the convection-diffusion equation (Eq. 3.23), (2) the concept of a gradient-type heat transfer mixing coefficient E_{Ty} is not valid until the thickness of the plume in the direction of transfer becomes larger than the eddies that are causing the transfer and (3) near the spreader the largest change in the magnitude of E_{Ty} occurs so that the assumption of E_{Ty} as constant with respect to X between consecutive sections is weakest in the region just downstream from the spreader.

3. Applicability of the Results: The preceeding analysis can be used to predict the downstream temperature profiles in a straight channel with two-dimensional uniform flow if the temperature profile at an upstream cross section is known. The conditions described in this thesis would be most likely to exist in a cooling canal or in a straight stretch of river.

The more rapidly mixing the flow, the more easily the

temperature profiles can be predicted. One reason for this is that the influence of the surface cooling on the temperature profile is less critical for rapidly mixing flows. In fact the Fickian model, which assumes zero heat loss, yields a reasonably good approximation ($\pm$ 20%) to the actual measured temperature profiles for flows with initial densimetric Froude numbers greater than about 8.0.

In applying the convection-diffusion equation with variable E_{Ty}, the rate of surface heat loss along the reach under investigation must be known. In an actual field situation, the heat loss models proposed by various investigators (3, 4, 10, 23) would have to be used to obtain the proper boundary condition at the surface. The influence of the surface heat loss becomes more important as the densimetric Froude number decreases. As the initial densimetric Froude number approaches unity, the cooling loss rate can be the main factor controlling the change in downsteam temperature profiles. It thus becomes clear that for the flows with lower initial densimetric Froude numbers, significant errors in the estimated heat loss rate will lead to corresponding errors in the predicted temperature profiles.

In the laboratory flume the smallest vertical grid increment for practical results was limited by the distance from the water surface to the uppermost measuring point. In the prototype situation where the length scales would be much larger, it may be possible to measure reverse temperature gradients near the water surface. This phenomenon could then be read into the initial temperature profile and the computer program could be expected to predict the variation in

temperatures near the surface more accurately than in the flume. In any case the minimum vertical step size would likely still be determined by the distance between the water surface and the highest level at which temperatures could be reliably measured.

In predicting the temperature distributions, the vertical distribution of E_{Ty} was considered constant over relatively large longitudinal intervals, corresponding to the distances between cross-sections where experimental readings were taken. For the run VR/25-3/10-25/A with DX = 1/10,000 and DY = .04 and 0.02 , computations were made wherein the distribution of E_{Ty} was updated at longitudinal intervals equal to one depth. By thus varying the vertical distribution of E_{Ty} along the flume length more frequently the temperature prediction was improved by about 5%, so that the predicted temperature profiles were within 15% of the experimentally measured values. For practical applications a longitudinal interval of about one river depth is recommended as the distance over which the distribution of E_{Ty} can be assumed to be constant.

Chapter VII

SUMMARY AND CONCLUSIONS

A. Summary

The vertical mixing, due to ambient turbulence, of a heated effluent downward from the free surface into an open-channel flow was investigated experimentally in a laboratory flume. A total of 44 experimental runs were conducted covering the range from very rapidly mixing flows to highly stratified flows. Parameters that were varied in these tests were depth of flow, average velocity, the ratio of effluent discharge to total discharge, entrance velocity of the effluent flow and the temperature difference between the effluent and ambient flows. For all flows extensive temperature distribution data at several cross sections were obtained and for some selected flows extensive sets of velocity profiles were also measured.

The experimental data yielded a direct measurement of the distance required for mixing for each run. More detailed analyses were based on the simplified Fickian form, and the width-averaged form of the steady-state convection-diffusion equation. The latter analysis included the heat transfer at the water surface. The two mixing coefficients derived from the above analyses were the bulk vertical mixing coefficient, K_y, and the y-dependent vertical heat transfer coefficient, E_{Ty}. The first parameter was presented as a function of the initial

densimetric Froude number of the flow, F_{DO}. The y-dependent vertical heat transfer coefficient was related to both the gross cross-sectional Froude number F_{DX}, and the width-averaged Richardson number, R_i. Finally the above mixing parameters were used with the convection-diffusion equation to mathematically model downstream temperature profiles for some selected runs.

B. Conclusions

The vertical mixing process has been described using several different parameters which are presented below. In general the results are presented in order of increasing detail and improved ability to portray the physical phenomena realistically.

(1) An experimental curve (Fig. 5.16) has been defined giving the dimensionless length $\frac{X_{0.2}u_*}{dU}$ necessary to achieve nearly complete mixing, i.e., $\frac{T_{top} - T_{bot}}{\bar{T}_x - T_{amb}} = 0.2$. $\frac{X_{0.2}u_*}{dU}$ was found to decrease from about 55 at $F_{DO} = 0.5$ to an asymptotic value of about 4.2 for $F_{DO} \geq 10$. Though the environmental conditions were not constant for all tests, the variation from test to test was sufficiently limited, so that the data for all flow conditions are described by a well-defined curve.

(2) Using the Fickian model and the reflection condition at the boundaries, experimentally-determined values of the bulk vertical mixing coefficient, K_y, were obtained for most experimental conditions, except for the most stratified flows for which the analysis is inapplicable. A plot of the dimensionless bulk vertical mixing coefficient as a function of the initial densimetric Froude number, F_{DO}, was obtained

(Fig. 5.17). The value of $K_y/u_* r_b$ increases from a value of about 0.005 at $F_{DO} \simeq 1.0$ to an asymptotic value of about 0.063 for $F_{DO} \geq 10$. Using these values of K_y with the simplified Fickian form of the convection-diffusion equation, is possible to predict with reasonable accuracy ($\pm 20\%$) the form of the downstream temperature profiles for rapidly mixing flows ($F_{DO} \geq 8.0$).

(3) The normalized y-dependent vertical heat transfer coefficient $\left.\frac{E_{Ty}}{E_{My}}\right|_\eta$ has been plotted as a function of the local width-averaged Richardson number, R_i (Fig. 6.6). The resultant empirical relationship, $\left.\frac{E_{Ty}}{E_{My}}\right|_\eta = \frac{1}{(1+3.33\ R_i)^{5/4}}$ agrees well with the results of other experimenters. The curve shows that E_{Ty} approaches the value of the vertical mass transfer coefficient, E_{My}, for well mixed flows (low R_i). The tendency for E_{Ty} to decrease markedly for stratified flows (high R_i) also illustrated.

(4) The Richardson number was found to be not very useful for the purposes of this investigation. This was because it was very sensitive to changes in the velocity distribution and the exact velocity distribution is rarely known in practical cases. Instead of using the local parameter R_i, two other parameters describing the overall mixing tendencies of the flow were used (1) the initial densimetric Froude number $F_{DO} = U/\sqrt{g r_b \Delta\rho/\rho_a}$, and (2) the cross-sectional densimetric Froude number $F_{DX} = U/\sqrt{g r_b \Delta\rho_x/\rho_b}$ for successive cross sections downstream.

(5) Empirical vertical distribution functions for the width-averaged vertical heat transfer coefficient, E_{Ty}, were obtained by

relating parameters of the beta distribution function from probability theory to F_{DX} (Figs. 6.2, 6.3, 6.4, and 6.5). In addition to the same trends for stratified and rapidly-mixing flows as described in (3) above, the empirical distribution functions indicated a distinct reduction of mixing in the uppermost portions of the flow where the temperature gradients were the greatest. Using the appropriate distributions of E_{Ty} for different F_{DX} values, the convection-diffusion equation, solved numerically in a step-wise fashion along the channel, gave vertical temperature distributions for downstream cross-sections. Knowing the surface heat loss, temperature profiles can be determined within reasonable tolerances. The differences of the normalized excess temperatures, $(\bar{T}^W - T_E)/\Delta T$, between the experimental values and the mathematical model were with $\pm$ 2.5% in the lower portion of the flow ($0 \leq \eta < .86$) and within $\pm$ 20% for the uppermost part of the flow ($0.86 < \eta \leq .96$) for the range of runs considered ($1.2 \leq F_{DO} \leq 8.3$).

C. Practical Applications

Various techniques for predicting downstream temperature profiles, in a straight channel with a heated effluent introduced at the surface, were devised during the course of this investigation.

Given a situation with the limited range of environmental conditions that were present during these tests (i.e., essentially summer conditions) it is possible to determine the length of channel necessary for nearly complete mising (F.g 5.16).

With rapidly mixing flows ($F_{DO} \geq 8.0$) temperature profiles can be computed using the Fickian equation as the mathematical

predictive model to a good order of accuracy. The heat loss rate need not be known and the computer program for solving this equation is simple and straightforward. If no computer is available, an analytical solution can be readily obtained.

For flows where the mixing is significantly inhibited by buoyancy effects, one must resort to the convection-diffusion equation using the empirical distribution functions for E_{Ty}. It is then necessary also to estimate the rate of surface heat loss.

One of the accomplishments achieved in this thesis is that buoyancy effects due to the heated effluent have been accounted for in the distribution of E_{Ty}. This approach does not describe all the mechanisms at work due to the presence of the heated effluent, but it does yield a practical method of predicting downstream temperature profiles, even for flows of a partially stratified nature. It is hoped that a start has been made toward the prediction of temperature profiles in more complex cases.

D. Suggestions for Future Research

During the progress of this research project various problems were encountered which were not investigated in detail. These phenomena could be topics for future research.

(1) Secondary currents, which have been described in this thesis, contribute convective dispersion to the vertical mixing process. Further investigations could determine the magnitude of these effects as well as attempt to derive a mathematical model to describe this phenomenon.

(2) It has been shown that the presence of a vertical density

gradient can alter the velocity distribution of the flowing stream. Further investigation may yield a workable mathematical model for describing this phenomenon, which would have utility for predicting velocity variations in stratified flows.

(3) Flowing heated water which is cooling at the surface apparently has a steep temperature gradient which is confined to a very thin layer near the surface. Further experimental studies, perhaps with the use of a radiometer, together with additional analysis, could help to determine the exact nature of the temperature profile very close to the water surface.

(4) A complete mathematical model for the cooling losses present in the flume was not achieved and verified in this investigation. For tests in the future involving the use of heated water, consideration should be given to insulating the bottom and perhaps sides of the flume. In addition the environmental air temperature and relative humidity should be monitored more frequently at more numerous locations around the flume. Use of a continously recording meteorograph above the water surface is recommended.

(5) This thesis has dealt with a simplified case of nearly two-dimensional, uniform flow in a straight channel. Further investigations could branch out into more complex flow conditions, as for example, the mixing of heated effluents in a meandering channel.

LIST OF REFERENCES

1. Abramovitch, G. N., 1963, The Theory of Turbulent Jets, M.I.T. Press, Cambridge, Mass.

2. Beckett, R. and Hurt, J., 1967, Numerical Calculations and Algorithms, McGraw-Hill, Inc.

3. Brady, D. K., Graves, W. L. and Geyer, J. C., 1969, "Surface Heat Exchange at Power Plant Cooling Lakes", Edison Electric Institute Publication No. 69-901.

4. Edinger, J. E. and Geyer, J. C., 1965, "Heat Exchange in the Environment", Edison Electric Institute Publication No. 65-902.

5. Elder, J. W., 1959, "The Dispersion of a Marked Fluid in a Turbulent Shear Flow", Journal of Fluid Mechanics, Vol. 5, Part 4, pp. 544-560.

6. Ellison, T. H. and Turner, J. S., 1959, "Turbulent Entrainment in Stratified Flows", Journal of Fluid Mechanics, Vol. 6, Part 3, pp. 423-447.

7. Ellison, T. H. and Turner, J. S., 1960, "Mixing of a Dense Fluid in a Turbulent Pipe Flow", Journal of Fluid Mechanics, Vol. 8, Part 4, pp. 514-544.

8. Fischer, H. B., 1967, "The Mechanics of Dispersion in Natural Streams", Journal of the Hydraulics Division, ASCE, Vol. 93, No. HY6, pp. 187-216.

9. Harleman, D. R. F., 1961, "Stratified Flow", Chapter 26 in Handbook of Fluid Mechanics, ed. Streeter, V. L., McGraw-Hill, Inc., pp. 26: 1-21.

10. Harleman, D. R. F. et al, 1972, Engineering Aspects of Heat Disposal, Summer Symposium Notes, Massachusetts Institute of Technology:
Ch. I, "Environmental Heat Transfer" by P. Ryan and K. D. Stolzenbach.
Ch. IX, "Temperature Distributions in the Far Field Region -- Partial Mixing" by J. D. Ditmars.

11. Hickox, G. H., 1946, "Evaporation from a Free Water Surface", ASCE Transactions, Vol. III, pp. 1-66.

12. Jobson, H. E., 1968, "Vertical Mass Transfer in Open-Channel Flow", U. S. Geological Survey, Open-File Report.

13. Jobson, H. E. and Sayre, W. W., 1970, "Vertical Transfer in Open-Channel Flow", Journal of the Hydraulics Division, ASCE, Vol. 96, No. HY3, pp. 703-724.

14. Jobson, H. E. and Sayre, W. W., 1970, "Predicting Concentration Profiles in Open Channels", Journal of the Hydraulics Division, ASCE, Vol. 96, No. HY10, pp. 1983-1996.

15. Kennedy, J. F. et al, 1971, "Hydraulic Relations for Alluvial Streams", Journal of the Hydraulics Division, ASCE, Vol. 97, No. HY1, pp. 101-141.

16. Koh, C. Y. and Fan, L., 1970, "Mathematical Models for the Prediction of Temperature Distributions Resulting from the Discharge of Heated Water into Large Bodies of Water", Water Pollution Control Research Series Report No. 16130DWO, Environmental Protection Agency.

17. Motz, L. H. and Benedict, B. A., 1971, "Heated Surface Jet Discharged into a Flowing Ambient Stream", Water Pollution Control Research Series Report No. 16130 FDQ, Environmental Protection Agency.

18. Parker, F. L. and Krenkel, P. A., 1969, Thermal Pollution: The Status of the Art, Vanderbilt University Press.

19. Parker, F. L. and Krenkel, P. A., 1969, Engineering Aspects of Thermal Pollution, Vanderbilt University Press.

20. Prych, E. A., 1970, "Effects of Density Differences on Lateral Mixing in Open-Channel Flows", Report No. KH-R-21, California Institute of Technology.

21. Richtmyer, R. D., 1957, Difference Methods for Initial Value Problems, Interscience Publishers Inc.

22. Sayre, W. W., 1968, "Dispersion of Mass in Open-Channel Flow", Hydraulics Paper No. 3, Colorado State University.

23. Shen, H.W., ed., 1973, Environmental Impact on Rivers, Shen Publishers:
Ch. 6, "Natural Mixing Processes in Rivers", by W.W. Sayre.
Ch. 10, "Heated Surface Discharges into Flowing Ambient Streams and Lakes", by E. Silberman.

24. Stefan, H. and Hayakawa, N., 1972, "Mixing Induced by an Internal Hydraulic Jump", Water Resources Bulletin, Vol. 8, No. 3, pp. 531-545.

25. Taylor, G.I., 1921, "Diffusion by Continuous Movements", Proc. London Math. Soc., Ser. 2, Vol. 20, pp. 196-211.

26. Stolzenbach, K.D. and Harleman, D.R.F., 1971, "An Analytical and Experimental Investigation of Surface Discharges of Heated Water", Water Pollution Control Research Series Report No. 16130 DJU, Environmental Protection Agency.

27. Turner, J.S., 1973, Buoyancy Effects in Fluids, Cambridge University Press.

28. Weil, J., 1972, "Mixing of a Heated Surface Jet in Turbulent Channel Flow", Waste Heat Management Report WHM-1, University of California at Berkeley.

29. Yeh, T.P., written communication.

30. Yih, C.S. and Guha, C.R., 1955, "Hydraulic Jump in a Fluid System of Two Layers", Tellus, Vol. 7, No. 3, pp. 358-365.

Appendix A

EXPERIMENTAL MEASUREMENTS AND PARAMETERS

Table A.1: Basic Parameters for the Experimental Runs.

Velocity (f.p.s.)	ΔT	Depth = 0.25 ft.								Depth = 0.5 ft.				
		← Entrance Conditions												
		A	B	C	D	A	B	A	A	Slope	A	A	B	A	Slope
0.1	5			X	X	X	X					X	X		
	15	X	X	X	X	X	X	X		1.810×10^{-5}		X	X		8.66×10^{-6}
	25			X	X	X	X								
0.3	5					X	X								
	15					X	X			1.429×10^{-4}					6.928×10^{-5}
	25					X	X	X				X	X		
0.5	5					X									
	15					X				3.247×10^{-4}		X			1.386×10^{-4}
	25					X	X	X							
0.7	5					X									
	15					X		X		5.629×10^{-4}					
	25					X									
0.9	5					X									
	15					X				9.050×10^{-4}					
	25					X									
1.5	5								X						
	15								X	2.338×10^{-3}					
	25								X						
$\varepsilon_{eff}/Q_{tot}$ ⟹		$\frac{1}{5}$		$\frac{1}{10}$				$\frac{1}{20}$	$\frac{1}{25}$		$\frac{1}{5}$	$\frac{1}{10}$		$\frac{1}{20}$	

Table A.2: Abbreviated Summary of Velocity Measurements.

Note: Cross sections in which ten velocity profiles were measured are listed in this table. There were in addition some cross sections, not listed in this table, where only a few selected velocity profiles were measured. In general the cross sections listed in this table were in the zone of best mixing along the flume.

Flow Designation	Cross Section (x/d)	Average κ Value For Middle 8 Readings
V/25-3/0-0 (Ambient Only)	30	0.48
	50	0.47
	90	0.49
V/25-3/10-5/A	30	0.47
	50	0.40
	90	0.44
V/25-3/10-5/B	30	0.49
V/25-3/10-15/A	30	0.44
	50	0.42
	90	0.39
V/25-3/10-15/B	30	0.44
V/25-3/10-25/A	30	0.49
	50	0.45
	90	0.42
	140	0.39
V/25-3/10-25/B	30	0.46
	50	0.42
	90	0.40
V/25-3/20-25/A	50	0.44
	90	0.40
	140	0.43
V/50-3/0-0 (Ambient)	45	0.50
V/50-3/10-25/A	45	0.47
	70	0.40
	100	0.39

Table A.2: (Cont.)

Flow Designation	Cross Section (X/d)	Average κ Value For Middle 8 Readings
V/25-5/0-0 (Ambient)	65	0.41
V/25-5/10-25/A	40	0.36
	65	0.38
	100	0.36
V/25-9/0-0 (Ambient)	10	0.37
	20	0.39
V/25-9/10-25/A	20	0.40
V/25-15/0-0 (Ambient)	5	0.39
	20	0.36
V/25-15/25-25/A	5	0.40

Table A.3: Derived Experimental Parameters.

Code	Run No.	Symbol	r_b (ft.)	u_* (fps.)	$\frac{U}{u_*}$	R_N (Multiply by 10^4)	F_{DO}
V/25-1/10-5/C	1		0.233	0.012	8.57	0.859	1.36
V/25-1/10-5/D	2		0.233	0.012	8.57	0.850	1.35
V/25-1/10-5/A	3	○	0.233	0.012	8.57	0.859	1.32
V/25-1/10-5/B	4	○	0.233	0.012	8.57	0.896	1.27
V/50-1/10-5/A	5	⌀	0.397	0.011	9.51	1.44	0.95
V/50-1/10-5/B	6	⌀	0.397	0.011	9.50	1.46	0.96
V/25-1/5-15/A	7	$\varnothing_5$	0.233	0.012	8.57	0.850	0.69
V/25-1/5-15/B	8	$\varnothing_5$	0.233	0.012	8.57	0.850	0.72
V/25-1/10-15/C	9		0.233	0.012	8.57	0.850	0.70
V/25-1/10-15/D	10		0.233	0.012	8.57	0.859	0.70
V/25-1/10-15/A	11	◑	0.233	0.012	8.57	0.859	0.67
V/25-1/10-15/B	12	◑	0.233	0.012	8.57	0.896	0.71
V/25-1/20-15/A	13	$◑_{20}$	0.233	0.012	8.57	0.850	0.73
V/50-1/10-15/A	14	⌀	0.397	0.011	9.50	1.47	0.53
V/50-1/10-15/B	15	⌀	0.397	0.011	9.50	1.46	0.54
V/25-1/10-25/C	16		0.233	0.012	8.57	0.850	0.58
V/25-1/10-25/D	17		0.233	0.012	8.57	0.850	0.57

Table A.3: (Cont.)

Code	Run No.	Symbol	r_b (ft.)	u_* (fps.)	$\frac{U}{u_*}$	R_N (Multiply by 10^4)	F_{DO}
V/25-1/10-25/A	18	●	0.233	0.012	8.57	0.859	0.56
V/25-1/10-25/B	19	●	0.233	0.012	8.57	0.896	0.54
V/25-3/10-5/A	20	□	0.234	0.033	9.14	2.55	4.09
V/25-3/10-5/B	21	□	0.235	0.033	9.13	2.69	3.85
V/25-3/10-15/A	22	◪	0.234	0.033	9.14	2.55	2.20
V/25-3/10-15/B	23	◪	0.235	0.033	9.13	2.69	2.11
V/25-3/10-25/A	24	■	0.234	0.033	9.14	2.55	1.61
V/25-3/10-25/B	25	■	0.235	0.033	9.13	2.69	1.53
V/25-3/20-25/A	26	■ 20	0.235	0.033	9.13	2.69	1.64
V/50-3/10-25/A	27	■	0.401	0.030	10.03	4.61	1.20
V/50-3/10-25/B	28	■	0.401	0.030	10.03	4.61	1.21
V/25-5/10-5/A	29	△	0.234	0.049	10.12	4.34	6.38
V/25-5/10-15/A	30	◭	0.234	0.049	10.12	4.34	3.58
V/50-5/10-15/A	31	◭	0.396	0.042	11.90	7.36	2.86
V/25-5/10-25/A	32	▲	0.234	0.049	10.12	4.34	2.87
V/25-5/10-25/B	33	▲	0.224	0.048	10.34	5.95	2.71
V/25-5/20-25/A	34	▲ 20	0.233	0.049	10.12	4.25	2.90
V/25-7/10-5/A	35	⧖	0.233	0.065	10.77	6.08	8.75
V/25-7/20-5/A	36	⧖ 20	0.233	0.065	10.77	6.01	8.83

Table A.3: (Cont.)

Code	Run No.	Symbol	r_b (ft.)	u_* (fps.)	$\frac{U}{u_*}$	R_N (Multiply by 10^4)	F_{DO}
V/25-7/10-15/A	37	⧗	0.233	0.065	10.77	6.08	5.05
V/25-7/10-25/A	38	⧗	0.233	0.065	10.77	6.48	3.93
V/25-9/10-5/A	39	◿	0.234	0.083	10.91	8.33	11.96
V/25-9/10-15/A	40	◿	0.234	0.083	10.91	8.33	6.47
V/25-9/10-25/A	41	◿	0.234	0.083	10.91	8.24	4.59
V/25-15/25-5/A	42	◺ 25	0.234	0.132	11.30	13.3	17.28
V/25-15/25-15/A	43	◺ 25	0.234	0.133	11.30	13.7	11.19
V/25-15/25-25/A	44	◺ 25	0.234	0.133	11.30	13.7	8.28

Table A.4: Background Experimental and Environmental Data.

Normalized Maximum Heat Loss	$(T_{amb}-T_E)$	Code	Date of Expt.	Cross Sections of Temp. Measurements	$\overline{\Delta T}$	$\overline{T_{amb}}$	$\overline{T_{air}}$	RH	T_E
(%)	(°F)			(X/d)	(°F)	(°F)	(°F)	(%)	(°F)
0.67	4.57	V/25-1/10-5/C	9/28/72	2,4,6,8,10,15, 20,30	5.24	75.51	75.0	83.0	71.1
0.50	7.05	V/25-1/10-5/D	9/28/72	2.5,5,7.5,10, 15,20,30,50	4.75	75.05	71.0	81.5	68.0
2.87	4.55	V/25-1/10-5/A	9/28/72	5,15,50,100, 140*,180	5.15	75.55	74.0	82.5	71.0
2.88	4.57	V/25-1/10-5/B	11/15/72	5,15,50,100, 140*,180,220	5.06	80.07	73.0	57.0	65.5
3.95	4.68	V/50-1/10-5/A	10/2/72	5,15,30,50,75, 110	6.31	72.98	73.5	69.5	68.3
2.01	7.00	V/50-1/10-5/B	11/21/72	5,15,30,50,75, 110	4.64	81.50	71.0	61.0	64.5
1.00	6.82	V/25-1/5-15/A	8/29/72	10,50,100*, 200	17.48	74.02	69.8	82.5	67.2
7.95	3.96	V/25-1/5-15/B	11/21/72	10,50,100*, 200	15.02	81.66	73.0	69.0	67.7
2.45	6.21	V/25-1/10-15/C	9/28/72	2.5,5,7.5,10, 20,50,90,150	16.54	75.21	71.8	82.0	69.0
6.73	4.95	V/25-1/10-15/D	9/28/72	10,30,50,80, 120,200	16.58	75.35	72.8	84.0	70.4
7.32	5.07	V/25-1/10-15/A	9/28/72	10,50,100*, 200	16.78	75.47	73.2	84.0	70.4
4.56	14.12	V/25-1/10-15/B	11/15/72	10,50,100*,200	15.20	80.02	73.2	59.0	65.9

Table A.4: (Cont.)

Normalized Maximum Heat Loss	$(T_{amb}-T_E)$	Code	Date of Expt.	Cross Sections of Temp. Measurements	$\overline{\Delta T}$	$\overline{T_{amb}}$	$\overline{T_{air}}$	RH	T_E
(%)	(°F)			(X/d)	(°F)	(°F)	(°F)	(%)	(°F)
4.65	6.34	V/25-1/20-15/A	8/29/72	6,20,50,134, 174*,214	16.36	74.14	71.0	80.0	67.8
3.45	4.89	V/50-1/10-15/A	10/2/72	5,25,50,100	17.38	73.59	74.0	69.5	68.7
3.91	15.74	V/50-1/10-15/B	11/21/72	5,25,50,100	14.96	81.64	71.2	69.0	65.9
6.38	6.82	V/25-1/10-25/C	9/29/72	4,8,12,26,42, 74,114,174	24.38	74.32	72.0	73.0	67.5
7.75	5.83	V/25-1/10-25/D	7/29/72	4,8,12,24,50, 80,120	24.26	74.23	71.8	78.0	68.4
8.25	6.40	V/25-1/10-25/A	9/29/72	10,50,100*, 200	24.55	74.20	71.3	80.0	67.8
6.68	13.40	V/25-1/10-25/B	11/15/72	10,50,100*, 200	24.85	80.00	74.3	58.0	66.6
1.45	5.81	V/25-3/10-5/A	8/30/72	4,8,12,20*,30*, 50,70*,90	5.01	73.91	70.8	82.0	68.1
0.96	12.32	V/25-3/10-5/B	11/7/72	4,8,12,20,30*, 50,70,90	5.23	80.42	73.8	66.0	68.1
4.17	5.71	V/25-3/10-15/A	8/30/72	5,10,30,50*, 90*,140*,200	16.24	73.21	71.8	73.0	67.5
2.37	13.62	V/25-3/10-15/B	11/9/72	5,10,30,50*, 90,140	16.03	80.52	72.5	67.0	66.9
7.50	5.22	V/25-3/10-25/A	8/30/72	5,10,30*,50*, 90*,140*,200	27.28	73.62	72.0	78.0	68.4

Table A.4: (Cont.)

Normalized Maximum Heat Loss	$(T_{amb}-T_E)$	Code	Date of Expt.	Cross Sections of Temp. Measurements	$\overline{\Delta T}$	$\overline{T_{amb}}$	$\overline{T_{air}}$	RH	T_E
(%)	(°F)			(X/d)	(°F)	(°F)	(°F)	(%)	(°F)
3.82	10.9	V/25-3/10-25/B	11/9/72	5,10,30,50, 90*,140,200	26.16	80.60	76.0	65.0	69.7
0.90	11.59	V/25-3/20-25/A	11/17/72	20,30,50,90, 140,200	24.37	79.69	73.8	66.0	68.1
2.92	6.36	V/50-3/10-25/A	11/14/72	5,15,25*,45, 70,100	25.61	81.36	72.0	59.0	65.0
3.80	10.91	V/50-3/10-25/B	11/14/72	5,15,25,45,70, 100	25.46	81.16	77.5	61.0	70.25
1.18	6.22	V/25-5/10-5/A	10/3/72	5,10,20*,40, 65,100	5.64	75.52	74.5	70.0	69.3
3.14	5.74	V/25-5/10-15/A	10/3/72	5,10,20*,40*, 65*,100,140	17.59	75.84	75.0	72.0	70.1
3.86	3.79	V/50-5/10-15/A	10/2/72	5,15,30,50*, 75,110	14.78	74.99	75.0	78.0	71.2
3.85	5.36	V/25-5/10-25/A	10/3/72	5,10,20*,40*, 65*,100*,150, 210	23.52	76.26	75.5	74.0	70.9
7.80	14.94	V/25-5/10-25/B	11/21/72	5,10,20*,40, 65,100,150	25.05	81.84	72.5	67.0	66.9
0.92	7.20	V/25-5/20-25/A	8/30/72	5,10,20*,40, 75,110	23.34	74.20	70.0	81.5	67.0
3.29	7.45	V/25-7/10-5/A	10/4/72	5,10,20*,30*, 50,70,90	5.84	75.85	73.0	73.0	68.4
0.39	7.46	V/25-7/20-15/A	8/30/72	5,10,15*,20, 40,70	5.73	74.46	69.8	81.5	67.0

Table A.4: (Cont.)

Normalized Maximum Heat Loss	$(T_{amb}-T_E)$	Code	Date of Expt.	Cross Sections of Temp. Measurements	$\overline{\Delta T}$	$\overline{T_{amb}}$	$\overline{T_{air}}$	RH	T_E
(%)	(°F)			(X/d)	(°F)	(°F)	(°F)	(%)	(°F)
2.39	7.38	V/25-7/10-15/A	10/4/72	5,10,20*,40*, 70*,110,150	15.74	76.18	73.8	69.5	68.8
3.45	6.41	V/25-7/10-25/A	10/4/72	5,15,*,30*, 50*,80,130,200	22.42	77.01	74.5	78.0	70.7
0.64	8.23	V/25-9/10-5/A	10/5/72	5,10,18*,30*, 50,80,120	4.83	76.63	72.8	73.0	69.4
2.01	7.44	V/25-9/10-15/A	10/5/72	5,10,20*,40*, 70*,120,180	14.96	76.84	73.8	73.5	69.4
2.98	6.89	V/25-9/10-25/A	10/5/72	5,10,20*,30*, 60*,100,150, 220	27.90	78.29	74.0	84.5	71.4
0.36	10.07	V/25-15/25-5/A	10/6/72	5,10,20*,30, 50,80,120	6.97	78.47	72.0	78.0	68.4
0.65	10.97	V/25-15/25-15/A	10/6/72	5,10,20*,30*, 50,80,120,170	14.00	78.17	72.5	69.0	67.2
0.98	9.94	V/25-15/25-25/A	10/6/72	5,10,20*,40*, 70,120,200	23.65	78.29	72.5	75.0	68.35

Appendix B

COMPUTER PROGRAMS FOR TEMPERATURE PREDICTION

PROGRAM B.1: FICKIAN EQUATION

```
C       PREDICTING TEMPERATURE PROFILES USING FICKIAN ASSUMPTIONS
C       RUN  V/25-3/10-5/A ,  DX=1/100 , DY=1/50
C       NOTE: THE ORDER OF THE SUBSCRIPTS IN T(I,J) HAS BEEN REVERSED
C       FROM THE ORDER USED IN THE THESIS TEXT
C       AK= VON KARMANS COEFFICIENT
C       XO= DIMENSIONLESS DISTANCE TO INITIAL CONDITIONS
C       USTAR= SHEAR VELOCITY
C       UAVUST= AVE VEL/ SHEAR VEL
C       AKY= CONSTANT DIFFUSION COEFFICIENT
C       VEL= AVE VEL
C       DELTEM= EFFLUENT TEMP-AMB TEMP
C       RB=CORRECTED EFFECTIVE DEPTH
C       NO= NUMBER OF HEAT LOSS READINGS READ IN
C       NP= NO OF PRINTOUTS AFTER INITIAL READING
      COMMON T(2,100),X(25),Y(25)
      READ(5,200) XO,UAVUST,AK,AKY,VEL,DELTEM,RB,USTAR,M,N,NO,NP
  200 FORMAT(8F10.5/4I5)
C       WRITE OUT MAIN PARAMETERS
      WRITE(6,202) XO,UAVUST,AK,AKY,VEL,DELTEM,RB,USTAR,M,N,NO,NP
  202 FORMAT (' XO,    UAVUST,  AK,  AKY,    VEL,     DELTEM  ,        RB,
     1    USTAR,     M,     N,     NO   ,NP '/8F10.5,4I5//)
      AN=N
      AM=M
      DY=1./AN
      DX=1./AM
      UI=1./UAVUST
C       READ IN INITIAL TEMP PROFILE
      READ(5,201) (T(1,J),J=1,N)
  201 FORMAT(10F8.4)
      WRITE(6,40) XO,(T(1,I),I=1,N)
   40 FORMAT (F8.3/(10F10.5))
C       READ IN CUMULATIVE SURFACE HEAT LOSS VS. X/D
      READ(5,44) (X(I),Y(I),I=1,NO)
   44 FORMAT(2F10.5)
      D=DX/(DY*DY)
C       M2= NUMBER OF STEPS BETWEEN PRINTOUTS
      M2=400
      AM2=M2
      XC=XO
      AX=AM2/AM
C       DO AS MANY TIMES AS PRINTOUTS
      DO 21 K=1,NP
      XC=XC+AX
      DO 4 I=1,M2
C       COMPUTE BOUNDARY VALUES
```

```
      T(2,1)=T(1,1)+D*AKY*UI*(T(1,2)-T(1,1))
      T(2,N)=T(1,N)+D*AKY*UI*(T(1,N-1)-T(1,N))
C      COMPUTE VALUES INTERIOR TO BOUNDARIES
      KA=N-1
      DO 5 J=2,KA
    5 T(2,J)=T(1,J)+D*UI*AKY*(T(1,J+1)-2.*T(1,J)+T(1,J-1))
      DO 4 J=1,N
    4 T(1,J)=T(2,J)
      IF(K.EQ.1) M2=400
      IF(K.EQ.2) M2=400
      IF(K.EQ.3) M2=800
      IF(K.EQ.4) M2=1000
      IF (K.EQ.5) M2=2000
      IF(K.EQ.6) M2=2000
      IF(K.EQ.7) M2=2000
      AM2=M2
      AX=AM2/AM
   21 WRITE(6,40) XC,(T(1,J),J=1,N)
      CALL EXIT
      END
```

PROGRAM B.2: CONVECTION-DIFFUSION EQUATION WITH E_{Ty}

```
C       PREDICTING TEMPERATURE PROFILES USING EMPIRICAL DISTRIBUTION
C       FUNCTIONS FOR ET(Y).
C       RUN V/25-3/10-25/A   , DX=1/10,000 ,  DY=1/50
C       NOTE: THE ORDER OF THE SUBSCRIPTS IN T(I,J) HAS BEEN REVERSED
C       FROM THE ORDER USED IN THE THESIS TEXT
C       AK= VON KARMAN'S COEFFICIENT
C       XO= DIMENSIONLESS DISTANCE TO THE INITIAL CONDITIONS
C       UAVUST= AVE VEL/ SHEAR VEL
C       NO= NUMBER OF SURFACE HEAT LOSS READINGS READ IN
C       DELTEM= EFFLUENT TEMP-AMB TEMP
C       TI,RI,CI= INITIAL VALUES OF BETA PARAMETERS
C       E(I)=TRANSFER COEFFICIENT*6/(AK*RB*USTAR)
C       RB= CORRECTED EFFECTIVE DEPTH
C       USTAR= SHEAR VELOCITY
C       NP= NO OF PRINTOUTS  AFTER INITIAL READING
        COMMON T(2,100),X(50),Y(50),CTPT(100),UD(100),UI(100),U(100)
       1,TEMP(60),DENS(60),FIDXA(60),TA(60),RA(60),CA(60),E(100),CTPTC(100
       2)
C       READ IN BASIC PARAMETERS FOR THE RUN
        READ(5,20) XO,AK,UAVUST,DELTEM,TI,RI,CI,RB,USTAR,QEFF,DP,AMBTP,M,N
       1,NO,NP
   20   FORMAT (8F10.5/4F10.5,4I8)
        WRITE(6,22)XO,AK,UAVUST,DELTEM,TI,RI,CI,RB,USTAR,QEFF,DP,AMBTP,M,N
       1,NO,NP
   22   FORMAT(' LIST OF BASIC PARAMETERS '/12F9.5/4I8)
C       NOTE: FIDX FOR INITIAL COND,AVG VEL,EQTEM AND QTOT ENTERED HERE
        FIDX=1.835
        VEL=0.3
        EQTEM=68.4
        QTOT=.1875
        AN=N
        AM=M
        DY=1./AN
        DX=1./AM
C       READ IN INITIAL TEMP PROFILE
        READ (5,201) (T(1,J),J=1,N)
  201   FORMAT (10F8.4)
        DO 190 J=1,N
  190   T(1,J)=(T(1,J)-EQTEM)/DELTEM
C       READ IN ETA LOCATIONS AT MID POINTS OF INCREMENTS
        READ(5,25) (CTPT(I),I=1,N)
   25   FORMAT(8F10.5)
C       CALCULATING UI(I) AT MID POINT OF EACH INCREMENT
C       FIRST CALCULATE THE TWO MOST BOTTOM VELOCITIES (ASSUME LINEAR RELATION)
```

```
      U(2)= (USTAR/AK)*((ALOG(CTPT(2)))+1.)+VEL
      U(1)=0.3333*U(2)
      UD(2)=U(2)/VEL
      UD(1)=U(1)/VEL
      UI(2)=1./UD(2)
      UI(1)=1./UD(1)
      DO 40 J=3,N
      U(J)=(USTAR/AK)*((ALOG(CTPT(J)))+1.)+VEL
      UD(J)=U(J)/VEL
   40 UI(J)=1./UD(J)
C      READ IN CUMULATIVE HEAT LOSS VS. X/D
      DO 46 I=1,NO
      READ(5,44) (X(I),Y(I))
   44 FORMAT (2F10.5)
   46 CONTINUE
C      READ IN TEMP AND DENSITY CURVE
      READ(5,27) (TEMP(NI),NI=1,51)
   27 FORMAT(10F8.3)
      READ(5,28) (DENS(NI),NI=1,51)
   28 FORMAT (8F10.6)
C      READ IN TABLES FOR BETA PARAMETERS FIDX,T,R,C
      DO 33 I=1,50
      READ(5,32) (FIDXA(I),TA(I),RA(I),CA(I))
   32 FORMAT (4F10.5)
   33 CONTINUE
C      USING ORIGINAL VALUES OF T,R,C CALCULATE ORIGINAL VALUES OF E(I)
C      E(I) MEASURED AT BOTTOM OF INCREMENT
      DO 29 J=1,N
   29 CTPTC(J)=CTPT(J)-0.01
      DO 30 J=1,N
   23 CCTPT=1.-CTPTC(J)
      RM=RI-1.
      DIFF=TI-RI
      TM=DIFF-1.
      E(J)=14.3*CI*CTPTC(J)**RM*CCTPT**TM
   30 CONTINUE
C      CALCULATE DEPTH AVERAGED VALUES AND NORMALIZED FLUX FOR
C      INITIAL CONDITION
C      INITIAL HEAT FLUX IN EXCESS OF EQTEM=EFLUX
C      ETHAV = AVE VALUE OF DIMENSIONLESS TRANSFER COEFFICIENT,ET/RB*USTAR
      EFLUX=((QEFF*DELTEM)+(QTOT*(AMBTP-EQTEM)))*62.4
      FLUX=0.0
      ETHAV=0.0
      DO 45 J=1,N
      FLUX=FLUX+T(1,J)*U(J)
   45 ETHAV=ETHAV+E(J)/AN
      ETHAV=ETHAV/14.3
      FLUX=FLUX*2.5*0.02*DP*62.4*DELTEM
      FLUXN=FLUX/EFLUX
      WRITE(6,50) XO,ETHAV,FLUXN,FIDX,(T(1,J),J=1,N)
   50 FORMAT(//4F10.5/(10F10.5))
      D=DX/(DY*DY)
      D1=DX/DY
C      M2= NUMBER OF STEPS BETWEEN PRINTOUTS
      M2=5.*AK*USTAR* 10000./(6.*VEL)
      AM2=M2
      AX= AM2/AM
      XC=XO
C      DO AS MANY TIMES AS PRINTOUT
      DO 21 K=1,NP
      XC=XC+AX
```

```
      CALL SURLOS(XC,YC,VEL,AK,USTAR,RB,DELTEM,NO)
      DO 4 I=1,M2
C      FIRST COMPUTE BOUNDARY VALUES
      T(2,1)=T(1,1)+D*E(2)*UI(1)*(T(1,2)-T(1,1))
      T(2,N)=T(1,N)+D*E(N)*UI(N)*(T(1,N-1)-T(1,N))-(YC*UI(N)*D1)
C      COMPUTE VALUES INTERIOR TO BOUNDARIES
      KA=N-1
      DO 5 J=2,KA
    5 T(2,J)=T(1,J)+D*UI(J)*(E(J+1)*(T(1,J+1)-T(1,J))-E(J)*(T(1,J)-T(1,J
     1-1)))
      DO 4 J=1,N
    4 T(1,J)=T(2,J)
C      COMPUTE NORMALIZED FLUX AND ETHAV AT PRINTOUT POSITION
      FLUX=0.0
      ETHAV=0.0
      DO 6 J=1,N
      ETHAV=ETHAV+E(J)/AN
    6 FLUX=FLUX+T(1,J)*U(J)
      ETHAV=ETHAV/14.3
      FLUX=FLUX*2.5*0.02*DP*62.4*DELTEM
      FLUXN=FLUX/EFLUX
C      COMPUTE T1,R AND C FOR NEXT STEP LENGTH
C      FIRST COMPUTE FIDX FOR TEMPS AT END OF PREVIOUS STEP (AND
C       THUS THE BEGINNING OF THE NEXT STEP )
      TMIN=0.5*(T(1,4)+T(1,5))
      TMAX=0.5*(T(1,N-1)+T(1,N-2))
      CALL RELDEN(TMAX,TMIN,DELDEN,DELTEM,AMBTP,EQTEM)
      FIDX=VEL/(SQRT(32.2*RB*DELDEN))
C      PRINT OUT RESULTS
      WRITE(6,60) XC,ETHAV,FLUXN,FIDX,(T(1,J),J=1,N)
   60 FORMAT(//4F10.5/(10F10.5))
      CALL BETPRO(FIDX,T1,R,C)
C      COMPUTE NEW VALUES OF E(I), MEAS AT BOTTOM OF INCREMENT
      DO 70 J=1,N
      CCTPT=1.-CTPTC(J)
      RM=R-1.
      DIFF=T1-R
      TM=DIFF-1.
   70 E(J)=14.3*C*CTPTC(J)**RM*CCTPT**TM
C      COMPUTE STEP LENGTH FOR THE NEXT PRINTOUT
      IF(K.EQ.1) GO TO 11
      IF(K.EQ.2) GO TO 12
      IF(K.EQ.3) GO TO 13
      IF(K.EQ.4) GO TO 14
      IF(K.EQ.5) GO TO 15
      GO TO 21
   11 M2=200000.*AK*USTAR/(6.*VEL)
      GO TO 19
   12 M2=200000.*AK*USTAR/(6.*VEL)
      GO TO 19
   13 M2= 400000.*AK*USTAR/(6.*VEL)
      GO TO 19
   14 M2= 500000.*AK*USTAR/(6.*VEL)
      GO TO 19
   15 M2=600000.*AK*USTAR/(6.*VEL)
   19 AM2=M2
      AX=AM2/AM
   21 CONTINUE
      CALL EXIT
      END
      SUBROUTINE SURLOS(XC,YC,VEL,AK,USTAR,RB,DELTEM,NO)
```

```
C       GIVEN A VALUE OF DIMENSIONLESS XC, GET A VALUE OF DIMENSIONLESS
C       SURFACE HEAT LOSS RATE YC
        COMMON T(2,100),X(50),Y(50),CTPT(100),UD(100),UI(100),U(100)
       1,TEMP(60),DENS(60),FIDXA(60),TA(60),RA(60),CA(60),E(100),CTPTC(100
       2)
C       TO CHANGE XC TO X/D
        XC=XC*(6.*VEL)/(AK*USTAR)
        DO 10 K=1,NO
        IF(X(K) .GT.XC) GO TO 20
   10   CONTINUE
   20   DX=X(K)-X(K-1)
        DY=Y(K)-Y(K-1)
        YC=DY/DX
        YC=YC*6.0/(2.5*62.4*AK*RB*USTAR*DELTEM)
        XC=XC*(AK*USTAR)/(6.*VEL)
        RETURN
        END
        SUBROUTINE RELDEN (TMAX,TMIN,DELDEN,DELTEM,AMBTP,EQTEM)
C       TO FIND DELTA RHO/RHO , TEMPS GIVEN  AS DIMENSIONLESS
        COMMON T(2,100),X(50),Y(50),CTPT(100),UD(100),UI(100),U(100)
       1,TEMP(60),DENS(60),FIDXA(60),TA(60),RA(60),CA(60),E(100),CTPTC(100
       2)
        TMIN=(((TMIN*DELTEM)+EQTEM)-32.)*5./9.
        TMAX=(((TMAX*DELTEM)+EQTEM)-32.)*5./9.
        DO 75 IN=2,51
        IF(TMIN.LT.TEMP(IN)) GO TO 77
   75   CONTINUE
C       INTERPOLATION PROCEDURE
   77   DIFF=TEMP(IN)-TMIN
        INB=IN-1
        DENSAM=DENS(IN)+(DIFF/0.5)*(DENS(INB)-DENS(IN))
        DO 78 IN=2,51
        IF(TMAX.LT.TEMP(IN)) GO TO 79
   78   CONTINUE
   79   DIFF= TEMP(IN)-TMAX
        INB=IN-1
        DENSEF =DENS(IN)+(DIFF/0.5)*(DENS(INB)-DENS(IN))
        DELDEN=(DENSAM-DENSEF)/DENSAM
        RETURN
        END
        SUBROUTINE BETPRO(FIDX,T1,R,C)
        COMMON T(2,100),X(50),Y(50),CTPT(100),UD(100),UI(100),U(100)
       1,TEMP(60),DENS(60),FIDXA(60),TA(60),RA(60),CA(60),E(100),CTPTC(100
       2)
        DO 20 I=2,50
        IF(FIDXA(I).GT.FIDX) GO TO 30
   20   CONTINUE
   30   DIFF=FIDXA(I)-FIDX
        BT=TA(I-1)-TA(I)
        AT=FIDXA(I)-FIDXA(I-1)
        DELTA=BT*DIFF/AT
        T1=TA(I)+DELTA
        BR=RA(I-1)-RA(I)
        DELRA=BR*DIFF/AT
        R=RA(I)+DELRA
        CR=CA(I-1)-CA(I)
        DELCA=CR*DIFF/AT
        C=CA(I)+DELCA
        RETURN
        END
```